UNIVERSITY OF HELSINKI REPORT SERIES IN PHYSICS

HU-P-D162

Exotic superfluid states of ultra-cold Fermi gases

Tomi Paananen

Division of Elementary Particle Physics
Department of Physics
Faculty of Science
University of Helsinki
Helsinki, Finland

ACADEMIC DISSERTATION
To be presented, with the permission of the Faculty of Science of the University of Helsinki, for public criticism in the Small Auditorium (E204) of Physicum, Gustaf Hällströmin katu 2a, on Thursday, May 28, 2009 at 12 o'clock.

Helsinki 2009

ISBN 978-952-10-4235-5 (printed version)
ISSN 0356-0961
ISBN 978-952-10-4236-2 (pdf-version)
http://ethesis.helsinki.fi
Yliopistopaino
Helsinki 2009

Abstract

This is a study of ultra-cold Fermi gases in different systems. This thesis is focused on exotic superfluid states, for an example on the three component Fermi gas and the FFLO phase in optical lattices. In the two-components case, superfluidity is studied mainly in the case of the spin population imbalanced Fermi gases and the phase diagrams are calculated from the mean-field theory. Different methods to detect different phases in optical lattices are suggested. In the three-component case, we studied also the uniform gas and harmonically trapped system. In this case, the BCS theory is generalized to three-component gases. It is also discussed how to achieve the conditions to get an $SU(3)$-symmetric Hamiltonian in optical lattices.

The thesis is divided in chapters as follows: Chapter 1 is an introduction to the field of cold quantum gases. In chapter 2 optical lattices and their experimental characteristics are discussed. Chapter 3 deals with two-components Fermi gases in optical lattices and the paired states in lattices. In chapter 4 three-component Fermi gases with and without a harmonic trap are explored, and the pairing mechanisms are studied. In this chapter, we also discuss three-component Fermi gases in optical lattices. Chapter 5 devoted to the higher order correlations, and what they can tell about the paired states. Chapter 6 concludes the thesis.

Acknowledgements

This thesis is based on research carried out at the University of Helsinki. The financial support from the Academy of Finland, is gratefully acknowledged.

First of all, I thank my supervisor Dr. Jani-Petri Martikainen for all his support and guidance. I also acknowledge Prof. Päivi Törmä, Dr. Timo Koponen, Dr. Reza Bakhtiari, and Dr. Emil Lundh for the collaboration.

I want to thank my friends Dr. Juha-Pekka Nikkarila, Mr. Reijo Keskitalo, and Mr. Jens Pomoell for the many illuminating discussions during the research.

Finally, I thank my parents and brothers for all the support.

Contents

List of Figures

List of included publications

This thesis consists the following publications.

I T. Paananen, J. -P. Martikainen, and P. Törmä,
Pairing in a three component Fermi gas,
Phys. Rev. A **73**, 053606 (2006)

II T. Paananen, P. Törmä, and J.-P. Martikainen,
Co-existence and shell structures of several superfluids in trapped three-component Fermi mixtures,
Phys. Rev. A **75**, 023622 (2007)

III T.K. Koponen, T. Paananen, J.-P. Martikainen,and P. Törmä,
Finite temperature phase diagram of a polarized Fermi gas in an optical lattice,
Phys. Rev. Lett. **99**, 120403 (2007)

IV T. Paananen, T. K. Koponen, P. Törmä, and J. -P. Martikainen,
Noise correlations of the ultra-cold Fermi gas in an optical lattice,
Phys. Rev. A **77**, 053602 (2008)

V T. Paananen,
Superfluid-density of the ultra-cold Fermi gas in optical lattices,
submitted to J. Phys. B, arXiv:0811.3623 (2008)

The author performed all the analytical calculations and most of the numerics in papers **I**, **II**, and **IV**. In paper **III** the author performed a part of the analytical calculations. The author is the main writer in paper **IV**, and has participated in writing publications **I**, **II**, and **III**.

Chapter 1

Introduction to ultra-cold atomic gases

1.1 Quantum statistics

Identical particles in classical physics are distinguishable. This means that one can label them and one can identify them at every moment by following their trajectories. The energy distribution of a large number of classical particles, in the thermal equilibrium, follows the Maxwell-Boltzmann distribution. Contrary to classical mechanics, in quantum mechanics, this kind of identification of identical particles is impossible. The intuitive concept of a trajectory does not belong quantum mechanics. Thus in quantum mechanics if one identifies the particles at time t_1, the particles cannot be identified at another time. Since one cannot follow the trajectories. Because the particles cannot be identified the energy distribution of particles in quantum mechanics is not the Maxwell-Boltzmann distribution.

It is an experimental fact that in three-dimensional space there are two kinds of particles, i.e there are two families of particle which have different energy distributions, or *statistics*. The families are called *fermions* and *bosons*. This is a main postulate of many body quantum mechanics. But this can be reasoned as the following way. Let us assume a system of two identical particles. The wavefunction of the system, in quantum mechanics a wavefunction i.e a complex function of all quantum numbers describes the system completely, is given by $\Psi(\chi_1, \chi_2)$, where χ_1 and χ_2 describe the quantum numbers of the particles. The square of the absolute value of the wave function gives probability of finding the system in a given quantum state. Because the particles are identical the probability does not change when the particles are reversed i.e. $|\Psi(\chi_1, \chi_2)|^2 = |\Psi(\chi_2, \chi_1)|^2$. Since the global phase of the wavefunction is not an observable in the three-dimensional system, there are two possibilities to achieve this condition, either $\Psi(\chi_1, \chi_2) = \Psi(\chi_2, \chi_1)$

or $\Psi(\chi_1, \chi_2) = -\Psi(\chi_2, \chi_1)$. The former holds for bosons and the later holds for fermions. In the other words the wavefunction for bosons is symmetric under the particle exchange for fermions it is asymmetric. Experiments have confirmed that all the particles belong either one of these groups. Both of these groups have their own energy distributions, Bose-Einstein distribution for bosons and Fermi-Dirac distribution for fermions. However, in two-dimensional system the phase of the wavefunction is an observable,and thus the equation $|\Psi(\chi_1, \chi_2)|^2 = |\Psi(\chi_2, \chi_1)|^2$ does not imply that $\Psi(\chi_1, \chi_2) = \pm\Psi(\chi_2, \chi_1)$. That is why in two dimensions particles are not either fermions or bosons, and their energy distributions can be,in principle, something else that the Fermi-Dirac- or the Bose-Einstein distributions. In two dimensions, the quantum mechanical particles are called *anyons*.

When the wavefunction is antisymmetric under the particle exchange and the quantum numbers of the particles are same, i.e. $\chi_1 = \chi_2$, then $\Psi(\chi_1, \chi_1) = -\Psi(\chi_1, \chi_1)$ and from this follows $\Psi(\chi_1, \chi_1) = 0$. This implies that the probability to find two identical fermions in the same quantum state is zero, and hence it is impossible for two or more identical fermions be in the same quantum state. This feature is known as the *Pauli exclusion principle*. Bosons or classical particles do not obey the exclusion principle. Arbitrary number of identical bosons can occupy the same quantum state.

The question whether a particle is a fermion or a boson is connected to the spin of the particle. If the spin is a half-integer ($s = \hbar/2, 3\hbar/2, \ldots$, where $\hbar = h/(2\pi)$,and h is the Planck's constant) the particle is a fermion. If the spin is an integer the particle is a boson.

A composite particle, a particle which consists of two or more particles, is a fermion if it includes odd number of fermions and it is a boson if it includes even number of fermions. An atom is a composite particle, which consists of fermions (protons, neutrons, and electrons) and its total number of fermions is $2F + N$, where F is the number of protons (and electrons) and N is the number of neutrons. Thus it is the number of neutrons that determine whether the atom is a fermion or not. If the number of neutrons is odd the atom is a fermion if even the atom is a boson. Although the chemical properties of an atom are determined, by electron cloud, the quantum statistical properties of an ultra-cold dilute gas are determined by the neutrons.

Originally the study of ultra cold atomic gases can be tracked back the studies of Satyendra Nath Bose and Albert Einsten [1, 2], they predicted theoretically a phenomenon which is nowadays called Bose-Einstein condensation (BEC). Their prediction was that when the a cloud of bosons is cooled down below some critical temperature a macroscopic number of the particles occupies the lowest energy state, and this macroscopic part of the cloud behaves like one coherent matter wave. First indications of BEC were seen from experiments with superfluid liquid helium. However, due the strong interactions in liquid helium these experiments lack the proof of pure BEC. The conclusive experimental proof of pure BEC

was given in year 1995 by groups of Carl Wieman and Eric Cornell at JILA and Wolfgang Ketterle at MIT. These experiments were done by using ultra-cold clouds of rubidium (JILA) and sodium (MIT) [3, 4]. After this atomic BECs have been observed in numerous laboratories all over the world.

1.2 Trapping and cooling

In experiments with ultra-cold gases, typically alkali metals are used. Alkali metals are in the order of the increasing number of protons, lithium (Li), sodium (Na), potassium (K), rubidium (Rb), cesium (Cs), and francium (Fr). Francium has not any stable isotopes, but the others have. Since the ground state phase of an alkali metal is solid,the alkali gases are unstable. However, if the gas is dilute and col enough the collisions, especially the three-body collisions, between the atoms are so rare that relaxation times become so long that the gas is almost stable. This is one of the main reasons why the gas has to be dilute.

The outermost electron of an alkali atom is in an *s*-orbit, other shells are closed, i.e they are full. For this reason inner shells have no net total angular momentum. Because the outermost electron is in an s-orbit, it has no orbital angular momentum. Thus the electron cloud has no total orbital angular momentum. The total angular momentum of the atom is connected to the total spin Z of the atom. The spin of the nucleus and the spin of the outermost electron interact between each other, and this interaction is called the hyperfine interaction. The total spin of the alkali atom is given by $Z = I \pm 1/2$, where I is the spin of the nucleus. The different hyperfine states have different hyperfine magnetic momenta $m_f = -F, -F+1, \ldots, F$. In the zero external magnetic field, the states with different total spin F have energy splitting between each other, but the hyperfine states with same total spin are degenerate. However, when the external magnetic field is switched on, the energy levels of the degenerate states split. This effect is called *Zeeman effect* and this energy splitting is called *Zeeman splitting*. Some of these hyperfine levels are called high field seeking levels. Since their energies decrease with increasing magnetic field, and others are called low field seeking levels.Since their energies increase with increasing magnetic field (bosons have also the neutral state, i.e. the state whose energy does not depend the magnetic field). This is seen in figure 1.1.

One way to trap cold atoms is to use a so-called magneto optical trap (MOT). In MOT there are two coils in an anti-Helmholtzian configuration [5]. This way one can create a magnetic trap, where the minimum of the amplitude of the magnetic field is at he center of the trap. This kind of trap can trap low field seeking hyperfine states. There is one major problem with these kind of traps, the magnetic field vanishes at the center of the trap. If the external field is zero, the hyperfine states become degenerate and the atoms can flip from one hyperfine state to another. This problem can be solved, for an example, by rotating the

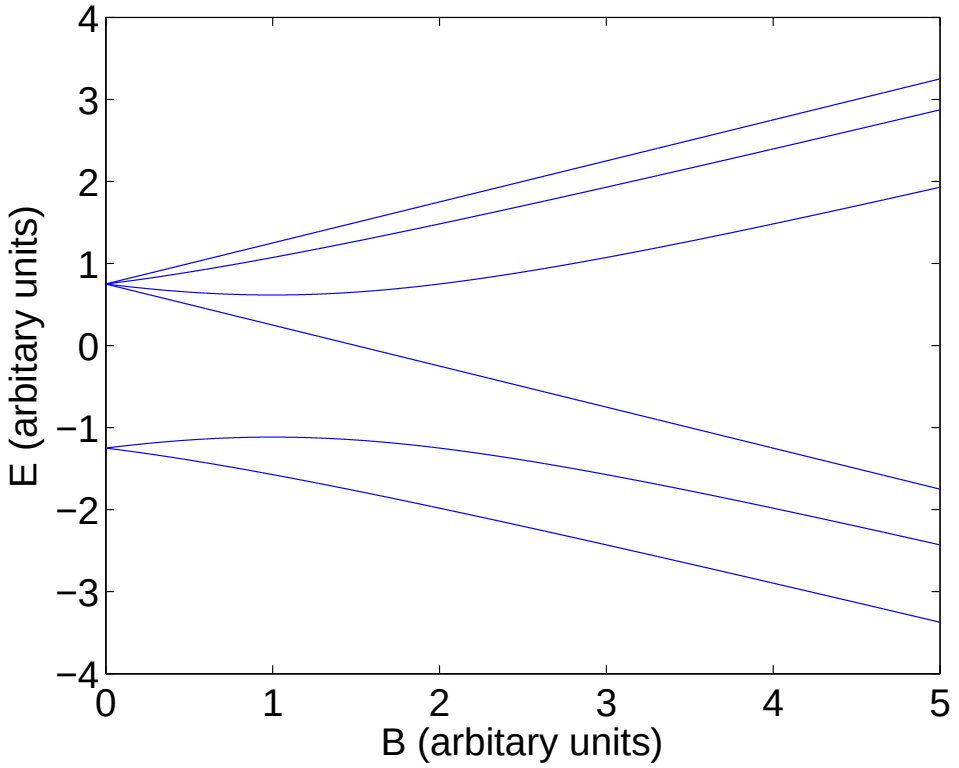

Figure 1.1: Schematic picture of the Zeeman effect for an atom with nuclear spin $I = 1$ (^{6}Li). The atom has two hyperfine states with the total spin $Z = 1/2$ and four the total spin $Z = 3/2$. In this picture three lowest energy states are high field seekers, other are low field seekers.

trap fast. This rotation forms a repulsive pseudo-potential at the center of the trap (JILA). Another way to solve this problem is to create an optical repulsive potential in the center of the trap by lasers (MIT).

The atoms can also be trapped optically. The trapping potential in an optical trap arises from the dipole electric field interaction as shown below. When an atom is in the external electric field it becomes charge polarized. In other words the electric field displaces the positively charged nucleus and the negatively charged electron cloud relative to each other, which renders the atom an electric dipole. When a charged particle is on the external electro-magnetic field it feels the Lorentz force, which is given by

$$\mathbf{F} = q\left(\mathbf{E} + \frac{d\mathbf{r}}{dt} \times \mathbf{B}\right),$$

where q is the charge of the particle and $\mathbf{E}$ and $\mathbf{B}$ are the electric- and the

magnetic fields, respectively. Now one can consider the atom as a dipole where two charges q and $-q$ with a displacement $\mathbf{r}_1 - \mathbf{r}_2 = \mathbf{d}$, thus the atom feels the force

$$\mathbf{F} = \mathbf{F}_1 - \mathbf{F}_2 = q\left(\mathbf{E}_1 - \mathbf{E}_2 + \frac{d\mathbf{d}}{dt} \times \mathbf{B}\right).$$

The displacement can be assumed small, and thus the force can be approximated as

$$\mathbf{F} = \mathbf{F}_1 - \mathbf{F}_2 = q\left((\mathbf{d} \cdot \nabla)\mathbf{E} + \frac{d\mathbf{d}}{dt} \times \mathbf{B}\right),$$

Furthermore one can determine the dipole moment as $\mathbf{p} = q\mathbf{d}$, and assume that the polarization is linear $\mathbf{p} = \alpha\mathbf{E}$, the force becomes

$$\mathbf{F} = \alpha\left((\mathbf{E} \cdot \nabla)\mathbf{E} + \frac{d\mathbf{E}}{dt} \times \mathbf{B}\right).$$

By using the following identities

$$(\mathbf{E} \cdot \nabla)\mathbf{E} = \frac{1}{2}\nabla E^2 - \mathbf{E} \times (\nabla \times \mathbf{E}),$$
$$\nabla \times \mathbf{E} = -\frac{\partial \mathbf{B}}{\partial t},$$

one finds

$$\mathbf{F} = \alpha\left(\frac{1}{2}\nabla E^2 + \frac{d}{dt}(\mathbf{E} \times \mathbf{B})\right).$$

The last term averages to zero, thus the force can be written as

$$\mathbf{F} = \nabla\frac{\alpha E^2}{2}.$$

Now the corresponding potential is given by

$$V = -\frac{\alpha E^2}{2}.$$

The atoms are attracted to the locations of the highest or the lowest intensity of the electric field (depending on the sign of α). Thus the atoms can be trapped in the middle of intersecting laser beams or in the local region of a single laser beam. The sign of the α depends on the frequency of the laser beams. Let us assume that the transition frequency between two different states $|1\rangle$ and $|2\rangle$ of an atom is f_0, and the frequency of the trapping laser is f. If $f > f_0$ (the laser is blue tuned), then $\alpha < 0$ and the atoms are attracted to the location of the lowest intensity. If $f < f_0$ (the laser is red tuned), then $\alpha > 0$ and the atoms are attracted to the location of the highest intensity.

Experiments are done the regime of quantum degeneracy at ultra-low temperatures (tens of nano Kelvins), therefore the gas has to be cooled. The requirement

for cold temperatures arises from the fact that superfluidity or the BEC are quantum phenomena. Temperatures have to be so low that atomic (center of mass) wavefunctions overlap. In other words, the de Broglie wavelength of the atoms has to be longer than the inter-particle distance. Since alkali gas are very dilute, temperatures, where the previous condition is achieved, are very low. There are different ways to cool the cloud. In a MOT one can use laser cooling. In laser cooling, perpendicular laser beams are directed to the cloud of the atoms, and the frequency f_l of the laser beams is chosen to be just below a transition frequency f_t between the ground state and an exited state of the atom. The cooling effect arises from the Doppler effect, when an atom is moving toward the laser beam it feels that the frequency of laser is higher than it really is, that is why the laser can excite the atom. When the excited state decays the atom emits a photon, which has frequency f_t. Now the atom looses from its kinetic energy the energy $hf_t - hf_l$ (h is the Planck's constant), and the gas cools.The temperature limit for this cooling method is the order of $10 - 100$ μK, and it comes from that the photon emmission from the atom is istropic, but excitation is direction depended (thus the laser beams are along side the axis) [5, 6, 7]. These temperatures are not often low enough for the experiments.

Lower temperatures can be achieved by using, for an example, the Sisyphus cooling [7]. In the Sisyphus cooling, laser beams, which are polarized in differently, connect different hyperfine states to each other. When the polarizations of the laser beams alternate, for an example, in z direction, the energy levels of of the hyperfine states also alternate, see figure 1.2. When the polarization of the laser changes the atom can jump from one hyperfine state to another. When the atom reaches the maximum of the potential of one hyperfine state, it can relax to the minimum of the potential of another hyperfine states, see figure 1.2. Thus the atoms climb constantly and looses its kinetic energy, - the gas cools. By using the Sisyphus cooling one can achieve temperatures order of $0.1 - 1$ μK [7].

If even lower temperatures are required, an useful cooling method is the evaporative cooling. The basic idea of the evaporative cooling is that the hottest atoms i.e the atoms, which have most kinetic energy, are allowed to leave the trap. This is done by lowering the trapping potential of the edges of the cloud. This lowering has to be done so slowly that the gas has time to thermalize. In other words, after lowering the trapping potential one has to wait until the gas has achieved a new thermal equilibrium and it has a new lower temperature energy distribution. By repeating this process very low temperatures can be achieved, even as low as 10 nK. Of course during the evaporative cooling a significant number of the atoms are lost.

One possible method to cool a gas, which is difficult to cool by using lasers, is called sympathetic cooling [8]. In the sympathetic cooling one uses two different types of atoms which interact with each others. These interactions can create some dissipation i.e. the interaction between atoms can excite atoms and gas

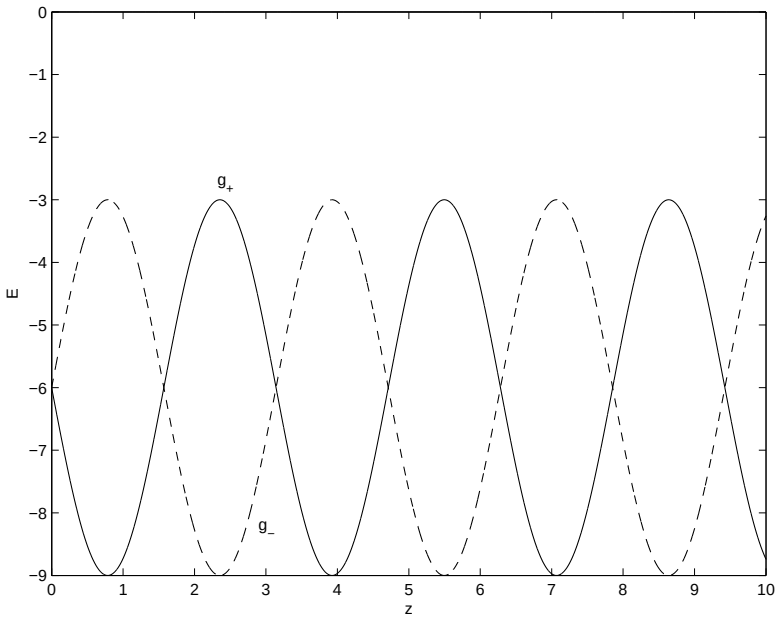

Figure 1.2: Schematic figure of the Sisyphus cooling. Lines g_+ and g_- describe the energy levels of two different hyperfine states of the same atom as a function of z. In this case the polarization of the laser beams alternate as a function of z. The units are arbitrary (E corresponds the energy).

can cool. Due to the interactions, the thermalization is much faster than without them. Lack of the s-wave interaction makes hard to cool a one component Fermi gas, since thermalization times are long. This is the reason why the evaporative cooling is much easier with a two-component Fermi gas than with an one component Fermi gas.

1.3 Interactions between atoms

Ultra-cold atomic gases are very dilute, with densities on the order of 10^{20} $1/\mathrm{m}^3$. This means that the inter-particle distance is on the order of 200 nm, and hence the two-body collisions are dominant. Thus the scattering phenomenon in the system can be handled as a two-body problem.

The interactions between two neutral alkali atoms arises from van der Waals interactions between electron clouds of the atoms. These van der Waals interactions occur only when the atoms are close to each other, i.e., in collisions. The real van der Waals potential considered here is of the following type, a hard core repulsion when distance between atoms $r \leq 2r_a$ (r_a is a radius of the atoms), and an attractive r^{-6} type potential when $r >> 2r_a$. This type of potential is

quite complicated and because the range of interactions is much smaller than the average distance between atoms, we can approximate the potential as a contact potential, which is given by [7]

$$V(\mathbf{r}_1, \mathbf{r}_2) = g\delta(\mathbf{r}_1 - \mathbf{r}_2) = \frac{2\pi\hbar^2 a}{m_r}\delta(\mathbf{r}_1 - \mathbf{r}_2),$$

where a is the s-wave scattering length, $\delta(\mathbf{r}_1 - \mathbf{r}_2)$ is the Dirac's delta-function and the reduced mass is given by

$$m_r = \frac{m_1 m_2}{m_1 + m_2},$$

with m_σ the mass of the atom σ. All the properties of this potential are characterized by one parameter, the s-wave scattering length a. This parameter can be controlled almost freely using magnetic fields and employing a phenomenon called the Feshbach resonance [9, 10, 11]. In the Feshbach resonance, in a scattering process a molecular state can couple resonantly to a free state via a virtual process. The s-wave scattering length depends on the energy difference between the molecular state and the free state and it can have, in principle, any value. When the energy of the free state is the lower one and difference is quite large, the scattering length is small and negative and the atoms form loosely bound Cooper pairs (BCS). When the energy of the free state is the higher one and difference is quite large, the scattering length is small and positive and the atoms form tightly bound molecules (BEC). On the resonance the energy difference between the molecular state and the free state becomes zero. This can be seen from figure 1.3.

By using the Feshbach resonance one can choose the effective interaction between atoms almost freely. This flexibility is one of the reasons why cold atoms are a good tool for modeling different quantum mechanical and solid state problems.

1.4 Superfluidity

At very low temperatures certain materials can lose their electric resistance, in other words they become *superconductors*. An analogous phenomenon for neutral particles is called *superfluidity*, where a fluid can flow without any friction. Actually one can think that superconductivity is superfluidity of charged particles. There two types of superconductors: low temperature superconductors and high temperature superconductors [12]. Low temperature superconductors are conventional metallic superconductors. A typical critical temperature T_c (below which the conductor is a superconductor) of a low temperature superconductor is a few Kelvins at maximum, and compared to the Fermi temperature T_F of

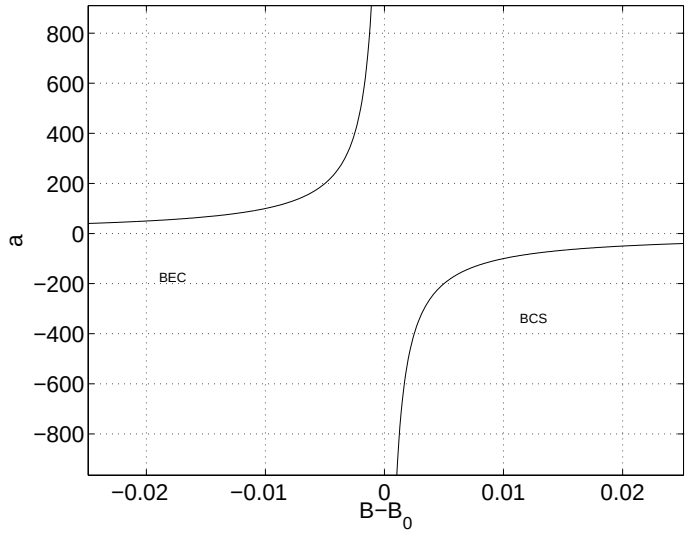

Figure 1.3: Schematic figure of the Feshbach resonance. Atom-atom s-wave scattering length as a function of external magnetic field near the resonance.The units are arbitrary.

electrons, it is order of $T_c/T_F \sim 0.001$. The theory by Bardeen, Cooper and Schieffer (BCS) [13] describes these low temperature superconductors very accurately. The critical temperatures of the high temperature superconductors are typically order of a few hundred of Kelvins, and $T_c/T_F \sim 0.01$. These high temperature superconductors are ceramic compounds. There is not a theory which describes well all the properties of these high temperature superconductors.

One of the reasons to study ultra-cold alkali gases is to achieve a better understanding of superconductivity. In superconductors the charge carriers are electrons, fermions, and thus it makes sense to study alkali Fermi gases. The superfluidity of bosons arises from the fact that at low temperatures they can condense to the same quantum state and form a Bose-Einstein condensate (BEC). In the case of fermions, the situation is more complicated, since fermions cannot form a BEC. However, the superfluidity of fermions can arises when the two different types of fermions form a pair, and these pairs can considered as (a kind of complicated) composite bosons.

Due to the Pauli principle, two identical fermions cannot form a pair. This is due to the lack of the s-wave interaction in a one-component Fermi gas unlike a two-components Fermi gas. That is why in experiments, two or more different hyperfine states of the same isotope are typically used. There are two different types of pairing mechanisms. Firstly the simple one is pairing in the real space, in

this type of pairing the interaction potential between the atoms is such that the two particle state is a bound state, a molecule. These molecules are bosons, thus they can form a BEC. This kind of pairing does not depend on the Fermi sea, i.e., the other fermions, it is only a two particle problem. The other type of pairing is called the BCS type of pairing, where the atoms with attractive interactions form pairs in the momentum space, these pairs are called Cooper pairs. In the simplest case, these pairs have zero net momentum, i.e., the paired atoms have momenta $\mathbf{k}$ and $-\mathbf{k}$. These pairs are not localized in the real space. This kind of pairing cannot happen without the Fermi sea, thus this pairing rises from the interactions between the atoms and the Fermi sea [14]. In this thesis we mainly deal with the generalization of the BCS pairing to more complicated systems, such as a three-component Fermi gas.

Molecules of ultra-cold fermions were observed the first time in year 2003 [15, 16, 17, 18]. In the same year the evidence of BEC of these molecules was reported [19, 20, 21, 22]. In year 2004, the first experimental evidence of the BCS type of pairing in ultra-cold alkali gases was reported [23, 24, 25, 26], and in year 2005 the phase transition between the normal phase and the superfluid phase was observed by measuring the heat capacity as a function of the temperature [27]. Finally, in 2005 the first direct observation of the superfluidity of an alkali Fermi gas took place, when the MIT group produced quantized vortices [28].

Chapter 2

Optical lattices

An optical lattice is made by counterpropagating lasers. The laser beams give rise to a periodic potential as shown below [29]. As shown in the previous section, interaction between light and an atom gives a potential which depends on the absolute value of the electric field. Two counterpropagating laser beams in the x direction, which have same amplitudes and wave lengths form a standing electric field wave which is given by

$$\mathbf{E} = 2A(r,\theta)\cos(kx)\hat{e},$$

where $A(r,\theta)$ is the amplitude of the electric field, θ is the polarization angle $k = 2\pi/\lambda$ is the wavenumber, and $\hat{e}$ is a unit vector. Thus the potential in the x direction is given by (see the previous section)

$$V(x) = -\alpha|A(r,\theta)|^2\cos^2(kx).$$

Thus the laser beams form a one-dimensional periodic lattice, whose period is $d = \lambda/2$, where d is called the lattice constant. By adding one more standing wave one gets a two-dimensional lattice, and adding third the lattice becomes a three-dimensional lattice.

When all the beams are orthogonal, the lattice is cubic. By varying the amplitudes, wave lengths of the lasers, or the angles between the lasers one can create lattices with different topologies [30, 31, 32, 33, 34, 35, 36]. The lattice potential can also be quasi-periodic. In this work, all the lattices are assumed to be cubic lattices.

The Schrödinger equation of a particle in a lattice is given by

$$\left(-\frac{\hbar^2\nabla^2}{2m} + V(\mathbf{r})\right)\Psi(\mathbf{r}) = E\Psi(\mathbf{r}),$$

where $V(\mathbf{r})$ is the lattice potential. The solutions to this equations are called the Bloch functions [37], and they are given by $\Psi_{\mathbf{k}}(\mathbf{r}) = u_{\mathbf{k}}(\mathbf{r})e^{i\mathbf{k}\cdot\mathbf{r}}$, where $u_{\mathbf{k}}(\mathbf{r})$ is

a periodic function and $\mathbf{k}$ is a reciprocal lattice vector. These Bloch functions are global functions, i.e., they are not localized in any lattice site. Instead of the Bloch functions, for deep lattices, it is often useful to use so called the Wannier functions. The Wannier functions are localized in each lattice sites, and one can calculate the Wannier functions from the Bloch functions by summing the Bloch functions [38] as follows

$$w_i(\mathbf{r}) = \frac{1}{\sqrt{M}} \sum_{\mathbf{k}} e^{-i\mathbf{k}\cdot\mathbf{R}_i} \Psi_{\mathbf{k}}(\mathbf{r}),$$

where M is the number of lattice sites, and $\mathbf{R}_i$ is a lattice vector. Although the Wannier functions are localized in the lattice sites, they decay exponentially, and thus the Wannier functions reach into the nearest neighbour sites and beyond. This makes the tunneling of the atoms possible. The question how fast the Wannier functions decay depends on the lattice depth, i.e., the intensity of the lasers. The deeper the lattice, the more localized are the Wannier functions. The lattice potential at the center of a lattice site is almost harmonic. Thus in the deep lattice, the Wannier functions can be approximated by using the eigenfunctions of the harmonic potential. This approximation is better for deeper the lattices.

The physics in the lattice is often described by using the so-called Hubbard model. If the lattice is deep enough, the tunnelling between other lattice sites than the nearest neighbours can be neglected. This nearest neighbours tunnelling is described, in the Hubbard model by the hopping strength J. If the atoms interact between each others and the absolute value of the s-wave scattering length $|a|$ is smaller than the lattice constant d, the interaction is a point like interaction, i.e., the atoms can interact only if they are in the same lattice site. This interaction is described by effective interaction parameter U. In the next chapter, the Hubbard model is described more precisely.

In experiments, the intensity profile of the laser beam as a function of the distance from the laser beam axis is not constant but almost like a Gaussian function. On the good side without this Gaussian profile the atoms would escape from the lattice, since the pure lattice potential allows the atoms to move. However, this Gaussian profile breaks the translational symmetry of the lattice, and because the profile is not a pure Gaussian profile it does not have the elliptical symmetry of the harmonic potential. The absence of these symmetries makes it more difficult to create accurate theoretical models.

Some great physics has been done by using optical lattices. For example, the Zürich group observed the Fermi surfaces of a two-components Fermi gas and fermionic molecules in optical lattices in years 2004 and 2005 [35, 39]. The same group has reported that they have achieved a fermionic Mott insulator state [40].

Another group in Mainz Germany observed the fermionic antibunching effect using the noise correlations [41]. This group made the pioneering observation of

quantum phase transition, a transition which is driven by the quantum fluctuations, using an optical lattice. This transition was the phase transition between the Mott-insulator phase, and it was observed using the noise correlations [42]. In 2006, the MIT group saw the first direct evidence of fermionic superfluidity in optical lattices [36].

Chapter 3

Two-component Fermi gases in optical lattices

We discuss in this chapter mainly the results, which have been published in paper **III**.

3.1 Exact Hamiltonian

Here we study a two-components Fermi gas in an optical lattice. Where the components are two different hyperfine states of the same isotope or two different isotopes. The components are labeled, as in the electron gas, by $\uparrow$ and $\downarrow$. The almost exact many body Hamiltonian is given by

$$\begin{aligned}\hat{H} = &\sum_{\sigma=\uparrow,\downarrow} \int d\mathbf{r}' \, \hat{\Psi}^\dagger_\sigma(\mathbf{r}) \left(-\frac{\hbar^2 \nabla^2}{2m_\sigma} + V_\sigma(\mathbf{r}) \right) \hat{\Psi}_\sigma(\mathbf{r}) \\ &+ \int \int d\mathbf{r} d\mathbf{r}' \, \hat{\Psi}^\dagger_\uparrow(\mathbf{r}) \hat{\Psi}^\dagger_\downarrow(\mathbf{r}') U(\mathbf{r}, \mathbf{r}') \hat{\Psi}_\downarrow(\mathbf{r}') \hat{\Psi}_\uparrow(\mathbf{r}),\end{aligned} \tag{3.1}$$

where $\hat{\Psi}^\dagger$ and $\hat{\Psi}$ are fermionic field operators, $V_\sigma(\mathbf{r})$ is the lattice potential for the component σ, and $U(\mathbf{r}, \mathbf{r}')$ is the interaction between the components. In the Hamiltonian we have neglected other than two-body interactions, since the gas is assumed to be very dilute.

The standard way to approximate the interaction between atoms is to take the interaction to be s-wave interaction. Under this approximation the interaction turns to be

$$U(\mathbf{r}, \mathbf{r}') = \frac{2\pi\hbar^2 a}{m_r} \delta(\mathbf{r} - \mathbf{r}'),$$

where $\delta(\mathbf{r} - \mathbf{r}')$ is the Dirac's δ-function and a is the s-wave scattering length,

and the reduced mass is given by

$$m_r = \frac{m_\uparrow m_\downarrow}{m_\uparrow + m_\downarrow}.$$

Thus the Hamiltonian is simplified as

$$\begin{aligned}\hat{H} = &\sum_{\sigma=\uparrow,\downarrow} \int d\mathbf{r}'\, \hat{\Psi}^\dagger_\sigma(\mathbf{r}) \left(-\frac{\hbar^2\nabla^2}{2m_\sigma} + V_\sigma(\mathbf{r}) \right) \hat{\Psi}_\sigma(\mathbf{r}) \\ &+ \frac{2\pi\hbar^2 a}{m_r} \int d\mathbf{r}\, \hat{\Psi}^\dagger_\uparrow(\mathbf{r}) \hat{\Psi}^\dagger_\downarrow(\mathbf{r}) \hat{\Psi}_\downarrow(\mathbf{r}) \hat{\Psi}_\uparrow(\mathbf{r}).\end{aligned} \tag{3.2}$$

The cubic lattice potential is given by

$$V_\sigma(\mathbf{r}) = \sum_{\alpha=x,y,z} V_{\sigma,\alpha} \sin^2(k_\alpha \alpha),$$

where $k_\alpha = \pi/d_\alpha$ and d_α is a lattice constant in the α direction.

As said in the previous section the eigenstates in a lattice are Bloch functions. Bloch functions can be represented as a series of well localized Wannier functions. The field operators can be expanded by using these localized Wannier functions as follows

$$\begin{aligned}\hat{\Psi}_\sigma(\mathbf{r}) &= \sum_i w_{\sigma,i}(\mathbf{r}) \hat{c}_{\sigma,i} \\ \hat{\Psi}^\dagger_\sigma(\mathbf{r}) &= \sum_i w^*_{\sigma,i}(\mathbf{r}) \hat{c}^\dagger_{\sigma,i},\end{aligned}$$

where $w_{\sigma,i}$ is Wannier function centered at a lattice site i of the component σ, $\hat{c}_{\sigma,i}$ and $\hat{c}^\dagger_{\sigma,i}$ are annihilation and creation operators of the component σ. This is the lowest band approximation. In the other words, here it is assumed that the atoms occupy only the lowest energy state of the sites. This is reasonable assumption, when temperatures are low i.e. $k_B T << E_{bg}$, where E_{bg} is the energy gap between bands, and the filling fractions $n_\sigma = N_\sigma/M < 1$, where N_σ is the number of particles of component σ and M is the number of the lattice sites.

3.2 Lowest band Hubbard model

When the lattice is deep enough the nearest neighbours approximation (also known as the tight binding approximation) can be used. Under this approximation the kinetic part of the Hamiltonian becomes

$$\sum_\sigma \sum_{\langle i,j \rangle} \int d\mathbf{r}\, w^*_{\sigma,i}(\mathbf{r}) \left(-\frac{\hbar^2\nabla^2}{2m_\sigma} + V_\sigma(\mathbf{r}) \right) w_{\sigma,j} \hat{c}^\dagger_{\sigma,i} \hat{c}_{\sigma,j},$$

where $\langle i,j\rangle$ means sum over the nearest neighbours, and the interaction part of the Hamiltonian becomes

$$\frac{2\pi\hbar^2 a}{m_r}\sum_i \int d\mathbf{r}\,|w_{\uparrow,i}(\mathbf{r})|^2|w_{\downarrow,i}(\mathbf{r})|^2\hat{c}^\dagger_{\uparrow,i}\hat{c}^\dagger_{\downarrow,i}\hat{c}_{\downarrow,i}\hat{c}_{\uparrow,i}.$$

We assume that the Wannier functions $w_{\sigma,i}$ are the same in every lattice sites, in other words the form of the Wannier function does not depend the lattice site. This condition holds when the depth of the lattice does not change from a lattice site to another. We can then define

$$\begin{aligned} J_{\sigma,\alpha} &= -\int d\mathbf{r}\, w^*_{\sigma,i}(\mathbf{r})\left(-\frac{\hbar^2\nabla^2}{2m_\sigma}+V_\sigma(\mathbf{r})\right)w_{\sigma,i+d_\alpha\hat{\alpha}}(\mathbf{r}) \\ U &= \frac{2\pi\hbar^2(m_\uparrow+m_\downarrow)}{m_\uparrow m_\downarrow}\int d\mathbf{r}\,|w_{\uparrow,i}(\mathbf{r})|^2|w_{\downarrow,i}(\mathbf{r})|^2, \end{aligned} \tag{3.3}$$

where $\hat{\alpha}$ is a unit vector in the α direction ($\alpha = x,y,z$). One finds the lowest band Hubbard Hamiltonian which is given by

$$\begin{aligned} \hat{H}-\mu_\uparrow\hat{N}_\uparrow-\mu_\downarrow\hat{N}_\downarrow = &-\sum_i(\mu_\uparrow\hat{c}^\dagger_{\uparrow,i}\hat{c}_{\uparrow,i}+\mu_\downarrow\hat{c}^\dagger_{\downarrow,i}\hat{c}_{\downarrow,i})+U\sum_i\hat{c}^\dagger_{\uparrow,i}\hat{c}^\dagger_{\downarrow,i}\hat{c}_{\downarrow,i}\hat{c}_{\uparrow,i} \\ &-\sum_{\sigma=\uparrow,\downarrow}\left(J_{\sigma,x}\sum_{\langle i,j\rangle_x}+J_{\sigma,y}\sum_{\langle i,j\rangle_y}+J_{\sigma,z}\sum_{\langle i,j\rangle_z}\right)\hat{c}^\dagger_{\sigma,i}\hat{c}_{\sigma,j}, \end{aligned} \tag{3.4}$$

where μ_σ is a chemical potential of the component σ. When we take the depth of the lattice to be a form $V_{\sigma,\alpha} = s_{\sigma,\alpha}E_{r,\uparrow}$, the recoil energy $E_{r,\uparrow} = \hbar^2\pi^2/(2m_\uparrow d^2)$ ($d_\alpha = d$), and approximate the Wannier functions with the harmonic oscillator ground states, the values of U and J are

$$\begin{aligned} J_{\sigma,\alpha} &= \frac{m_\uparrow}{m_\sigma}E_{r,\uparrow}e^{-\frac{\pi^2\sqrt{s_{\sigma,\alpha}}}{4}}\left[\left(\frac{\pi^2 s_{\sigma,\alpha}}{4}-\frac{\sqrt{s_{\sigma,\alpha}}}{2}\right)-\frac{s_{\sigma,\alpha}}{2}\left(1+e^{-\frac{1}{\sqrt{s_{\sigma,\alpha}}}}\right)\right] \\ U &= E_{r,\uparrow}\frac{4\pi^{1/2}(s_{\uparrow,x}s_{\uparrow,y}s_{\uparrow,z})^{3/12}(s_{\downarrow,x}s_{\downarrow,y}s_{\downarrow,z})^{3/12}(m_\uparrow+m_\downarrow)a}{m_\downarrow((s_{\uparrow,x}s_{\uparrow,y}s_{\uparrow,z})^{1/6}+(s_{\downarrow,x}s_{\downarrow,y}s_{\downarrow,z})^{1/6})^{3/2}d}. \end{aligned}$$

For fermions, the lowest band Hubbard Hamiltonian can be used only when the filling fractions n_σ are smaller than one. Due to the Pauli exclusion principle if the filling fraction is larger than one, the component starts occupy also the second band. Furthermore the interaction between the components is too strong, the lowest band Hubbard model is of limited accuracy. More precisely, when the interaction energy is larger than the band gap between the bands, one has to take into account also the higher bands.

3.3 Mean-field approximation

The exact Hubbard Hamiltonian can be solved only when the lattice is very small. The states used for solving the exact Hubbard Hamiltonian are the Fock states and the number of the relevant Fock states scales as 4^M a function of the number of sites M. When the lattice is bigger than 12 lattice sites the exact diagonalization of the Hubbard Hamiltonian cannot be done at reasonable time. When the lattice is small ($M < 100$) we cannot say that the system is macroscopic. Thus if we deal with a macroscopic system, we have to approximate the Hubbard Hamiltonian. Here we approximate the interaction part by using mean-field method. An operator $\hat{O}$ can be written as $\hat{O} = \langle\hat{O}\rangle + \hat{O} - \langle\hat{O}\rangle$, where $\langle\hat{O}\rangle$ is the mean value (i.e, the quantum mechanical expectation value) of the operator and $\delta\hat{O} = \hat{O} - \langle\hat{O}\rangle$ is the fluctuation around the mean value. Now we can rewrite the four-operator product of the interaction part as

$$\begin{aligned}\hat{c}^\dagger_{\uparrow,i}\hat{c}^\dagger_{\downarrow,i}\hat{c}_{\downarrow,i}\hat{c}_{\uparrow,i} &= (\langle\hat{c}^\dagger_{\uparrow,i}\hat{c}^\dagger_{\downarrow,i}\rangle + \hat{c}^\dagger_{\uparrow,i}\hat{c}^\dagger_{\downarrow,i} - \langle\hat{c}^\dagger_{\uparrow,i}\hat{c}^\dagger_{\downarrow,i}\rangle)(\langle\hat{c}_{\downarrow,i}\hat{c}_{\uparrow,i}\rangle + \hat{c}_{\downarrow,i}\hat{c}_{\uparrow,i} - \langle\hat{c}_{\downarrow,i}\hat{c}_{\uparrow,i}\rangle)\\ &= \langle\hat{c}^\dagger_{\uparrow,i}\hat{c}^\dagger_{\downarrow,i}\rangle\langle\hat{c}_{\downarrow,i}\hat{c}_{\uparrow,i}\rangle + \langle\hat{c}^\dagger_{\uparrow,i}\hat{c}^\dagger_{\downarrow,i}\rangle(\hat{c}_{\downarrow,i}\hat{c}_{\uparrow,i} - \langle\hat{c}_{\downarrow,i}\hat{c}_{\uparrow,i}\rangle) + \langle\hat{c}_{\downarrow,i}\hat{c}_{\uparrow,i}\rangle(\hat{c}^\dagger_{\uparrow,i}\hat{c}^\dagger_{\downarrow,i} - \langle\hat{c}^\dagger_{\uparrow,i}\hat{c}^\dagger_{\downarrow,i}\rangle)\\ &+ (\hat{c}^\dagger_{\uparrow,i}\hat{c}^\dagger_{\downarrow,i} - \langle\hat{c}^\dagger_{\uparrow,i}\hat{c}^\dagger_{\downarrow,i}\rangle)(\hat{c}_{\downarrow,i}\hat{c}_{\uparrow,i} - \langle\hat{c}_{\downarrow,i}\hat{c}_{\uparrow,i}\rangle).\end{aligned}$$

Now if it is assumed that the fluctuations are small the last term

$$\delta\hat{c}^\dagger_{\uparrow,i}\hat{c}^\dagger_{\downarrow,i}\delta\hat{c}_{\downarrow,i}\hat{c}_{\uparrow,i} = (\hat{c}^\dagger_{\uparrow,i}\hat{c}^\dagger_{\downarrow,i} - \langle\hat{c}^\dagger_{\uparrow,i}\hat{c}^\dagger_{\downarrow,i}\rangle)(\hat{c}_{\downarrow,i}\hat{c}_{\uparrow,i} - \langle\hat{c}_{\downarrow,i}\hat{c}_{\uparrow,i}\rangle),$$

can be neglected. Thus the four-operator product can be approximated as

$$\hat{c}^\dagger_{\uparrow,i}\hat{c}^\dagger_{\downarrow,i}\hat{c}_{\downarrow,i}\hat{c}_{\uparrow,i} \approx \hat{c}^\dagger_{\uparrow,i}\hat{c}^\dagger_{\downarrow,i}\langle\hat{c}_{\downarrow,i}\hat{c}_{\uparrow,i}\rangle + \hat{c}_{\downarrow,i}\hat{c}_{\uparrow,i}\langle\hat{c}^\dagger_{\uparrow,i}\hat{c}^\dagger_{\downarrow,i}\rangle - \langle\hat{c}^\dagger_{\uparrow,i}\hat{c}^\dagger_{\downarrow,i}\rangle\langle\hat{c}_{\downarrow,i}\hat{c}_{\uparrow,i}\rangle.$$

This is the key approximation of the usual BCS theory of superconductivity. It is clear that this approximation is poor if the fluctuations are large or if they dominate the system. In one-dimensional systems, the fluctuations are usually dominant. Thus mean-field approximation does not work well. Also if the interactions between the components are strong i.e. near the Feshbach resonance thermal fluctuations are important. Quantum Monte-Carlo calculations have shown that the BCS theory overestimates the critical temperature [43]. Furthermore if the filling fraction is quite large in the lattice the fluctuations are important.

Let us introduce the pairing field $\Delta(i) = U\langle\hat{c}_{\downarrow,i}\hat{c}_{\uparrow,i}\rangle$ as the order parameter of the system. Because the lattice the translational symmetry, it is reasonable to assume that the simplest pairing field, which breaks down this symmetry has a periodic phase. For now on the pairing field is assumed to be of the one mode FFLO (Fulde, Ferrel, Larkin, Ovchinnikov) type [44, 45]. With the one mode FFLO ansatz the pairing field is given by

$$\Delta(i) = \Delta e^{2i\mathbf{q}\cdot\mathbf{R}_i},$$

where $\Delta \geq 0$ is the absolute value of the pairing gap, $\mathbf{q}$ is a quasi-momentum vector and $\mathbf{R}_i$ is a lattice vector. The position dependence of the pairing field could be multimode, but these types of pairing fields can only make the FFLO areas larger in the phase diagram. Therefore, the above ansatz gives the "worst case" behaviour for the appearance of states breaking the translational invariance.

When the mean-field approximation and the pairing gap ansatz are put in the Hubbard Hamiltonian, the Hamiltonian becomes

$$\begin{aligned}\hat{H} - \mu_\uparrow \hat{N}_\uparrow - \mu_\downarrow \hat{N}_\downarrow = &- \sum_l (\mu_\uparrow \hat{c}^\dagger_{\uparrow,l} \hat{c}_{\uparrow,l} + \mu_\downarrow \hat{c}^\dagger_{\downarrow,l} \hat{c}_{\downarrow,l}) \\ &+ \sum_l \left(\Delta e^{2i\mathbf{q}\cdot\mathbf{R}_l} \hat{c}^\dagger_{\uparrow,l} \hat{c}^\dagger_{\downarrow,l} + \Delta e^{-2i\mathbf{q}\cdot\mathbf{R}_l} \hat{c}_{\downarrow,l} \hat{c}_{\uparrow,l} - \frac{\Delta^2}{U} \right) \\ &- \sum_{\sigma=\uparrow,\downarrow} \left(J_{\sigma,x} \sum_{\langle l,j\rangle_x} + J_{\sigma,y} \sum_{\langle l,j\rangle_y} + J_{\sigma,z} \sum_{\langle l,j\rangle_z} \right) \hat{c}^\dagger_{\sigma,l} \hat{c}_{\sigma,j}.\end{aligned} \tag{3.5}$$

This Hamiltonian is easier to handle in the (quasi-)momentum space. To represent the Hamiltonian in the momentum space one has to take the Fourier transform of the operators

$$\begin{aligned}\hat{c}_{\sigma,l} &= \frac{1}{\sqrt{M}} \sum_{\mathbf{k}} e^{i\mathbf{k}\cdot\mathbf{R}_l} \hat{c}_{\sigma,\mathbf{k}} \\ \hat{c}^\dagger_{\sigma,l} &= \frac{1}{\sqrt{M}} \sum_{\mathbf{k}} e^{-i\mathbf{k}\cdot\mathbf{R}_l} \hat{c}^\dagger_{\sigma,\mathbf{k}},\end{aligned}$$

where the sum goes over all the (quasi-)momenta of the reciprocal lattice. Let us calculate the Fourier transform of the Hamiltonian. in parts, starting from the Fourier transform the density part

$$\begin{aligned}\sum_{\sigma,l} \mu_\sigma \hat{c}^\dagger_{\sigma,l} \hat{c}_{\sigma,l} &= \frac{1}{M} \sum_{\sigma,l} \mu_\sigma \sum_{\mathbf{k},\mathbf{k}'} e^{i(\mathbf{k}-\mathbf{k}')\cdot\mathbf{R}_l} \hat{c}^\dagger_{\sigma,\mathbf{k}'} \hat{c}_{\sigma,\mathbf{k}} \\ &= \frac{1}{M} \sum_{\sigma,\mathbf{k},\mathbf{k}'} \hat{c}^\dagger_{\sigma,\mathbf{k}'} \hat{c}_{\sigma,\mathbf{k}} \sum_l \mu_\sigma e^{i(\mathbf{k}-\mathbf{k}')\cdot\mathbf{R}_l} \\ &= \frac{1}{M} \sum_{\sigma,\mathbf{k},\mathbf{k}'} \hat{c}^\dagger_{\sigma,\mathbf{k}'} \hat{c}_{\sigma,\mathbf{k}} \mu_\sigma M \delta_{\mathbf{k},\mathbf{k}'} \\ &= \sum_{\sigma,\mathbf{k}} \mu_\sigma \hat{c}^\dagger_{\sigma,\mathbf{k}} \hat{c}_{\sigma,\mathbf{k}}.\end{aligned}$$

The Fourier transform of the interaction part is not more complicated and is

given by

$$\begin{aligned}
&\sum_l \left(\Delta e^{2i\mathbf{q}\cdot\mathbf{R}_l} \hat{c}^\dagger_{\uparrow,l} \hat{c}^\dagger_{\downarrow,l} + \Delta e^{-2i\mathbf{q}\cdot\mathbf{R}_l} \hat{c}_{\downarrow,l} \hat{c}_{\uparrow,l} - \frac{\Delta^2}{U} \right) \\
&= \sum_l \left[\frac{1}{M} \sum_{\mathbf{k},\mathbf{k}'} \left(\Delta e^{i(2\mathbf{q}-\mathbf{k}-\mathbf{k}')\cdot\mathbf{R}_l} \hat{c}^\dagger_{\uparrow,\mathbf{k}} \hat{c}^\dagger_{\downarrow,\mathbf{k}'} + \Delta e^{i(\mathbf{k}+\mathbf{k}'-2\mathbf{q})\cdot\mathbf{R}_l} \hat{c}_{\downarrow,\mathbf{k}'} \hat{c}_{\uparrow,\mathbf{k}} \right) - \frac{\Delta^2}{U} \right] \\
&= \frac{1}{M} \sum_{\mathbf{k},\mathbf{k}'} \left(\Delta M \delta_{2\mathbf{q},\mathbf{k}+\mathbf{k}'} \hat{c}^\dagger_{\uparrow,\mathbf{k}} \hat{c}^\dagger_{\downarrow,\mathbf{k}'} + \Delta M \delta_{2\mathbf{q},\mathbf{k}+\mathbf{k}'} \hat{c}_{\downarrow,\mathbf{k}'} \hat{c}_{\uparrow,\mathbf{k}} \right) - \frac{M\Delta^2}{U} \\
&= \sum_{\mathbf{k}} \left(\Delta \hat{c}^\dagger_{\uparrow,\mathbf{k}+\mathbf{q}} \hat{c}^\dagger_{\downarrow,-\mathbf{k}+\mathbf{q}} + \Delta \hat{c}_{\downarrow,-\mathbf{k}+\mathbf{q}} \hat{c}_{\uparrow,\mathbf{k}+\mathbf{q}} - \frac{\Delta^2}{U} \right).
\end{aligned}$$

Finally the Fourier transform of the kinetic part is given by

$$\begin{aligned}
&-\sum_{\sigma,\alpha} \sum_{\langle l,j \rangle_\alpha} J_{\sigma,\alpha} \hat{c}^\dagger_{\sigma,l} \hat{c}_{\sigma,j} = -\sum_{\sigma,\alpha} \sum_l J_{\sigma,\alpha} (\hat{c}^\dagger_{\sigma,l} \hat{c}_{\sigma,l+d\hat{x}_\alpha} + \hat{c}^\dagger_{\sigma,l} \hat{c}_{\sigma,l-d\hat{x}_\alpha}) \\
&= \frac{-1}{M} \sum_{\sigma,\alpha} J_{\sigma,\alpha} \sum_{\mathbf{k},\mathbf{k}'} \sum_l \left(e^{-i(\mathbf{k}-\mathbf{k}')\cdot\mathbf{R}_l + ik'_\alpha d} \hat{c}^\dagger_{\sigma,\mathbf{k}} \hat{c}_{\sigma,\mathbf{k}'} + e^{-i(\mathbf{k}-\mathbf{k}')\cdot\mathbf{R}_l - ik'_\alpha d} \hat{c}^\dagger_{\sigma,\mathbf{k}} \hat{c}_{\sigma,\mathbf{k}'} \right) \\
&= \frac{-1}{M} \sum_{\sigma,\alpha} J_{\sigma,\alpha} \sum_{\mathbf{k},\mathbf{k}'} \left(M \delta_{\mathbf{k},\mathbf{k}'} e^{ik'_\alpha d} \hat{c}^\dagger_{\sigma,\mathbf{k}} \hat{c}_{\sigma,\mathbf{k}'} + M \delta_{\mathbf{k},\mathbf{k}'} e^{-ik'_\alpha d} \hat{c}^\dagger_{\sigma,\mathbf{k}} \hat{c}_{\sigma,\mathbf{k}'} \right) \\
&= -\sum_{\sigma,\alpha} J_{\sigma,\alpha} \sum_{\mathbf{k}} \left(e^{ik_\alpha d} + e^{-ik_\alpha d} \right) \hat{c}^\dagger_{\sigma,\mathbf{k}} \hat{c}_{\sigma,\mathbf{k}} \\
&= \sum_{\sigma,\alpha} \sum_{\mathbf{k}} (-2J_{\sigma,\alpha} \cos(k_\alpha d) \hat{c}^\dagger_{\sigma,\mathbf{k}} \hat{c}_{\sigma,\mathbf{k}}).
\end{aligned}$$

By combining all these terms, we find the mean-field Hubbard Hamiltonian in the momentum space

$$\begin{aligned}
\hat{H} - \mu_\uparrow \hat{N}_\uparrow - \mu_\downarrow \hat{N}_\downarrow &= \sum_{\mathbf{k}} \epsilon_{\uparrow,\mathbf{k}} \hat{c}^\dagger_{\uparrow,\mathbf{k}} \hat{c}_{\uparrow,\mathbf{k}} + \epsilon_{\downarrow,\mathbf{k}} \hat{c}^\dagger_{\downarrow,\mathbf{k}} \hat{c}_{\downarrow,\mathbf{k}} \\
&+ \sum_{\mathbf{k}} \left(\Delta \hat{c}^\dagger_{\uparrow,\mathbf{k}+\mathbf{q}} \hat{c}^\dagger_{\downarrow,-\mathbf{k}+\mathbf{q}} + \Delta \hat{c}_{\downarrow,-\mathbf{k}+\mathbf{q}} \hat{c}_{\uparrow,\mathbf{k}+\mathbf{q}} - \frac{\Delta^2}{U} \right),
\end{aligned} \tag{3.6}$$

where $\epsilon_{\sigma,\mathbf{k}} = \sum_{\alpha=x,y,z} 2J_{\sigma,\alpha}(1 - \cos(k_\alpha d)) - \mu_\sigma$ are the single particle dispersions. To get these single particle dispersions we have added a constant term $\sum_{\sigma,\alpha} 2J_{\sigma,\alpha} \hat{N}_\sigma$, where the number operators are $\hat{N}_\sigma = \sum_{\mathbf{k}} \hat{c}^\dagger_{\sigma,\mathbf{k}} \hat{c}_{\sigma,\mathbf{k}}$. Of course this term does not change the physics of the system, because the term commutates with the Hamiltonian.

The mean-field Hamiltonian can be rewritten in an equivalent matrix form as

$$\begin{aligned}\hat{H} - \mu_\uparrow \hat{N}_\uparrow - \mu_\downarrow \hat{N}_\downarrow &= \sum_{\mathbf{k}} \epsilon_{\uparrow,\mathbf{k}+\mathbf{q}} \hat{c}^\dagger_{\uparrow,\mathbf{k}+\mathbf{q}} \hat{c}_{\uparrow,\mathbf{k}+\mathbf{q}} + \epsilon_{\downarrow,-\mathbf{k}+\mathbf{q}} (1 - \hat{c}_{\downarrow,-\mathbf{k}+\mathbf{q}} \hat{c}^\dagger_{\downarrow,-\mathbf{k}+\mathbf{q}}) \\ &+ \sum_{\mathbf{k}} \left(\Delta \hat{c}^\dagger_{\uparrow,\mathbf{k}+\mathbf{q}} \hat{c}^\dagger_{\downarrow,-\mathbf{k}+\mathbf{q}} + \Delta \hat{c}_{\downarrow,-\mathbf{k}+\mathbf{q}} \hat{c}_{\uparrow,\mathbf{k}+\mathbf{q}} - \frac{\Delta^2}{U} \right) \\ &= \sum_{\mathbf{k}} \begin{pmatrix} \hat{c}^\dagger_{\uparrow,\mathbf{k}+\mathbf{q}} & \hat{c}_{\downarrow,-\mathbf{k}+\mathbf{q}} \end{pmatrix} \begin{pmatrix} \epsilon_{\uparrow,\mathbf{k}+\mathbf{q}} & \Delta \\ \Delta & -\epsilon_{\downarrow,-\mathbf{k}+\mathbf{q}} \end{pmatrix} \begin{pmatrix} \hat{c}_{\uparrow,\mathbf{k}+\mathbf{q}} \\ \hat{c}^\dagger_{\downarrow,-\mathbf{k}+\mathbf{q}} \end{pmatrix} \\ &+ \sum_{\mathbf{k}} \left(\epsilon_{\downarrow,-\mathbf{k}+\mathbf{q}} - \frac{\Delta^2}{U} \right). \end{aligned} \tag{3.7}$$

We can diagonalize this Hamiltonian by using unitary matrices, as,

$$\sum_{\mathbf{k}} \begin{pmatrix} \hat{c}^\dagger_{\uparrow,\mathbf{k}+\mathbf{q}} & \hat{c}_{\downarrow,-\mathbf{k}+\mathbf{q}} \end{pmatrix} U^\dagger_{\mathbf{k},\mathbf{q}} U_{\mathbf{k},\mathbf{q}} \begin{pmatrix} \epsilon_{\uparrow,\mathbf{k}+\mathbf{q}} & \Delta \\ \Delta & -\epsilon_{\downarrow,-\mathbf{k}+\mathbf{q}} \end{pmatrix} U^\dagger_{\mathbf{k},\mathbf{q}} U_{\mathbf{k},\mathbf{q}} \begin{pmatrix} \hat{c}_{\uparrow,\mathbf{k}+\mathbf{q}} \\ \hat{c}^\dagger_{\downarrow,-\mathbf{k}+\mathbf{q}} \end{pmatrix}$$

where $U^\dagger_{\mathbf{k},\mathbf{q}} U_{\mathbf{k},\mathbf{q}} = 1$. Now the unitary matrices have to be chosen in a way that they diagonalize the 2×2-matrix in the Hamiltonian i.e. the following equation holds

$$U_{\mathbf{k},\mathbf{q}} \begin{pmatrix} \epsilon_{\uparrow,\mathbf{k}+\mathbf{q}} & \Delta \\ \Delta & -\epsilon_{\downarrow,-\mathbf{k}+\mathbf{q}} \end{pmatrix} U^\dagger_{\mathbf{k},\mathbf{q}} = \begin{pmatrix} E_{+,\mathbf{k},\mathbf{q}} & 0 \\ 0 & -E_{-,\mathbf{k},\mathbf{q}} \end{pmatrix},$$

where the minus sign is only a convention. The eigenvalues can be solved from the determinant equations and it turns out that

$$E_{\pm,\mathbf{k},\mathbf{q}} = E_{\mathbf{k},\mathbf{q}} \pm \frac{\epsilon_{\uparrow,\mathbf{k}+\mathbf{q}} - \epsilon_{\downarrow,-\mathbf{k}+\mathbf{q}}}{2} = \sqrt{\left(\frac{\epsilon_{\uparrow,\mathbf{k}+\mathbf{q}} + \epsilon_{\downarrow,-\mathbf{k}+\mathbf{q}}}{2} \right)^2 + \Delta^2} \pm \frac{\epsilon_{\uparrow,\mathbf{k}+\mathbf{q}} - \epsilon_{\downarrow,-\mathbf{k}+\mathbf{q}}}{2}.$$

Furthermore it turns out that the unitary matrices can be chosen as

$$U_{\mathbf{k},\mathbf{q}} = \begin{pmatrix} u_{\mathbf{k},\mathbf{q}} & -v_{\mathbf{k},\mathbf{q}} \\ v_{\mathbf{k},\mathbf{q}} & u_{\mathbf{k},\mathbf{q}} \end{pmatrix},$$

where

$$\begin{aligned} u^2_{\mathbf{k},\mathbf{q}} &= \frac{1}{2} \left(1 + \frac{\epsilon_{\uparrow,\mathbf{k}+\mathbf{q}} + \epsilon_{\downarrow,-\mathbf{k}+\mathbf{q}}}{2E_{\mathbf{k},\mathbf{q}}} \right) \\ v^2_{\mathbf{k},\mathbf{q}} &= \frac{1}{2} \left(1 - \frac{\epsilon_{\uparrow,\mathbf{k}+\mathbf{q}} + \epsilon_{\downarrow,-\mathbf{k}+\mathbf{q}}}{2E_{\mathbf{k},\mathbf{q}}} \right). \end{aligned}$$

We can determine quasiparticle operators by using this unitary transformation

$$\begin{aligned} \hat{\gamma}_{+,\mathbf{k},\mathbf{q}} &= u_{\mathbf{k},\mathbf{q}} \hat{c}_{\uparrow,\mathbf{k}+\mathbf{q}} + v_{\mathbf{k},\mathbf{q}} \hat{c}^\dagger_{\downarrow,-\mathbf{k}+\mathbf{q}}, \\ \hat{\gamma}_{-,\mathbf{k},\mathbf{q}} &= u_{\mathbf{k},\mathbf{q}} \hat{c}_{\downarrow,-\mathbf{k}+\mathbf{q}} - v_{\mathbf{k},\mathbf{q}} \hat{c}^\dagger_{\uparrow,\mathbf{k}+\mathbf{q}}. \end{aligned}$$

This transformation, which is called the Bogoliubov transformation, is a canonical transformation. In other words it preserves the anticommutation relations

$$\{\hat{\gamma}^{\dagger}_{\alpha,\mathbf{k},\mathbf{q}}, \hat{\gamma}_{\beta,\mathbf{k}',\mathbf{q}}\} = \hat{\gamma}^{\dagger}_{\alpha,\mathbf{k},\mathbf{q}}\hat{\gamma}_{\beta,\mathbf{k}',\mathbf{q}} + \hat{\gamma}_{\beta,\mathbf{k}',\mathbf{q}}\hat{\gamma}^{\dagger}_{\alpha,\mathbf{k},\mathbf{q}} = \delta_{\alpha\beta}\delta_{\mathbf{k},\mathbf{k}'}$$
$$\{\hat{\gamma}_{\alpha,\mathbf{k},\mathbf{q}}, \hat{\gamma}_{\beta,\mathbf{k}',\mathbf{q}}\} = \{\hat{\gamma}^{\dagger}_{\alpha,\mathbf{k},\mathbf{q}}, \hat{\gamma}^{\dagger}_{\beta,\mathbf{k}',\mathbf{q}}\} = 0.$$

The quasiparticles are linear combinations of particles and holes.

The diagonalized Hamiltonian is given by

$$\hat{H}_{mf} = \sum_{\mathbf{k}} E_{+,\mathbf{k},\mathbf{q}}\hat{\gamma}^{\dagger}_{+,\mathbf{k},\mathbf{q}}\hat{\gamma}_{+,\mathbf{k},\mathbf{q}} + E_{-,\mathbf{k},\mathbf{q}}\hat{\gamma}^{\dagger}_{-,\mathbf{k},\mathbf{q}}\hat{\gamma}_{-,\mathbf{k},\mathbf{q}} - E_{-,\mathbf{k},\mathbf{q}} + \epsilon_{\downarrow,-\mathbf{k}+\mathbf{q}} - \frac{\Delta^2}{U}. \tag{3.8}$$

The diagonalized Hamiltonian is the Hamiltonian of a two-components free gas, where the components are two different types of quasiparticles, and furthermore the eigenenergies are the quasiparticle dispersions. Thus we can write down the eigenstates of the diagonalized mean-field Hamiltonian as

$$|i\rangle = \prod_{\mathbf{k}\in G_2} \hat{\gamma}^{\dagger}_{-,\mathbf{k},\mathbf{q}} \prod_{\mathbf{k}\in G_1} \hat{\gamma}^{\dagger}_{+,\mathbf{k},\mathbf{q}}|0\rangle,$$

where G_1 and G_2 are domains in the momentum space and $|0\rangle$ denotes the vacuum state. The eigenstates of mean-field Hamiltonian are the Fock states for the quasiparticles. However, the ground state is

$$|GS\rangle = \prod_{\mathbf{k}\in G_2} \hat{\gamma}^{\dagger}_{-,\mathbf{k},\mathbf{q}} \prod_{\mathbf{k}\in G_1} \hat{\gamma}^{\dagger}_{+,\mathbf{k},\mathbf{q}}|0\rangle,$$

where in domain G_1 $E_{+,\mathbf{k},\mathbf{q}} < 0$ and in domain G_2 $E_{-,\mathbf{k},\mathbf{q}} < 0$.

The one mode FFLO ansatz which is used above includes four different phases. Firstly the standard BCS phase, where the quasimomentum $\mathbf{q}$ and the polarization

$$P = \frac{N_\uparrow - N_\downarrow}{N_\uparrow + N_\downarrow} = \frac{n_\uparrow - n_\downarrow}{n_\uparrow + n_\downarrow}$$

vanish and the pairing gap is finite. Physically this means that the Fermi surfaces of the components totally overlap, and the total momentum of a pair is zero. Furthermore the pairing gap is uniform. Secondly the Sarma/BP (Breach Pairing) phase [46, 47], corresponds to $P \neq 0$, $\Delta > 0$, and $\mathbf{q} = 0$. This means that the Fermi surfaces do not fully overlap and a part of the atoms remains unpaired. Basically this Sarma/BP phase is the phase separation in the momentum space, a part of the momentum space includes non-polarized paired gas and another part polarized normal gas. In this phase, the pairing gap is also uniform. In the coordinate space of course the pairs occur everywhere. Thirdly, the one mode FFLO

phase corresponds to situation where $P \neq 0$, $\Delta > 0$, and $\mathbf{q}$ is non-zero. Also in this phase, the Fermi surfaces do not fully overlap, but they have been shifted by the momentum $\mathbf{q}$ and the pairs have total momentum $2\mathbf{q}$. The momentum $\mathbf{q}$ has to be chosen such that the free-energy is minimized, which turns out to be roughly equivalent with the condition that the overlapping between the Fermi surfaces is maximized. The normal phase means vanishing order parameter, i.e, $\Delta = 0$.

3.4 Self consistent equations and free-energy

3.4.1 Gap and number equations

Using the inverse Bogoliubov transformation, we can derive three equations: the gap equation, and the number equations for the both components. From these equations, one can solve the order parameter Δ and the chemical potentials μ_σ self consistently. The gap equation can be derived from the definition of the order parameter by substituting the quasiparticle operators into the definition. More precisely we get

$$
\begin{aligned}
\Delta &= U e^{-2i\mathbf{q}\cdot\mathbf{R}_i}\langle \hat{c}_{\downarrow,i}\hat{c}_{\uparrow,i}\rangle \\
&= \frac{U}{M}\sum_{\mathbf{k},\mathbf{k}'} e^{i(\mathbf{k}+\mathbf{k}'-2\mathbf{q})\cdot\mathbf{R}_i}\langle \hat{c}_{\downarrow,\mathbf{k}}\hat{c}_{\uparrow,\mathbf{k}'}\rangle \\
&= \frac{U}{M}\sum_{\mathbf{k},\mathbf{k}'} e^{i(\mathbf{k}+\mathbf{k}'-2\mathbf{q})\cdot\mathbf{R}_i}\langle (u_{-\mathbf{k}'+\mathbf{q},\mathbf{q}}\hat{\gamma}_{-,-\mathbf{k}'+\mathbf{q},\mathbf{q}} + v_{,-\mathbf{k}'+\mathbf{q},\mathbf{q}}\hat{\gamma}^\dagger_{+,-\mathbf{k}'+\mathbf{q},\mathbf{q}})\times \\
&(u_{\mathbf{k}-\mathbf{q},\mathbf{q}}\hat{\gamma}_{+,\mathbf{k}-\mathbf{q},\mathbf{q}} - v_{\mathbf{k}-\mathbf{q},\mathbf{q}}\hat{\gamma}^\dagger_{-,\mathbf{k}-\mathbf{q},\mathbf{q}})\rangle \\
&= \frac{U}{M}\sum_{\mathbf{k},\mathbf{k}'} e^{i(\mathbf{k}+\mathbf{k}'-2\mathbf{q})\cdot\mathbf{R}_i}\Big(u_{-\mathbf{k}'+\mathbf{q},\mathbf{q}}u_{\mathbf{k}-\mathbf{q},\mathbf{q}}\langle \hat{\gamma}_{-,-\mathbf{k}'+\mathbf{q},\mathbf{q}}\gamma_{+,\mathbf{k}-\mathbf{q},\mathbf{q}}\rangle \\
&- u_{-\mathbf{k}'+\mathbf{q},\mathbf{q}}v_{\mathbf{k}-\mathbf{q},\mathbf{q}}\langle \hat{\gamma}_{-,-\mathbf{k}'+\mathbf{q},\mathbf{q}}\hat{\gamma}^\dagger_{-,\mathbf{k}-\mathbf{q},\mathbf{q}}\rangle + v_{-\mathbf{k}'+\mathbf{q},\mathbf{q}}u_{\mathbf{k}-\mathbf{q},\mathbf{q}}\langle \hat{\gamma}^\dagger_{+,-\mathbf{k}'+\mathbf{q},\mathbf{q}}\hat{\gamma}_{+,\mathbf{k}'-\mathbf{q},\mathbf{q}}\rangle \\
&- v_{-\mathbf{k}'+\mathbf{q},\mathbf{q}}v_{\mathbf{k}-\mathbf{q},\mathbf{q}}\langle \hat{\gamma}^\dagger_{+,-\mathbf{k}'+\mathbf{q},\mathbf{q}}\hat{\gamma}^\dagger_{-,\mathbf{k}-\mathbf{q},\mathbf{q}}\rangle\Big) \\
&= \frac{U}{M}\sum_{\mathbf{k}} u_{\mathbf{k},\mathbf{q}}v_{\mathbf{k},\mathbf{q}}[1 - f(E_{+,\mathbf{k},\mathbf{q}}) - f(E_{-,\mathbf{k},\mathbf{q}})] \\
&= \frac{-U}{M}\sum_{\mathbf{k}} \frac{\Delta[1 - f(E_{+,\mathbf{k},\mathbf{q}}) - f(E_{-,\mathbf{k},\mathbf{q}})]}{2E_{\mathbf{k},\mathbf{q}}},
\end{aligned}
\tag{3.9}
$$

where the Fermi-Dirac distribution is given by

$$f(E) = \frac{1}{e^{E/k_BT}+1}.$$

Here, k_B is the Boltzmann constant T is the temperature. Above, we have used results of the equilibrium statistical physics

$$\langle\hat{\gamma}^\dagger_{\alpha,\mathbf{k}',\mathbf{q}}\hat{\gamma}_{\beta,\mathbf{k}',\mathbf{q}}\rangle = \delta_{\alpha\beta}\delta_{\mathbf{k},\mathbf{k}'}f(E_{\alpha,\mathbf{k},\mathbf{q}})$$
$$\langle\hat{\gamma}^\dagger_{\alpha,\mathbf{k}',\mathbf{q}}\hat{\gamma}^\dagger_{\beta,\mathbf{k}',\mathbf{q}}\rangle = \langle\hat{\gamma}_{\alpha,\mathbf{k}',\mathbf{q}}\hat{\gamma}_{\beta,\mathbf{k}',\mathbf{q}}\rangle = 0.$$

When the gap equation (3.9) is divided by Δ, we get the standard BCS gap equation

$$1 = \frac{-U}{M}\sum_{\mathbf{k}}\frac{1 - f(E_{+,\mathbf{k},\mathbf{q}}) - f(E_{-,\mathbf{k},\mathbf{q}})}{2E_{\mathbf{k},\mathbf{q}}}. \tag{3.10}$$

In the same way, we get the number equations and they are given by

$$\begin{aligned} N_\uparrow &= \sum_{\mathbf{k}} u^2_{\mathbf{k},\mathbf{q}} f(E_{-,\mathbf{k},\mathbf{q}}) + v^2_{\mathbf{k},\mathbf{q}}(1 - f(E_{+,\mathbf{k},\mathbf{q}})), \\ N_\downarrow &= \sum_{\mathbf{k}} u^2_{\mathbf{k},\mathbf{q}} f(E_{+,\mathbf{k},\mathbf{q}}) + v^2_{\mathbf{k},\mathbf{q}}(1 - f(E_{-,\mathbf{k},\mathbf{q}})). \end{aligned} \tag{3.11}$$

Because the Fermi-Dirac distribution becomes the Heaviside step function in the zero-temperature limit, i.e.

$$\lim_{T\to 0} f(E) = \Theta(-E) = \begin{cases} 0, & E > 0 \\ 0.5, & E = 0 \\ 1, & E < 0, \end{cases}$$

if the system is polarized at least one of the quasiparticle dispersion has to change its sign at zero temperature.

If $\mathbf{q}$ is assumed to be zero, there are only three unknown variables to solve: the chemical potentials and the absolute value of the gap. In this case we can solve the gap equations and the number equations iteratively.

There are some limits where the solution is even simple. When the interaction between components is weak the chemical potentials can be approximated with the Fermi energies (as is done with metallic superconductors). If the gas is balanced, i.e, the number of particles are equal (and the masses or hopping strengths are same), the chemical potentials can be chosen to be same $\mu_\uparrow = \mu_\downarrow$. Thus there is only one number equation left in this case.

If $\mathbf{q}$ is not assumed to vanish one has three extra unknown variables to solve: q_x, q_y, q_z. Thus it can be more convenient to calculate the Helmholtz free energy and minimize that, rather than solve the gap- and the number equations separately.

3.4.2 Free energy

To calculate the Helmholtz free energy $F = \Omega + \mu_\uparrow N_\uparrow + \mu_\downarrow N_\downarrow$, we must first calculate the grand canonical potential

$$\Omega = -k_B T \log(\mathcal{Z}) = -k_B T \log\left(\mathrm{Tr}\left[e^{-\beta \hat{H}_{mf}}\right]\right),$$

where $\beta = 1/k_B T$. The grand canonical partition function $\mathcal{Z}$ it is easy to calculate for the free Fermi gas, as shown below.

$$\begin{aligned}\mathcal{Z} &= \mathrm{Tr}\left[e^{-\beta \hat{H}_{mf}}\right] = \sum_i \langle i| e^{-\beta \hat{H}_{mf}} |i\rangle \\ &= \sum_i \langle i| \prod_{\mathbf{k}} e^{-\beta E_{+,\mathbf{k},\mathbf{q}} \hat{\gamma}^\dagger_{+,\mathbf{k},\mathbf{q}} \hat{\gamma}_{+,\mathbf{k},\mathbf{q}}} e^{-\beta E_{-,\mathbf{k},\mathbf{q}} \hat{\gamma}^\dagger_{-,\mathbf{k},\mathbf{q}} \hat{\gamma}_{-,\mathbf{k},\mathbf{q}}} e^{-\beta c_{\mathbf{k}}} |i\rangle,\end{aligned}$$

where $|i>$ is an eigenstate of the mean-field Hamiltonian, and

$$c_{\mathbf{k}} = -E_{-,\mathbf{k},\mathbf{q}} + \epsilon_{\downarrow,-\mathbf{k}+\mathbf{q}} - \frac{\Delta^2}{U}.$$

Since

$$e^{-\beta E_{\alpha,\mathbf{k},\mathbf{q}} \hat{\gamma}^\dagger_{\alpha,\mathbf{k},\mathbf{q}} \hat{\gamma}_{\alpha,\mathbf{k},\mathbf{q}}} |i\rangle = |i\rangle e^{-\beta E_{\alpha,\mathbf{k},\mathbf{q}} n_{\alpha,\mathbf{k},i}},$$

$n_{\alpha,\mathbf{k},i}$ is the occupation number of a quasiparticle type α in the momentum state $\mathbf{k}$ in $|i\rangle$,

$$\mathcal{Z} = e^{-\beta \sum_{\mathbf{k}} c_{\mathbf{k}}} \sum_i \prod_{\mathbf{k}} e^{-\beta E_{+,\mathbf{k},\mathbf{q}} n_{+,\mathbf{k},i}} e^{-\beta E_{-,\mathbf{k},\mathbf{q}} n_{-,\mathbf{k},i}}.$$

Since the sum over the eigenstates runs over all possible combinations once and the occupation number $n_{\alpha,\mathbf{k},i}$ is either 0 or 1, the grand canonical partition function becomes

$$\mathcal{Z} = e^{-\beta \sum_{\mathbf{k}} c_{\mathbf{k}}} \prod_{\mathbf{k}} \left(1 + e^{-\beta E_{+,\mathbf{k},\mathbf{q}}}\right)\left(1 + e^{-\beta E_{-,\mathbf{k},\mathbf{q}}}\right).$$

Thus the grand canonical potential is given by

$$\begin{aligned}\Omega_{FFLO} = \sum_{\mathbf{k}} \Bigg[&- k_B T \log\left(1 + e^{-\beta E_{+,\mathbf{k},\mathbf{q}}}\right) - k_B T \log\left(1 + e^{-\beta E_{-,\mathbf{k},\mathbf{q}}}\right) \\ &- E_{-,\mathbf{k},\mathbf{q}} + \epsilon_{\downarrow,-\mathbf{k}+\mathbf{q}} - \frac{\Delta^2}{U}\Bigg],\end{aligned} \tag{3.12}$$

and furthermore

$$\begin{aligned}F_{FFLO} = \sum_{\mathbf{k}} \Bigg[&- k_B T \log\left(1 + e^{-\beta E_{+,\mathbf{k},\mathbf{q}}}\right) - k_B T \log\left(1 + e^{-\beta E_{-,\mathbf{k},\mathbf{q}}}\right) \\ &- E_{-,\mathbf{k},\mathbf{q}} + \epsilon_{\downarrow,-\mathbf{k}+\mathbf{q}} - \frac{\Delta^2}{U}\Bigg] + \mu_\uparrow N_\uparrow + \mu_\downarrow N_\downarrow.\end{aligned} \tag{3.13}$$

In the thermal equilibrium the right value, of the order parameter minimizes the free energy. It depends on the system whether it is useful to use the grand canonical potential or the Helmholtz free energy. If the lattice is in a trap, the number of particles can change as a function of the distance from the center of the trap, and in this case it is better to use the grand canonical potential. But if the external potential is uniform, it is better to use the Helmholtz free energy.

If the grand potential is used, there is a so-called Clogston limit [48], which tells how big the chemical potential difference $|\delta\mu| = |\mu_\uparrow - \mu_\downarrow|$ (in the case where the masses or the hopping strengths are equal) has to be for it to be possible to find other solutions than the standard BCS solution at zero temperature. Clogston showed [48] that in the free space, the limit is $|\delta\mu| = \sqrt{2}\Delta_0$, where Δ_0 is the gap when $|\delta\mu| = 0$. In a lattice the value of the Clogston limit is the same [49]. However, this work did not consider phase separation, which could be relevant in some systems.

Even in the case where $\mathbf{q} = 0$ one can find a non-zero gap solution for the gap equation above the Clogston limit, but this solution, which is called the Sarma/BP phase, is unstable at zero temperature. It turns out that this Sarma/BP solution is a local maximum of the grand potential at zero temperature [50], thus it is not energetically favorable. However, due to thermal fluctuations it becomes energetically favorable at non-zero temperatures.

If the external trapping potential is flat or uniform, it is useful to fix the numbers of the particles and use Helmholtz free-energy. In the case of the one mode FFLO ansatz, one can find non-BCS type solution for arbitrary polarizations. But at low temperatures and low polarizations this FFLO type pairing is not the minimum energy state, since one should take into account also the possibility of the phase separation between the normal gas and the BCS pairing. This means that in a part of the lattice there is a polarized normal gas and parts are occupied by a non-polarized superfluid gas, at low temperatures and low polarizations this phase separation is the minimum energy solution. When the phase separation is taken account, we have to compare two different free energy densities $\tilde{F}_{FFLO} = F_{FFLO}/M$ and

$$\tilde{F}_{PS} = \frac{x}{M} F_{BCS} + \frac{(1-x)}{M} F_{normal},$$

where F_{BCS} is same as F_{FFLO} in the case where $\mathbf{q} = 0$, $\mu_\uparrow = \mu_\downarrow$, and $N_\uparrow = N_\downarrow = N_{BCS}$, and F_{normal} is F_{FFLO} in the case where $\Delta = 0$, and $N_{normal,\uparrow} = N_\uparrow - N_{BCS}, N_{normal,\downarrow} = N_\downarrow - N_{BCS}$. The x above represents the fraction of the lattice sites, which is occupied by the BCS phase. In this phase separation free energy formula we have two new free minimization parameters N_{BCS} and x.

The one mode FFLO phase occupies a large part of a polarization-temperature phase diagram as shown in figure 3.1. This is a main difference between the free space - and the lattice phase diagrams. In free space the FFLO area is almost

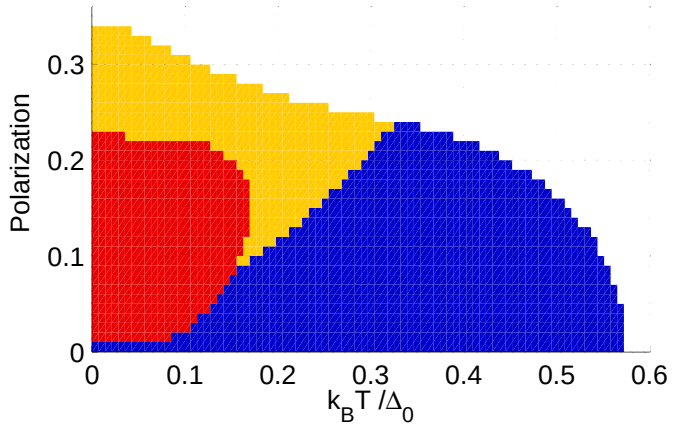

Figure 3.1: Polarization-temperature phase diagram for a two-components Fermi gas in a three-dimensional cubic lattice. The average filling fraction $n_{av} = (n_\uparrow + n_\downarrow)/2 = 0.2$. The other parameters which were used are $U = -0.26E_r$, $J = 0.07E_R$, and wavelength of the laser $\lambda = 1030\,\mathrm{nm}$. The components are two different hyperfine states of Lithium-6. Here Δ_0 means the gap at $T = 0$ and $P = 0$. The color coding is such as: FFLO=yellow, Sarma/BP/BCS=blue (BCS only when $P = 0$), Phase separation=red, and Normal=white.

negligible. This difference between the free space and the lattice phase diagrams is due the shape difference between the Fermi surfaces. In a cubic lattice the Fermi surfaces are like dodecahedrons, but in the free space they are spheres. If the Fermi surfaces are dodecahedrons, the overlapping of the surfaces can be made much greater by shifting the surfaces than if they are spheres. This phenomenon is called nesting.

Figure 3.1 shows that there are several phase transitions in the phase diagram. The FFLO-Sarma/BP phase transition is a second order phase transition, where the order parameter is $\mathbf{q}$. The Sarma/PB phase is transnational symmetric, but the FFLO phase is not. Thus the FFLO phase breaks spontaneously the translational symmetry. All the phase transitions which include the phase separation, i.e., the BCS-phase separation transition, the phase separation-Sarma/PB transition and the phase separation-FFLO transition, are first order transitions [50, 51]. The phase transitions to the normal phase are second order transitions, where the order parameter is the absolute value of the pairing gap. The normal-superfluid phase transition breaks the local $U(1)$-symmetry of the Hamiltonian.

3.5 Interband model in optical lattices

If the interaction strengths are strong or the filling fractions are larger than unity, the lowest band Hubbard model is not valid. One has to use a multiband model. Both experimental and theoretical multiband studies have been already done in optical latices [35, 52, 53].

Here we study the case where the components can have filling fraction larger than unity, but smaller than four (the maximum filling fraction of the p-band is three) in order to explore novel paired phases. Since the gas is fermionic, the component, whose filling fraction is bigger than unity not only occupies the lowest band, but also the first excited band. This is due to the Pauli exclusion principle.

The exact Hamiltonian of this system is the same as before and is given by

$$\begin{aligned}\hat{H} = &\sum_{\sigma=\uparrow,\downarrow} \int d\mathbf{r}\, \hat{\Psi}^\dagger_\sigma(\mathbf{r}) \left(-\frac{\hbar^2\nabla^2}{2m_\sigma} + V_\sigma(\mathbf{r}) \right) \hat{\Psi}_\sigma(\mathbf{r}) \\ &+ \frac{2\pi\hbar^2 a}{m_r} \int d\mathbf{r}\, \hat{\Psi}^\dagger_\uparrow(\mathbf{r}) \hat{\Psi}^\dagger_\downarrow(\mathbf{r}) \hat{\Psi}_\downarrow(\mathbf{r}) \hat{\Psi}_\uparrow(\mathbf{r}),\end{aligned} \tag{3.14}$$

Let us assume that component $\uparrow$ has filling fraction bigger than unity. The field operators can be expanded by using the Wannier functions, and are given by

$$\hat{\Psi}_\sigma(\mathbf{r}) = \sum_i w_{\sigma,0,i}(\mathbf{r})\hat{c}_{\sigma,0,i} + w_{\sigma,x,i}(\mathbf{r})\hat{c}_{\sigma,x,i} + w_{\sigma,y,i}(\mathbf{r})\hat{c}_{\sigma,y,i} + w_{\sigma,z,i}(\mathbf{r})\hat{c}_{\sigma,z,i},$$

where $w_{\sigma,\alpha,i}(\mathbf{r})$ ($\sigma = \uparrow,\downarrow$ and $\alpha = 0, x, y, z$) are the Wannier functions and $\hat{c}_{\alpha,\sigma,i}$ are the annihilation operators. There are three different types of fermions (x,y,z) in the excited band, and they have their own Wannier functions and creation and annihilation operators. This is due the fact that the excited band is the p-band and it has three different states.

If the lattice is deep, we can derive the corresponding Hubbard Hamiltonian, as we did in the lowest band case. The Hubbard Hamiltonian is given by

$$\begin{aligned}\hat{H} = &-\sum_{\alpha,\sigma} \left(\left[J_{\sigma,\alpha,x} \sum_{\langle i,j\rangle_x} + J_{\sigma,\alpha,y} \sum_{\langle i,j\rangle_y} + J_{\sigma,\alpha,z} \sum_{\langle i,j\rangle_z} \right] \hat{c}^\dagger_{\sigma,\alpha,i}\hat{c}_{\sigma,\alpha,j} \right) \\ &+ \sum_{\alpha,i} (E_{pg,\uparrow,\alpha} - \mu_\uparrow)\hat{c}^\dagger_{\uparrow,\alpha,i}\hat{c}_{\uparrow,\alpha,i} + (E_{pg,\downarrow,\alpha} - \mu_\downarrow)\hat{c}^\dagger_{\downarrow,\alpha,i}\hat{c}_{\downarrow,\alpha,i} \\ &+ \sum_{\alpha,\beta} U_{\alpha\beta}\hat{c}^\dagger_{\uparrow,\alpha,i}\hat{c}_{\uparrow,\alpha,i}\hat{c}^\dagger_{\downarrow,\beta,i}\hat{c}_{\downarrow,\beta,i}\end{aligned} \tag{3.15}$$

where $E_{pg,\sigma,\alpha}$ ($E_{pg,\sigma,0} = 0$) are the band gaps, $\langle i,j\rangle_\beta$ denotes sum over the nearest

neighbours in the β direction, and

$$J_{\sigma,\alpha,\beta} = \int d\mathbf{r}\, w^*_{\sigma,\alpha,i}(\mathbf{r}) \left(-\frac{\hbar^2\nabla^2}{2m_\sigma} + V_\sigma(\mathbf{r}) \right) w_{\sigma,\alpha,i+d\hat{x}_\beta}(\mathbf{r}),$$
$$U_{\alpha\beta} = \frac{2\pi\hbar^2 a}{m_r} \int d\mathbf{r}\, |w_{\uparrow,\alpha,i}(\mathbf{r})|^2 |w_{\downarrow,\beta,i}(\mathbf{r})|^2,$$

where d is the lattice constant and $\hat{x}_\beta$ is the unit vector in the β direction. When these integrals are calculated, one finds that $J_{\sigma,\alpha,\alpha}$ is negative, when $\alpha \neq 0$. Note that the Hamiltonian does not include the terms like $\hat{c}^\dagger_{\sigma,\alpha,i}\hat{c}_{\sigma,\beta,j}$, $(\alpha \neq \beta)$ this is due to the (anti-)symmetry of Wannier functions, i.e. when one calculates the corresponding hopping term, one finds that it is zero. This implies that the fermions cannot change their type through the hoping. The particles can change their type through the interactions, but in this work this types of interactions are not considered.

One can do the same mean-field approximation as we did in the lowest band model, and under this approximation the Hamiltonian becomes in the momentum space

$$\begin{aligned} \hat{H} = &\sum_{\sigma,\alpha,\mathbf{k}} \epsilon_{\sigma,\alpha,\mathbf{k}} \hat{c}^\dagger_{\sigma,\alpha,\mathbf{k}} \hat{c}_{\sigma,\alpha,\mathbf{k}} + \\ &\sum_{\alpha,\beta,\mathbf{k}} \Delta_{\alpha\beta} \hat{c}^\dagger_{\uparrow,\alpha,\mathbf{k}} \hat{c}^\dagger_{\downarrow,\beta,-\mathbf{k}} + \Delta^*_{\alpha\beta} \hat{c}_{\downarrow,\beta,-\mathbf{k}} \hat{c}_{\uparrow,\alpha,\mathbf{k}} - \sum_{\alpha,\beta} \frac{|\Delta_{\alpha\beta}|^2}{U_{\alpha\beta}}, \end{aligned} \tag{3.16}$$

where the pairing fields are defined by $\Delta_{\alpha\beta} = U_{\alpha\beta}\langle c_{\downarrow,\beta,i} c_{\uparrow,\alpha,i}\rangle$ and the one particle dispersions are given by

$$\epsilon_{\sigma,\alpha,\mathbf{k}} = E_{pg,\sigma,\alpha} + \sum_{\beta=x,y,z} 2J_{\sigma,\alpha,\beta}(1 - \cos^2(k_\beta d)) - \mu_\sigma.$$

Here we have, for simplicity, assumed that the pairing fields are constants i.e. the pairings are the BCS type of pairings.

To simplify the situation we assume that only the $\uparrow$-component has filling fraction larger than unity. Since $\downarrow$-component lies on the lowest band, only pairing fields, which can be non-zero are $\Delta_{\alpha 0}$. In this special case the mean-field Hamiltonian becomes

$$\begin{aligned} \hat{H} = &\sum_{\mathbf{k}} \epsilon_{\downarrow,0,\mathbf{k}} \hat{c}^\dagger_{\downarrow,0,\mathbf{k}} \hat{c}_{\downarrow,0,\mathbf{k}} + \epsilon_{\uparrow,0,\mathbf{k}} \hat{c}^\dagger_{\uparrow,0,\mathbf{k}} \hat{c}_{\uparrow,0,\mathbf{k}} + \epsilon_{\uparrow,x,\mathbf{k}} \hat{c}^\dagger_{\uparrow,x,\mathbf{k}} \hat{c}_{\uparrow,x,\mathbf{k}} \\ &+ \epsilon_{\uparrow,y,\mathbf{k}} \hat{c}^\dagger_{\uparrow,y,\mathbf{k}} \hat{c}_{\uparrow,y,\mathbf{k}} + \epsilon_{\uparrow,z,\mathbf{k}} \hat{c}^\dagger_{\uparrow,z,\mathbf{k}} \hat{c}_{\uparrow,z,\mathbf{k}} \\ &+ \sum_{\alpha,\mathbf{k}} \Delta_{\alpha 0} \hat{c}^\dagger_{\uparrow,\alpha,\mathbf{k}} \hat{c}^\dagger_{\downarrow,0,-\mathbf{k}} + \Delta^*_{\alpha 0} \hat{c}_{\downarrow,0,-\mathbf{k}} \hat{c}_{\uparrow,\alpha,\mathbf{k}} - \sum_{\alpha} \frac{|\Delta_{\alpha 0}|^2}{U_{\alpha 0}}. \end{aligned} \tag{3.17}$$

This Hamiltonian can be written in the matrix form as

$$\begin{aligned}\hat{H} = \sum_{\mathbf{k}} \hat{\mathbf{\Psi}}^{\dagger}_{\mathbf{k}} \begin{pmatrix} \epsilon_{\uparrow,0,\mathbf{k}} & 0 & 0 & 0 & \Delta_{00} \\ 0 & \epsilon_{\uparrow,x,\mathbf{k}} & 0 & 0 & \Delta_{x0} \\ 0 & 0 & \epsilon_{\uparrow,y,\mathbf{k}} & 0 & \Delta_{y0} \\ 0 & 0 & 0 & \epsilon_{\uparrow,z,\mathbf{k}} & \Delta_{z0} \\ \Delta^{*}_{00} & \Delta^{*}_{x0} & \Delta^{*}_{y0} & \Delta^{*}_{z0} & -\epsilon_{\downarrow,0,-\mathbf{k}} \end{pmatrix} \hat{\mathbf{\Psi}}_{\mathbf{k}} \\ + \sum_{\mathbf{k}} \epsilon_{\downarrow,0,-\mathbf{k}} - \sum_{\alpha} \frac{|\Delta_{\alpha 0}|^2}{U_{\alpha 0}},\end{aligned} \tag{3.18}$$

where the five component spinor is defined by

$$\hat{\mathbf{\Psi}}_{\mathbf{k}} = \begin{pmatrix} \hat{c}_{\uparrow,0,\mathbf{k}} \\ \hat{c}_{\uparrow,x,\mathbf{k}} \\ \hat{c}_{\uparrow,y,\mathbf{k}} \\ \hat{c}_{\uparrow,z,\mathbf{k}} \\ \hat{c}^{\dagger}_{\downarrow,0,-\mathbf{k}} \end{pmatrix}.$$

This Hamiltonian can be diagonalized by means of the Bogoliubov transformation and we can write the diagonalized Hamiltonian

$$\begin{aligned}\hat{H} = &\sum_{\mathbf{k}} E_{1,\mathbf{k}} \hat{\gamma}^{\dagger}_{1,\mathbf{k}} \hat{\gamma}_{1,\mathbf{k}} + E_{2,\mathbf{k}} \hat{\gamma}^{\dagger}_{2,\mathbf{k}} \hat{\gamma}_{2,\mathbf{k}} \\ &+ E_{3,\mathbf{k}} \hat{\gamma}^{\dagger}_{3,\mathbf{k}} \hat{\gamma}_{3,\mathbf{k}} + E_{4,\mathbf{k}} \hat{\gamma}^{\dagger}_{4,\mathbf{k}} \hat{\gamma}_{4,\mathbf{k}} + E_{5,\mathbf{k}} \hat{\gamma}^{\dagger}_{5,\mathbf{k}} \hat{\gamma}_{5,\mathbf{k}} \\ &+ \sum_{\mathbf{k}} \epsilon_{\downarrow,0,\mathbf{k}} - E_{5,\mathbf{k}} - \sum_{\alpha} \frac{|\Delta_{\alpha 0}|^2}{U_{\alpha 0}},\end{aligned} \tag{3.19}$$

where $E_{i,\mathbf{k}}$ are the quasiparticle dispersions, and $\hat{\gamma}^{\dagger}_{i,\mathbf{k}}$ and $\hat{\gamma}_{i,\mathbf{k}}$ are the quasiparticle creation and annihilation operators, respectively. Term $\sum_{\mathbf{k}} \epsilon_{\downarrow,0,\mathbf{k}} - E_{5,\mathbf{k}}$ arises from the normal ordering of the operators. One can find the quasiparticle dispersions, and the quasiparticle operators by the diagonalization of the Hamiltonian numerically.

Since the diagonalized Hamiltonian is the ideal Fermi gas Hamiltonian for the quasiparticles, we can write the grand canonical potential as

$$\Omega = -k_B T \sum_{i,\mathbf{k}} \log\left(1 + e^{-\beta E_{i,\mathbf{k}}}\right) + \sum_{\mathbf{k}} \epsilon_{\downarrow,0,\mathbf{k}} - E_{5,\mathbf{k}} - \sum_{\alpha} \frac{|\Delta_{\alpha 0}|^2}{U_{\alpha 0}}. \tag{3.20}$$

Of course, one obtains also the Helmholtz free-energy $F = \Omega + \mu_{\uparrow} N_{\uparrow} + \mu_{\downarrow} N_{\downarrow}$.

We can vary many different variables of the system such as the chemical potentials, interaction strengths, temperature, or filling fractions. By minimizing the free energy, one can find the phase diagrams describing possible paired phases.

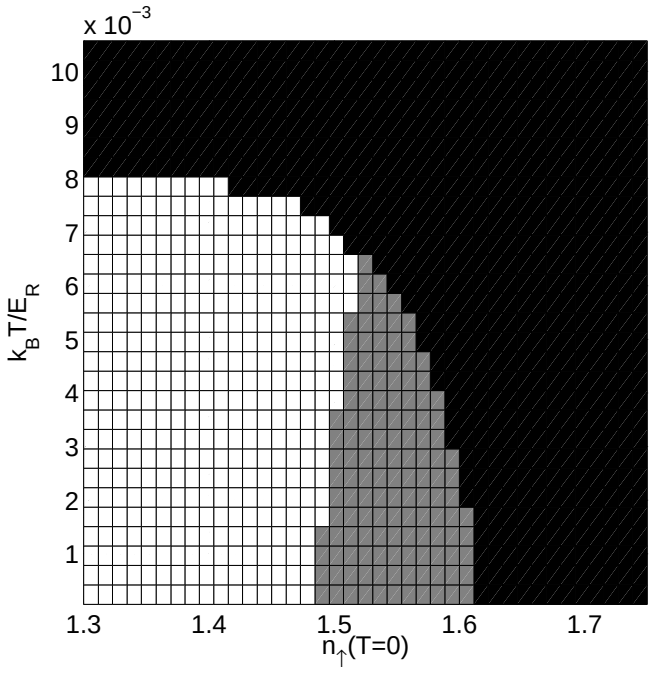

Figure 3.2: Phase diagram with a fixed scattering length $a = -80a_B$ and (a_B is the Bohr radius) the minority component chemical potential which corresponds to half-filling for the ideal system at $T = 0$. The x-axis shows the filling fraction of the ideal gas of majority atoms at $T = 0$ Shading: symmetric state = light, on-axis state = gray, normal state=dark. E_r is the recoil energy.

For a cubic lattice in the case where the components are two different hyperfine states of the same isotope, the filling fraction of component $\uparrow$ is greater than unity, attractive interactions, which we have implicitly assumed, there are three different competing phases in the system: The first one is the antisymmetric superfluid phase, which means that only one of pairing fields $\Delta_{x0}, \Delta_{y0}, \Delta_{z0}$ is non-zero and $\Delta_{00} = 0$, the second one is the symmetric superfluid phase, where $\Delta_{x0} = \Delta_{y0} = \Delta_{z0} > 0$, and the third one is the normal gas, where all the pairing fields are zero [54]. These phase can be seen from figure 3.2. The pairing can take place when the Fermi surfaces overlap. That is why $\Delta_{00} = 0$, when the filling fraction of component $\uparrow$ is greater than unity.

The appearance of three pairing channels at once is quite remarkable and we will demonstrated below this is not what is expected in a system with several different component.

These different phases could be experimentally observed using the noise correlations [55, 42], or the pairing gaps could also be observed through radio-frequency spectroscopy [56, 57, 58].

If the interactions are repulsive, one can find anti-ferromagnetic ordering. This topic was further explored in reference [54].

Chapter 4

Three-component Fermi gases

In this chapter we concentrate the physics, which has been discussed in papers **I** and **II**.

In the previous section we discussed pairing in the first excited band of the lattice. Here, we explore a three-component Fermi gas. Like in the interband case we can have here several different pairing fields

A three-component Fermi gas consists three different types of fermions. The components can be three different hyperfine states of the same alkali isotope, different isotopes, different elements, or they can be even quarks [59]. It has been suggested that in the core of a neutron star the baryonic matter is degenerate and quarks form a superfluid liquid. This superfluidity of quarks is called color superconductivity. There are tree types of quarks in the baryonic matter two different spin states of up quark and one down quark. Some interest towards ultra-cold three-component Fermi gases have been recently shown [60, 61, 62]. This is due that this color superconductivity has close analogs with a three-component alkali Fermi gas. These are our main motivations to study a three-component Fermi gas.

4.1 BCS-theory of a three-component Fermi gas

Although we study free space physics here, the theory we present is also applicable in optical lattices if the filling fractions are much smaller than unity and the dispersions can be approximated as parabolic.

The easiest way to create a theory for an ultra-cold three-component Fermi gas with attractive interactions is to generalize the standard BCS-theory. Let us consider a three-component Fermi gas, the components of which are three different types of alkali atoms. Furthermore, let us assume that the components interact with each other and all the interactions are attractive. The Hamiltonian

of the system is given by

$$\begin{aligned}\hat{H} = &\sum_{\sigma=1,2,3} \int d\mathbf{r}\, \hat{\Psi}_\sigma^\dagger(\mathbf{r}) \left(-\frac{\hbar^2\nabla^2}{2m_\sigma} - \mu_\sigma + V_\sigma(\mathbf{r}) \right) \hat{\Psi}_\sigma(\mathbf{r}) \\ &+ \int\int d\mathbf{r}\, d\mathbf{r}'\, \hat{\Psi}_1^\dagger(\mathbf{r}) \hat{\Psi}_2^\dagger(\mathbf{r}') U_{12}(\mathbf{r},\mathbf{r}') \hat{\Psi}_2(\mathbf{r}') \hat{\Psi}_1(\mathbf{r}) \\ &+ \int\int d\mathbf{r}\, d\mathbf{r}'\, \hat{\Psi}_1^\dagger(\mathbf{r}) \hat{\Psi}_3^\dagger(\mathbf{r}') U_{13}(\mathbf{r},\mathbf{r}') \hat{\Psi}_3(\mathbf{r}') \hat{\Psi}_1(\mathbf{r}) \\ &+ \int\int d\mathbf{r}\, d\mathbf{r}'\, \hat{\Psi}_2^\dagger(\mathbf{r}) \hat{\Psi}_3^\dagger(\mathbf{r}') U_{23}(\mathbf{r},\mathbf{r}') \hat{\Psi}_3(\mathbf{r}') \hat{\Psi}_2(\mathbf{r}),\end{aligned} \tag{4.1}$$

where $\hat{\Psi}^\dagger, \hat{\Psi}$ are the fermionic field operators, μ_σ is the chemical potential of component σ, $V_\sigma(\mathbf{r})$ is the external potential felt by component σ, and $U_{\alpha\beta}(\mathbf{r},\mathbf{r}')$ is the interaction between components α and β ($\alpha, \beta = 1, 2, 3$). In this Hamiltonian, the three-particle scattering processes are ruled out, this limitation is reasonable because the gas is considered very dilute. Thus the three particle scattering processes are very rare. If the gas is not dilute enough three-body losses may be a problem [62]. In a dilute gas, we can approximate the interactions as usual by

$$U_{\alpha\beta}(\mathbf{r},\mathbf{r}') = \frac{2\hbar^2\pi(m_\alpha + m_\beta)a_{\alpha\beta}}{m_\alpha m_\beta}\delta(\mathbf{r}-\mathbf{r}') = g_{\alpha\beta}\delta(\mathbf{r}-\mathbf{r}'),$$

where $a_{\alpha\beta}$ is the s-wave scattering length between components α and β. For this kind of contact interactions, the Hamiltonian reduced into

$$\begin{aligned}\hat{H} = &\sum_{\sigma=1,2,3} \int d\mathbf{r}\, \hat{\Psi}_\sigma^\dagger(\mathbf{r}) \left(-\frac{\hbar^2\nabla^2}{2m_\sigma} - \mu_\sigma - V_\sigma(\mathbf{r}) \right) \hat{\Psi}_\sigma(\mathbf{r}) \\ &+ g_{12} \int d\mathbf{r}\, \hat{\Psi}_1^\dagger(\mathbf{r}) \hat{\Psi}_2^\dagger(\mathbf{r}) \hat{\Psi}_2(\mathbf{r}) \hat{\Psi}_1(\mathbf{r}) \\ &+ g_{13} \int d\mathbf{r}\, \hat{\Psi}_1^\dagger(\mathbf{r}) \hat{\Psi}_3^\dagger(\mathbf{r}) \hat{\Psi}_3(\mathbf{r}) \hat{\Psi}_1(\mathbf{r}) \\ &+ g_{23} \int d\mathbf{r}\, \hat{\Psi}_2^\dagger(\mathbf{r}) \hat{\Psi}_3^\dagger(\mathbf{r}) \hat{\Psi}_3(\mathbf{r}) \hat{\Psi}_2(\mathbf{r}).\end{aligned}$$

In the same way as shown in chapter 3, one can do the mean-field approximation,

and derive the mean-field Hamiltonian which is given by

$$\begin{aligned}\hat{H} = &\sum_{\sigma=1,2,3} \int d\mathbf{r}\, \hat{\Psi}^\dagger_\sigma(\mathbf{r}) \left(-\frac{\hbar^2\nabla^2}{2m_\sigma} - \mu_\sigma - V_\sigma(\mathbf{r}) \right) \hat{\Psi}_\sigma(\mathbf{r}) \\ &+ \int d\mathbf{r}\, \Delta_{12}(\mathbf{r})\hat{\Psi}^\dagger_1(\mathbf{r})\hat{\Psi}^\dagger_2(\mathbf{r}) + \Delta^*_{12}(\mathbf{r})\hat{\Psi}_2(\mathbf{r})\hat{\Psi}_1(\mathbf{r}) \\ &+ \int d\mathbf{r}\, \Delta_{13}(\mathbf{r})\hat{\Psi}^\dagger_1(\mathbf{r})\hat{\Psi}^\dagger_3(\mathbf{r}) + \Delta^*_{13}(\mathbf{r})\hat{\Psi}_3(\mathbf{r})\hat{\Psi}_1(\mathbf{r}) \\ &+ \int d\mathbf{r}\, \Delta_{23}(\mathbf{r})\hat{\Psi}^\dagger_2(\mathbf{r})\hat{\Psi}^\dagger_3(\mathbf{r}) + \Delta^*_{23}(\mathbf{r})\hat{\Psi}_3(\mathbf{r})\hat{\Psi}_2(\mathbf{r}) \\ &- \int d\mathbf{r} \left(\frac{|\Delta_{12}(\mathbf{r})|^2}{g_{12}} + \frac{|\Delta_{13}(\mathbf{r})|^2}{g_{13}} + \frac{|\Delta_{23}(\mathbf{r})|^2}{g_{23}} \right),\end{aligned} \tag{4.2}$$

where the pairing fields are defined by

$$\Delta_{\alpha\beta}(\mathbf{r}) = g_{\alpha\beta}\langle\Psi_\beta(\mathbf{r})\Psi_\alpha(\mathbf{r})\rangle.$$

In the absence of the external potentials, the gas is uniform. In this case, it is reasonable to assume as the first approximation that the pairing fields are constant i.e. $\Delta_{\alpha\beta}(\mathbf{r}) = \Delta_{\alpha\beta}$ (the standard BCS ansatz). For the uniform gas it is useful to do the Fourier transform, and the Hamiltonian in the momentum space becomes

$$\begin{aligned}\hat{H} = &\sum_{\sigma,\mathbf{k}} \epsilon_{\sigma,\mathbf{k}} \hat{c}^\dagger_{\sigma,\mathbf{k}} \hat{c}_{\sigma,\mathbf{k}} \\ &+ \sum_{\mathbf{k}} \Big[\Delta_{12}\hat{c}^\dagger_{1,\mathbf{k}}\hat{c}^\dagger_{2,-\mathbf{k}} + \Delta^*_{12}\hat{c}_{2,-\mathbf{k}}\hat{c}_{1,\mathbf{k}} + \Delta_{13}\hat{c}^\dagger_{1,\mathbf{k}}\hat{c}^\dagger_{3,-\mathbf{k}} + \Delta^*_{13}\hat{c}_{3,-\mathbf{k}}\hat{c}_{1,\mathbf{k}} \\ &+ \Delta_{23}\hat{c}^\dagger_{2,-\mathbf{k}}\hat{c}^\dagger_{3,\mathbf{k}} + \Delta^*_{23}\hat{c}_{3,\mathbf{k}}\hat{c}_{2,-\mathbf{k}} \Big] - \frac{V|\Delta_{12}|^2}{g_{12}} - \frac{V|\Delta_{13}|^2}{g_{13}} - \frac{V|\Delta_{23}|^2}{g_{23}},\end{aligned} \tag{4.3}$$

where $\epsilon_{\sigma,\mathbf{k}} = \hbar^2|\mathbf{k}|^2/(2m_\sigma) - \mu_\sigma$, and V is the quantization volume.

When one of the interactions is assumed much weaker than others, one can ignore the corresponding pairing field. Let us assume that $g_{13} = 0$. In this case,

the mean-field Hamiltonian can be expressed as

$$\begin{aligned}\hat{H} &= \sum_{\sigma,\mathbf{k}} \epsilon_{\sigma,\mathbf{k}} \hat{c}^\dagger_{\sigma,\mathbf{k}} \hat{c}_{\sigma,\mathbf{k}} \\ &+ \sum_{\mathbf{k}} \left[\Delta_{12} \hat{c}^\dagger_{1,\mathbf{k}} \hat{c}^\dagger_{2,-\mathbf{k}} + \Delta^*_{12} \hat{c}_{2,-\mathbf{k}} \hat{c}_{1,\mathbf{k}} - \Delta_{23} \hat{c}^\dagger_{3,\mathbf{k}} \hat{c}^\dagger_{2,-\mathbf{k}} - \Delta^*_{23} \hat{c}_{2,-\mathbf{k}} \hat{c}_{3,\mathbf{k}} \right] \\ &- \frac{V|\Delta_{12}|^2}{g_{12}} - \frac{V|\Delta_{23}|^2}{g_{23}} \\ &= \sum_{\mathbf{k}} \begin{pmatrix} \hat{c}^\dagger_{1,\mathbf{k}} & \hat{c}_{2,-\mathbf{k}} & \hat{c}^\dagger_{3,\mathbf{k}} \end{pmatrix} \begin{pmatrix} \epsilon_{1,\mathbf{k}} & \Delta_{12} & 0 \\ \Delta^*_{12} & -\epsilon_{2,-\mathbf{k}} & -\Delta^*_{23} \\ 0 & -\Delta_{23} & \epsilon_{3,\mathbf{k}} \end{pmatrix} \begin{pmatrix} \hat{c}_{1,\mathbf{k}} \\ \hat{c}^\dagger_{2,-\mathbf{k}} \\ \hat{c}_{3,\mathbf{k}} \end{pmatrix} \\ &+ \sum_{\mathbf{k}} \epsilon_{2,\mathbf{k}} - \frac{V|\Delta_{12}|^2}{g_{12}} - \frac{V|\Delta_{23}|^2}{g_{23}}.\end{aligned}$$

The matrix part can be diagonalized by using unitary transformation matrices $U_{\mathbf{k}}$. Thus the matrix part can be written as

$$\begin{aligned}&\begin{pmatrix} \hat{c}^\dagger_{1,\mathbf{k}} & \hat{c}_{2,-\mathbf{k}} & \hat{c}^\dagger_{3,\mathbf{k}} \end{pmatrix} U^\dagger_{\mathbf{k}} U_{\mathbf{k}} \begin{pmatrix} \epsilon_{1,\mathbf{k}} & \Delta_{12} & 0 \\ \Delta^*_{12} & -\epsilon_{2,-\mathbf{k}} & -\Delta^*_{23} \\ 0 & -\Delta_{23} & \epsilon_{3,\mathbf{k}} \end{pmatrix} U^\dagger_{\mathbf{k}} U_{\mathbf{k}} \begin{pmatrix} \hat{c}_{1,\mathbf{k}} \\ \hat{c}^\dagger_{2,-\mathbf{k}} \\ \hat{c}_{3,\mathbf{k}} \end{pmatrix} \\ &= \begin{pmatrix} \hat{\gamma}^\dagger_{1,\mathbf{k}}\hat{} & \hat{\gamma}_{2,\mathbf{k}} & \hat{\gamma}^\dagger_{3,\mathbf{k}} \end{pmatrix} \begin{pmatrix} E_{1,\mathbf{k}} & 0 & 0 \\ 0 & -E_{2,\mathbf{k}} & 0 \\ 0 & 0 & E_{3,\mathbf{k}} \end{pmatrix} \begin{pmatrix} \hat{\gamma}_{1,\mathbf{k}} \\ \hat{\gamma}^\dagger_{2,\mathbf{k}} \\ \hat{\gamma}_{3,\mathbf{k}} \end{pmatrix},\end{aligned}$$

where the minus sign is only a convention. This diagonalization can be done analytically, but the formulas are lengthy. However, the analytical formulas are much simpler in the case where $\epsilon_{1,\mathbf{k}} = \epsilon_{3,\mathbf{k}}$ i.e. $m_1 = m_3$ and $\mu_1 = \mu_3$. In this special case the Bogoliubov dispersions are

$$\begin{aligned}E_{1,\mathbf{k}} &= E_{\mathbf{k}} + \frac{\epsilon_{1,\mathbf{k}} - \epsilon_{2,-\mathbf{k}}}{2} = \sqrt{\left(\frac{\epsilon_{1,\mathbf{k}} + \epsilon_{2,-\mathbf{k}}}{2}\right)^2 + |\Delta_{12}|^2 + |\Delta_{23}|^2} + \frac{\epsilon_{1,\mathbf{k}} - \epsilon_{2,-\mathbf{k}}}{2}, \\ E_{2,\mathbf{k}} &= E_{\mathbf{k}} - \frac{\epsilon_{1,\mathbf{k}} - \epsilon_{2,-\mathbf{k}}}{2} = \sqrt{\left(\frac{\epsilon_{1,\mathbf{k}} + \epsilon_{2,-\mathbf{k}}}{2}\right)^2 + |\Delta_{12}|^2 + |\Delta_{23}|^2} - \frac{\epsilon_{1,\mathbf{k}} - \epsilon_{2,-\mathbf{k}}}{2}, \\ E_{3,\mathbf{k}} &= \epsilon_{3,\mathbf{k}},\end{aligned}$$

and the corresponding unitary matrices are given by

$$U_{\mathbf{k}} = \begin{pmatrix} u_{\mathbf{k}} & -v_{\mathbf{k}} & 0 \\ v_{\mathbf{k}} & u_{\mathbf{k}} & 0 \\ 0 & 0 & 1, \end{pmatrix},$$

where

$$u_{\mathbf{k}}^2 = \frac{1}{2}\left(1 + \frac{\epsilon_{1,\mathbf{k}} + \epsilon_{2,-\mathbf{k}}}{2E_{\mathbf{k}}}\right),$$
$$v_{\mathbf{k}}^2 = \frac{1}{2}\left(1 - \frac{\epsilon_{1,\mathbf{k}} + \epsilon_{2,-\mathbf{k}}}{2E_{\mathbf{k}}}\right).$$

The Hamiltonian can be diagonalized in every case numerically without any difficulties. For $g_{13} = 0$ the diagonalized mean-field Hamiltonian is given by

$$\begin{aligned}\hat{H} = &\sum_{\mathbf{k}} E_{1,\mathbf{k}}\hat{\gamma}_{1,\mathbf{k}}^\dagger\hat{\gamma}_{1,\mathbf{k}} + E_{2,\mathbf{k}}\hat{\gamma}_{2,\mathbf{k}}^\dagger\hat{\gamma}_{2,\mathbf{k}} + E_{3,\mathbf{k}}\hat{\gamma}_{3,\mathbf{k}}^\dagger\hat{\gamma}_{3,\mathbf{k}} \\ &+ \sum_{\mathbf{k}}(\epsilon_{2,\mathbf{k}} - E_{2,\mathbf{k}}) - \frac{V|\Delta_{12}|^2}{g_{12}} - \frac{V|\Delta_{23}|^2}{g_{23}}.\end{aligned} \tag{4.4}$$

We can derive the gap and the number equations in the same way as in chapter 3. The gap and the number equations are given by

$$\begin{aligned}\Delta_{12} &= \frac{g_{12}}{V}\sum_{\mathbf{k}} u_{11,\mathbf{k}}^* u_{12,\mathbf{k}} f(E_{1,\mathbf{k}}) + u_{21,\mathbf{k}}^* u_{22,\mathbf{k}} f(-E_{2,\mathbf{k}}) + u_{31,\mathbf{k}}^* u_{32,\mathbf{k}} f(E_{3,\mathbf{k}}), \\ \Delta_{23} &= \frac{g_{23}}{V}\sum_{\mathbf{k}} u_{13,\mathbf{k}}^* u_{12,\mathbf{k}} f(E_{1,\mathbf{k}}) + u_{23,\mathbf{k}}^* u_{22,\mathbf{k}} f(-E_{2,\mathbf{k}}) + u_{33,\mathbf{k}}^* u_{32,\mathbf{k}} f(E_{3,\mathbf{k}}), \\ n_1 &= \frac{1}{V}\sum_{\mathbf{k}} |u_{11,\mathbf{k}}|^2 f(E_{1,\mathbf{k}}) + |u_{21,\mathbf{k}}|^2 f(-E_{2,\mathbf{k}}) + |u_{31,\mathbf{k}}|^2 f(E_{3,\mathbf{k}}), \\ n_2 &= \frac{1}{V}\sum_{\mathbf{k}} |u_{12,\mathbf{k}}|^2 f(-E_{1,\mathbf{k}}) + |u_{22,\mathbf{k}}|^2 f(E_{2,\mathbf{k}}) + |u_{32,\mathbf{k}}|^2 f(-E_{3,\mathbf{k}}), \\ n_3 &= \frac{1}{V}\sum_{\mathbf{k}} |u_{13,\mathbf{k}}|^2 f(E_{1,\mathbf{k}}) + |u_{23,\mathbf{k}}|^2 f(-E_{2,\mathbf{k}}) + |u_{33,\mathbf{k}}|^2 f(E_{3,\mathbf{k}}),\end{aligned} \tag{4.5}$$

where $f(E)$ is the Fermi-Dirac distribution and $u_{ij,\mathbf{k}}$ are the matrix elements of the unitary matrix.

As it was shown for the two-components case in chapter 3, it is usually better to use the free energy rather than the gap equations. If $g_{13} = 0$ and the external potential is uniform the grand canonical potential is given by

$$\begin{aligned}\Omega = -k_B T \sum_{\mathbf{k}} \Bigg[&\log\left(1 + e^{-\beta E_{1,\mathbf{k}}}\right) + \log\left(1 + e^{-\beta E_{2,\mathbf{k}}}\right) \\ &+ \log\left(1 + e^{-\beta E_{3,\mathbf{k}}}\right)\Bigg] + \sum_{\mathbf{k}}[\epsilon_{2,\mathbf{k}} - E_{2,\mathbf{k}}] - \frac{V|\Delta_{12}|^2}{g_{12}} - \frac{V|\Delta_{23}|^2}{g_{23}}.\end{aligned} \tag{4.6}$$

4.1.1 Renormalization

In the continuum limit, the sum in equation (4.6) can be replaced with integral as follows

$$\sum_{\mathbf{k}} \to \frac{V}{(2\pi)^3}\int d^3k = \frac{V}{2\pi^2}\int_0^\infty k^2 dk,$$

but the integral form of the grand potential is ultraviolet divergent. This divergence is caused by the unphysical short distance behavior of the contact interaction. However, it can be removed, in the usual way, by subtracting the divergent contribution from the grand potential. The renormalized grand potential density in the continuum limit is given by

$$\begin{aligned}\tilde{\Omega} = \frac{\Omega}{V} = \frac{1}{2\pi^2}\int_0^\infty k^2 dk\Bigg[- k_B T\Bigg(\log\left(1+e^{-\beta E_{1,k}}\right) + \log\left(1+e^{-\beta E_{2,k}}\right) \\ + \log\left(1+e^{-\beta E_{3,k}}\right)\Bigg) + \epsilon_{2,k} - E_{2,k} - \frac{|\Delta_{12}|^2}{\xi_{12,k}} - \frac{|\Delta_{23}|^2}{\xi_{23,k}}\Bigg] \\ - \frac{|\Delta_{12}|^2}{g_{12}} - \frac{|\Delta_{23}|^2}{g_{23}},\end{aligned} \tag{4.7}$$

where

$$\xi_{\alpha\beta,k} = \frac{\hbar^2(m_\alpha + m_\beta)k^2}{4m_\alpha m_\beta}.$$

The number equations in the continuum limit are given by

$$\begin{aligned} n_1 &= \frac{1}{2\pi^2}\int_0^\infty k^2 dk\, |u_{11,k}|^2 f(E_{1,k}) + |u_{21,k}|^2 f(-E_{2,k}) + |u_{31,\mathbf{k}}|^2 f(E_{3,k}) \\ n_2 &= \frac{1}{2\pi^2}\int_0^\infty k^2 dk\, |u_{12,k}|^2 f(-E_{1,k}) + |u_{22,k}|^2 f(E_{2,k}) + |u_{32,\mathbf{k}}|^2 f(-E_{3,k}) \\ n_1 &= \frac{1}{2\pi^2}\int_0^\infty k^2 dk\, |u_{13,k}|^2 f(E_{1,k}) + |u_{23,k}|^2 f(-E_{2,k}) + |u_{33,\mathbf{k}}|^2 f(E_{3,k}). \end{aligned} \tag{4.8}$$

There is no need to renormalize the number equations. Since they are not divergent.

4.2 Pairing mechanism

For $g_{13} = 0$ two different pairing fields are left in the problem. There are four different possibilities for the pairing fields $(\Delta_{12}, \Delta_{23})$, $(\Delta_{12}, 0)$, $(0, \Delta_{23})$, and $(0, 0)$. The first one corresponds the case where the system has two different non-zero pairing fields at the same time. The last one is the case where the gas is in the normal phase. The two other cases indicate that there is only one type of pairing present in the simultaneously.

Now a question arises, how the system chooses between these two pairing fields or can they coexist? It turns out that for fixed parameters there can be only one non-zero order parameter in the system. In the case where $\epsilon_{1,\mathbf{k}} = \epsilon_{3,\mathbf{k}}$, there can be two different non-zero pairing gaps co-existing in the system, but it turns out that in this case the right order parameter is of form $\sqrt{\Delta_{12}^2 + \Delta_{23}^2}$. In this case the system has a changing symmetry between components 1 and 3. In other words, one can change a 1-particle to a 3-particle without any physical difference, as shown in figure 4.1. But for $\epsilon_{1,\mathbf{k}} = \epsilon_{3,\mathbf{k}}$, there can be formally two different non-zero pairing fields in the system only if $g_{12} = g_{23}$. Otherwise only one pairing field can be finite.

If $\epsilon_{1,\mathbf{k}} \neq \epsilon_{3,\mathbf{k}}$, there can be only one finite pairing gap co-existing. The question how the system chooses which one of the pairing gaps is non-zero depends on the interaction strengths, the chemical potentials (densities), the masses of the components, and the temperature **I**.

In the weak coupling regime some general rules can be found to predict the phase which is energetically favorable at zero temperature. Firstly, pairing will occur only for matched Fermi surfaces. This means that the pairing happens when the Fermi surfaces overlap. For the Fermi surfaces of components α and β to overlap the chemical potentials have to fulfill the condition

$$\mu_\alpha \approx \frac{m_\beta}{m_\alpha}\mu_\beta.$$

This condition can be derived from the fact if the Fermi surfaces overlap, the length of the Fermi vectors k_f must be equal and in the weakly interacting limit, the chemical potentials correspond the Fermi energies

$$E_{f,\sigma} = \frac{\hbar^2 k_f^2}{2m_\sigma}.$$

The Fermi energy is the energy of the highest energy state which is occupied at zero temperature. How closely the surfaces must be matched depends on the coupling strengths; stronger coupling implies greater tolerance for a Fermi surface mismatch. Secondly, if several pairing channels have same coupling strengths the pairing will occur in the channel involving the heavy fermion. This effect is due to the density of states increasing with mass which translates into lower energy. However, it should be kept in mind that this density of states effect can be masked by increasing the coupling in the channel involving the light fermion.

The condition for chemical potentials is not absolute, i.e., there can be some difference between the chemical potential before the pairing disappears. If the masses are equal, the limit is roughly $\delta\mu = \sqrt{2}\Delta_0$ (Δ_0 is a pairing gap when $\delta\mu = 0$), in accordance with the Clogston limit.

If the remaining interactions are equal and all the masses are equal, the system chooses the pairing channel in which the average chemical potential potential

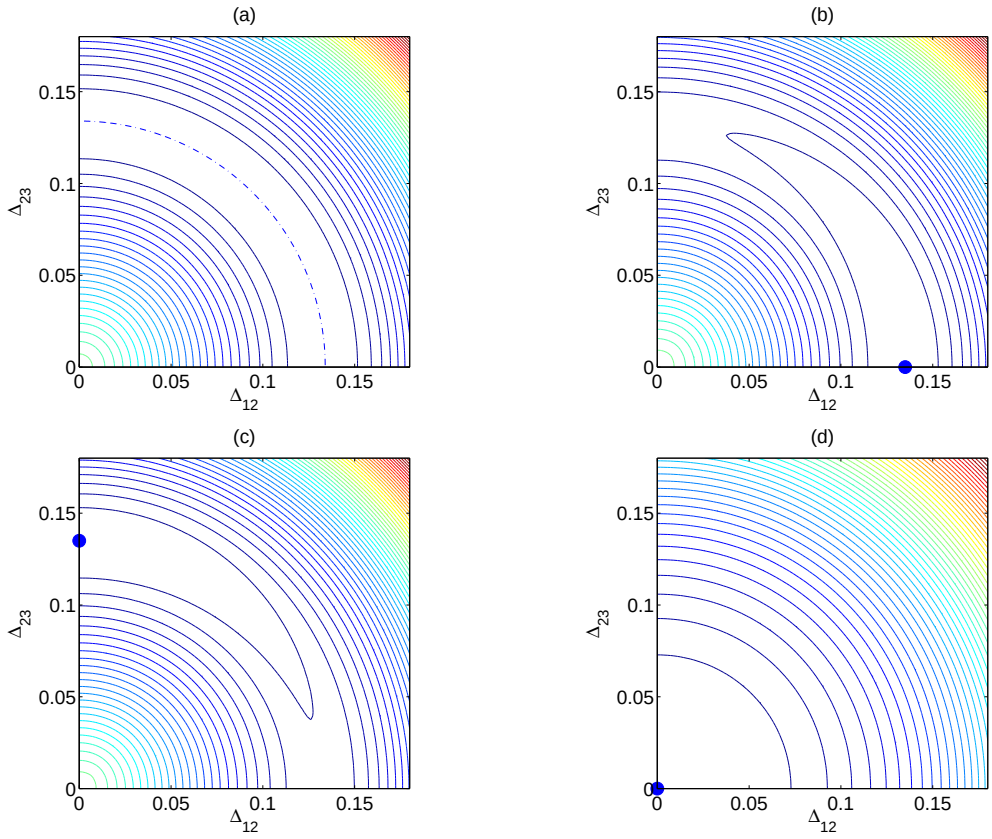

Figure 4.1: The free energy landscape as a function of Δ_{12} and Δ_{23} if all three components having the same mass. The dash-dotted line in (a) and the filled circles in (b)-(d) show the location of the global minimum. The coupling strengths are $g_{12} = g_{23} = -0.50$ and the figures (a)-(c) were calculated at zero temperature while the figure (d) was calculated at $k_B T/\epsilon_F = 0.08$ which is above the critical temperature. The chemical potentials we such that in the figure (a) $\mu_1 = \mu_2 = \mu_3 = 1$, in (b) $\mu_1 = 1.01$, $\mu_2 = 1$, $\mu_3 = 0.99$, in (c) $\mu_1 = 0.99$, $\mu_2 = 1$, $\mu_3 = 1.01$, and finally in (d) $\mu_1 = \mu_2 = \mu_3 = 1$. The energy units are the Fermi energy of component 2.

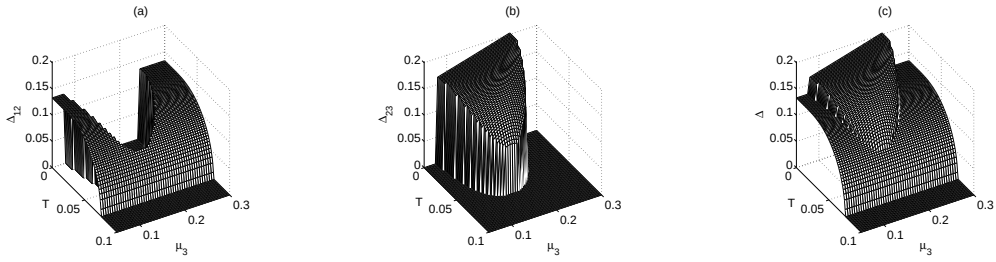

Figure 4.2: The gap parameters as a function of temperature T and of the third component chemical potential μ_3. We used the mass ratio $m_1/m_3 = 0.15$ ($m_1 = m_2$), $\mu_1 = \mu_2 = 1$, and the coupling strengths were $g_{12} = g_{23} = -0.5$. The figure (c) shows $\Delta = \sqrt{\Delta_{12}^2 + \Delta_{23}^2}$ and demonstrates clearly the sharp change in the order parameter at zero temperature as well as the smoother transition from the Δ_{23} superfluid to Δ_{12} superfluid at a finite temperature. The energy units are the Fermi energy of component 2.

is the largest. In other words, the system has two different average chemical potentials $(\mu_1 + \mu_2)/2$ and $(\mu_3 + \mu_2)/2$ and the pairing channel with the higher average chemical potential is chosen, unless the difference between the chemical potentials are not too big (the Clogston limit), as shown in figure 4.1. The average chemical potential corresponds to the density and it is the same for the both paired components at zero temperature. Higher average chemical potential indicates higher density and higher density implies larger pairing gap.

For the $g_{13} = 0$ there are two competing two-components systems. The system chooses from these competing pairing fields the one which gives a larger pairing gap if the system was a two-components system. This is demonstrated in figure 4.2. Note that a quantum phase transition is also possible as is clear in figure 4.2. The phase transition between the pairing channels in figure 4.2 is a quantum phase transition, since it happens at zero temperature. At zero temperature, all the thermal fluctuations are frozen and the transition can be only driven by the quantum fluctuations. Here, the quantum phase transition is related to the Clogston limit.

If one uses the Helmholtz free energy instead of the grand potential, i.e. the number of the particles are fixed, then the Fermi surface condition assumes the form

$$n_\alpha = n_\beta,$$

where n_α and n_α are the densities of components α and β. Of course this condition holds only for the BCS type of pairing, where the total momentum of the pairs is zero. Other type of pairings like the FFLO or phase separation are in principle possible when the densities are not equal, but these are not addressed here.

4.3 Three-component Fermi gas in a harmonic trap

Experiments with three-component Fermi gases are done in traps [62]. That is why it is important to study this system in a harmonic trap. In the mean-field approximation, there are two different ways to handle this system theoretically: the local density approximation (LDA) and the Bogoliubov-de Gennes equations. If the Bogoliubov-de Gennes equations are, used (in the two-components case), one performs first the Bogoliubov transformation for the field operators as

$$\hat{\Psi}_\uparrow(\mathbf{r}) = \sum_\eta u_\eta(\mathbf{r})\hat{\gamma}_{+,\eta} - v_\eta^*(\mathbf{r})\hat{\gamma}_{-,\eta}^\dagger$$
$$\hat{\Psi}_\downarrow(\mathbf{r}) = \sum_\eta u_\eta(\mathbf{r})\hat{\gamma}_{-,\eta} + v_\eta^*(\mathbf{r})\hat{\gamma}_{+,\eta}^\dagger,$$

where η indicates the different eigen modes. One can then solve functions $u_\eta(\mathbf{r})$ and $v_\eta(\mathbf{r})$ from the following equation

$$\begin{pmatrix} H_{0,\uparrow} & \Delta(\mathbf{r}) \\ \Delta^*(\mathbf{r}) & -H_{0,\downarrow} \end{pmatrix} \begin{pmatrix} u_\eta(\mathbf{r}) \\ v_\eta(\mathbf{r}) \end{pmatrix} = E_{\eta,\pm} \begin{pmatrix} u_\eta(\mathbf{r}) \\ v_\eta(\mathbf{r}) \end{pmatrix},$$

where $E_{\eta,\pm}$ are the eigenenegies and $\pm$ indicates that two different eigenenergies correspond to every η-mode, and

$$H_{0,\sigma} = \frac{-\hbar^2\nabla^2}{2m_\sigma} - \mu_\sigma + V_\sigma(\mathbf{r}),$$

where $V_\sigma(\mathbf{r})$ is the external potential. When this eigenequation is solved iteratively with the gap and the number equations which are given by

$$\Delta(\mathbf{r}) = -g\sum_\eta u_\eta(\mathbf{r})v_\eta^*(\mathbf{r})[1 - f(E_{\eta,+}) - f(E_{\eta,-})],$$
$$N_\sigma = \int n_\sigma(\mathbf{r})\, d\mathbf{r} = \int d\mathbf{r} \sum_\eta |u_\eta(\mathbf{r})|^2 f(E_{\eta,\alpha}) + |u_\eta(\mathbf{r})|^2(1 - f(E_{\eta,-\alpha})),$$

one can find the gap and the density profiles [63, 64, 65]. In the LDA, it is assumed that the gas is locally uniform, thus one can minimize the uniform grand canonical potential (4.7) and number equations in every spatial point separately. The chemical potentials in the center of the is chosen such that one obtains the desired atom number.

In principle, using the Bogoliubov-de Gennes equation in the three-component case is straightforward. However, as shown above in the two-components case one has to handle five coupled equations simultaneously. In the three-component case, there are eight coupled equations which we have to solve simultaneously. This is a challenging numerical problem. Because of this and the fact that the LDA

works fairly well, we employ here the LDA. In the LDA, the external potentials are included the effective chemical potentials as follows

$$\mu_{eff,\sigma}(\mathbf{r}) = \mu_\sigma - V_\sigma(\mathbf{r}).$$

At every point one calculates the grand canonical potential in the momentum space (4.7) with the local chemical potentials $\mu_{eff,\sigma}(\mathbf{r})$ and finds at the minimum the local pairing gaps $\Delta_{\alpha\beta}(\mathbf{r})$. The local densities can be calculated by using the number equations in the momentum space (4.8) with the local chemical potentials and the local pairing gaps. The total number of particles in the trap is given by integrating the local densities over the trap. The chemical potentials in the center of the trap can be fixed by fixing the number of particles in the trap **II**.

In the two-components case the LDA gives a reasonable agreement with the experiments [66, 67, 68, 69], and hence we assume that it works as well in a three-component case. The LDA fails when the gap or the density profiles change sharply, i.e., when one cannot assume that the gas is locally uniform. Of course, LDA does not handle the surface tension effects [70, 71, 72].

In our case, we assume that the trap is spherical, in other words, the external potential is given by

$$V_\sigma(\mathbf{r}) = \frac{1}{2} m_\sigma \omega_\sigma^2 r^2.$$

It is, however, easy to relax this assumption. Here, we assume that the trapping frequencies ω_σ can be different for different components. For concreteness, we assume that components 1 and 2 are two different hyperfine states of Lithium-6 (^{6}Li) and component 3 is a hyperfine state of potassium-40 (^{40}K). Of course, qualitative results obtained apply also for every combination of alkali fermions with attractive interactions.

The pairing mechanism in the trap is basically the same as in the uniform case, the pairing can only happen when the local Fermi spheres overlap. This implies that if the following condition is fulfilled $\mu_\alpha(r) \approx (m_\beta/m_\alpha)\mu_\beta(r)$, components α and β can pair. However, a three-component Fermi gas in a harmonic trap is a much richer system than the uniform case. Since one can vary many variables of the system such as the trapping frequencies, the number of particles, temperature, and the interactions between components. By varying these different variables one can obtain different types of pairings in different locations in the trap. An example of this is shown in figure 4.3. One can also observe from this figure that the phase transitions are of the first order and because they happen at zero temperature they can be considered as quantum phase transitions. As said in the uniform case, if components α and β are paired, the local densities of these components have to be the same. This is shown in figure 4.3 (b), which includes doubly integrated density differences, where the pairing areas can be observed as plateaus. This doubly integrated density can me measured in experiments by taking a picture from the cloud of atoms [70, 71]. It is clear that by varying

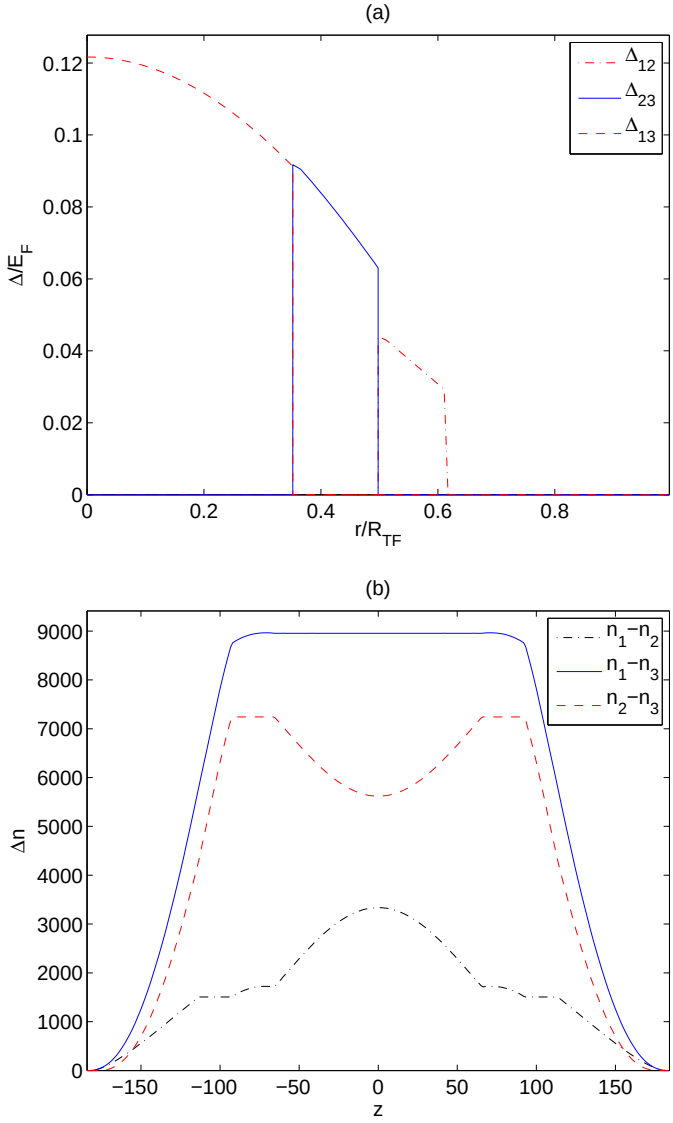

Figure 4.3: (a) Gaps as a function of position (R_{TF} is the ideal gas Thomas-Fermi radius of the second component). (b) Doubly integrated density differences. We used the parameters $N_1 = 6 \cdot 10^4$, $N_2 = 5 \cdot 10^4$, and $N_3 = 2 \cdot 10^4$, $k_F a_{12} = -1.04$, $(1 + 1/r_m)k_F a_{13} = -1.03$, $(1 + 1/r_m)k_F a_{23} = -1.15$, where $r_m = m_{Li}/m_K$ and $\omega_3/\omega_1 = 0.4$.

different variables of the system one finds different types of phase diagrams. The different phases form a shell structure. In this shell structure the different phases are located in different places in the trap. An example of this shell structure is shown in figure 4.3. Whereas a couple examples of phase diagrams are shown in figure 4.4. These phase diagrams can be quite exotic for example we predict the possibility of a normal gas core in the center of the trap surrounded by a superfluid shell, see figure 4.4 (b). This kind of normal gas core has never been seen in the two-components case. These exotic phase diagrams, might for some parameters be artifacts which are caused by using the BCS ansatz or the LDA. However, this is not likely. Bogoliubov-de Gennes calculations show that there can be some kind of FFLO type of pairing in the case of polarized two-components Fermi gas in a trap [73], whereas the LDA calculations show a phase separation [68, 50, 74, 72, 69]. Experiments with a two-components imbalanced Fermi gas show that there is an unpolarized superfluid (BCS) core in the center of the trap surrounded by a normal gas [66, 67, 70].

4.4 Three-component Fermi gas in optical lattices

In this section, we discuss a three-component Fermi gas in optical lattices, and how one can tune the lattices in such a way that the Hamiltonian approaches $SU(3)$-symmetric form. Most of the results presented in this section are still unpublished.

Experimentally, it may be beneficial to study a three-component Fermi gas in an optical lattice. Since one can change the masses (the hopping strengths correspond the effective masses) and interactions almost freely.

In lattices, a three-component Fermi gas is described by the Hubbard Hamiltonian which is given by

$$\hat{H} = -\sum_{\sigma} J_{\sigma} \sum_{\langle i,j \rangle} \hat{c}^{\dagger}_{\sigma,i} \hat{c}_{\sigma,j} + \sum_{\sigma \neq \sigma'} \sum_{i} \frac{U_{\sigma,\sigma'}}{2} \hat{n}_{\sigma,i} \hat{n}_{\sigma',i}, \tag{4.9}$$

where $\hat{n}_{\sigma,i} = \hat{c}^{\dagger}_{\sigma,i} \hat{c}_{\sigma,i}$. Here, we have assumed that the hopping strengths are direction independent. Furthermore, we take the lattice potentials to be

$$V_{\sigma}(\mathbf{r}) = s_{\sigma} E_{r,1} \sum_{\alpha} \sin^2(x_{\alpha}),$$

where the recoil energy

$$E_{r,1} = \frac{\hbar^2 \pi^2}{2 m_1 d^2}$$

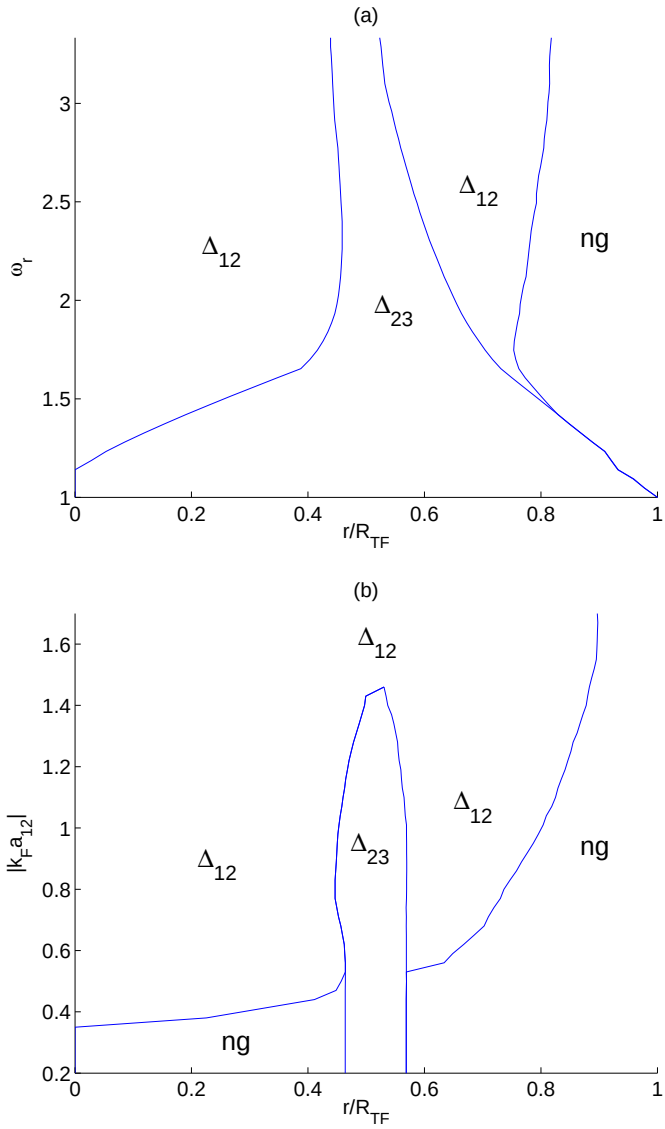

Figure 4.4: (a) Zero temperature phase diagram as a function of the dimensionless frequency ratio $\omega_r = m_{\mathrm{K}}\omega_{\mathrm{K}}/m_{\mathrm{Li}}\omega_{\mathrm{Li}}$ and r/R_{TF} with $(1+1/r_m)k_F a_{23} = -1$ and $k_F a_{12} = -1$. (b) Phase diagram in the trap as functions $-k_F a_{12}$ and r/R_{TF} for $\omega_r = 2.67$ and $(1+1/r_m)k_F a_{23} = -1$ In both figure we used parameters $N_{1,2,3} = 5.5 \cdot 10^4$, and $|a_{23}| > |a_{13}|$. Sharp corners in the figures are due to numerical uncertainties.

and d is the lattice constant. Now $U_{\sigma,\sigma'}$ and J_σ:s are given by

$$J_\sigma = \frac{m_1}{m_\sigma} E_{r,1} e^{-\frac{\pi^2\sqrt{s_\sigma}}{4}} \left[\left(\frac{\pi^2 s_\sigma}{4} - \frac{\sqrt{s_\sigma}}{2} \right) - \frac{s_\sigma}{2} \left(1 + e^{-\frac{1}{\sqrt{s_\sigma}}} \right) \right],$$

$$U_{\sigma,\sigma'} = E_{r,1} \frac{4\pi^{1/2} s_\sigma^{3/4} s_{\sigma'}^{3/4} (m_\sigma + m_{\sigma'}) m_1 a_{\sigma,\sigma'}}{m_\sigma m_{\sigma'} ((s_\sigma)^{1/2} + (s_{\sigma'})^{1/2})^{3/2} d}.$$

4.4.1 $SU(3)$-symmetric model in deep lattices

A three-component Fermi gas in optical lattices can have close analogs to quantum chromodynamics (QCD). The QCD is almost SU(3)-symmetric theory. There is a small difference between the masses of u-quark d-quark, but this difference is so small that one can often consider the QCD as a $SU(3)$-symmetric theory.

In the free space, $SU(3)$-symmetry is unlikely. In a lattice however, we can make the above Hamiltonian $SU(3)$-symmetric by changing the lattice depths and the s-wave scattering lengths. In particular, by creating spin depended lattices [75, 76], we can create $SU(3)$-symmetric interactions even if the scattering lengths in the continuum differ.

If all the interaction parameters are equal and all the hoping strengths are equal, the Hamiltonian has a global $SU(3)$ symmetry [61]. This is similar to QCD. Of course the uniform case can formally realize this $SU(3)$ condition as well, but this requires that all the scattering lengths and masses are equal [60].

When all the masses are the same, i.e, all the components are same isotope, $SU(3)$-symmetry can be achieved only when all the lattice depths and scattering lengths are equal. This is highly unlikely in practice. However, in a deep lattice the $SU(3)$ condition can be achieved for different masses as shown below. Let us assume that components 1 and 2 are of the same isotope and have mass m_1, and furthermore we assume that component 3 is of a different isotope than two others and has mass m_3. These assumptions directly imply that s_1 and s_2 have to be equal to get J_1 and J_2 to be equal, and a_{13} and a_{23} have to be equal to get U_{12} and U_{13} to be equal. Furthermore to get $U_{12} = U_{13}$ the lattice depths have to obey a condition

$$s_1 = s_2 = s_3 \left(\frac{2^{3/2}(m_3 + m_1)a_{13}}{m_3 a_{12}} - 1 \right)^2.$$

Now we have two equations for the lattice depths and the scattering lengths, the first one is given above and the second one is given by $J_1 = J_3$. These equations have to be satisfied simultaneously. This scenario is hard to achieve in experiments since the condition $a_{13} = a_{23}$ is somewhat unrealistic. If all the masses are unequal, there are more possibilities to fix the lattice depths such that the Hamiltonian becomes $SU(3)$-symmetric.

Although the pure $SU(3)$ condition is hard to achieve, it turns out that if all the scattering lengths are negative (positive), one can find a combination of the lattice depths such that all the interaction parameters are equal. If the interactions are yhe dominant part of the Hamiltonian, the kinetic term can be handled as a perturbation. Let us assume that all the components are of same isotope and that the scattering lengths are given by $a_{12} = a$, $a_{13} = a + \delta a_1$, and $a_{23} = a + \delta a_2$. We write the lattice depths as $s_1 = s$, $s_2 = s + \delta s_2$ and $s_3 = s + \delta s_3$. If we take all the interaction parameters to be equal, we get the following condition for δs_2 and δs_3

$$\delta s_2 = \left[\left(\frac{(1+\delta a_1/a)^{2/3} - (1+\delta a_2/a)^{2/3} + 1}{(1+\delta a_2/a)^{2/3} - (1+\delta a_1/a)^{2/3} + 1} \right)^2 - 1 \right] s,$$

$$\delta s_3 = \left[\left(\frac{(1+\delta a_1/a)^{2/3} - (1+\delta a_2/a)^{2/3} + 1}{(1+\delta a_1/a)^{2/3} + (1+\delta a_2/a)^{2/3} - 1} \right)^2 - 1 \right] s.$$

If $|\delta a_i/a| \ll 1$ then δs_i are small. Thus in this case the Hamiltonian can be written as $\hat{H} = \hat{H}_0 + \hat{H}'$, where $\hat{H}_0$ is the pure $SU(3)$ symmetric Hamiltonian and

$$\hat{H}' = -\sum_{\langle i,j \rangle} (\delta J_2 \hat{c}^\dagger_{2,i} \hat{c}_{2,j} + \delta J_3 \hat{c}^\dagger_{3,i} \hat{c}_{3,j}),$$

where $\delta J_\sigma = J_\sigma - J_1$. We can handle $\hat{H}'$ as a small perturbation about the $SU(3)$-symmetric case. Such a theory amounts to a strong coupling expansion where the interaction term is $SU(3)$-symmetric whereas the kinetic term breaks the symmetry and vanishes in the limit of infinitely deep lattice. In QCD the $SU(3)$-symmetry is broken by the kinetic term, thus this deep lattice model is similar to QCD. From figure 4.5 we observe that, if the difference between the scattering lengths is of the order of 10%, and the lattice depths are chosen so that the interactions are same, then δJ_2 and δJ_3 are of the order of J at most.

The ground state of a three-component Fermi gas with attractive interactions in a lattice depends on the interaction strengths. If $|U|$:s are small, the ground state is the superfluid state and if $|U|$:s are great enough the ground state is a so called trion-state, where the atoms form three-body bound states [61]. In the $SU(3)$-symmetric case, the transition between the superfluid state and the trion-state is analogous to the transition between color superconductivity and baryonic matter.

Although optical lattices seem to be promising systems to study a three-component Fermi gas, there might be some experimental problems. In an optical lattice, the densities can be quite high, and hence the probability to get three different particles at same lattice site can also be quite high. There are different types of three particle bound states, for example the Efimov states [77, 78, 79],

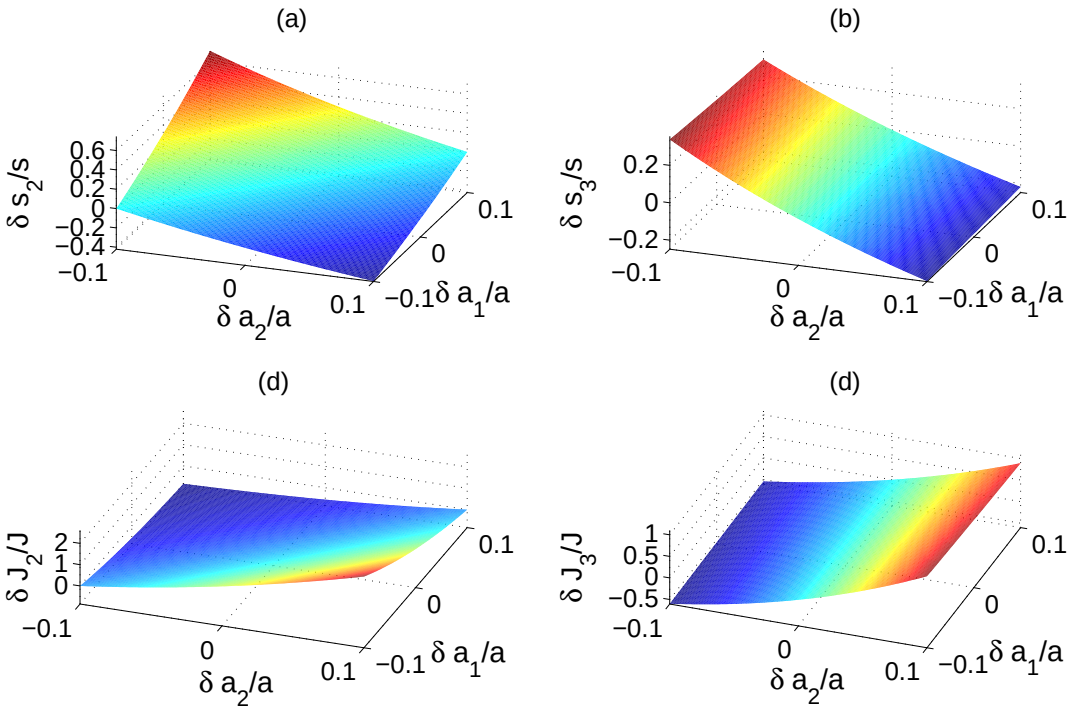

Figure 4.5: Figures (a) and (b) show how the lattice depths has to be chosen to get the interaction strength to match, for different scattering lengths. Figures (c) and (d) show how this effect the hopping terms. Here we have chosen $s = 10$.

and their binding energy can be so high that they can escape from the lattice. For this reason three body-losses may be a problem in lattices. This issue should be analyzed in greater detail in the future.

Chapter 5

Higher than the first order correlations

In this chapter we discuss the higher than the first order correlations. The first section is connected to paper **IV** and the second section is connected to paper **V**.

BCS like theory of pairing only involves the computation of first order correlation functions (i.e. two operator products). However, important information can be found in higher order correlations. In this chapter we will explore these for two concrete examples. Firstly, we will compute density-density correlations in a lattice. Secondly, we will outline how one can draw conclusions about superfluidity for the BCS theory by computing the superfluid density.

5.1 Density noise correlations in optical lattices

Density-density correlations tell us how atomic densities at different positions are correlated. Noise correlations are density-density correlations, from which the mean densities are sutracted away. Noise correlations offer a tool to observe different phases in optical lattices. The densities can be very similar for different phases, while the noise correlations can show a huge difference. An example of using noise correlations as an indicator of phase transition is the phase transition between the superfluid Bose gas and the Mott insulator [55, 42]. Noise correlations have also been used as an indicator of the fermionic anti-bunching for ideal fermions in a lattice [41].

In this study, we assume a two-components Fermi gas with attractive interactions in optical lattices. The gas can be polarized. The density-density correlations are defined as

$$D_{\sigma\sigma'}(\mathbf{r},\mathbf{r}',t) = \langle \hat{n}_\sigma(\mathbf{r},t)\hat{n}_\sigma(\mathbf{r}',t)\rangle,$$

where $\hat{n}_\sigma(\mathbf{r},t) = \hat{\Psi}^\dagger_\sigma(\mathbf{r},t)\hat{\Psi}_\sigma(\mathbf{r},t)$, and $\Psi^\dagger_\sigma(\mathbf{r},t)$ and $\hat{\Psi}_\sigma(\mathbf{r},t)$ are the field operators

at time t. If the mean densities are substracted out, we obtain the definitions of noise correlations [55] as

$$G_{\sigma\sigma'}(\mathbf{r},\mathbf{r}',t) = \langle \hat{n}_\sigma(\mathbf{r},t)\hat{n}_\sigma(\mathbf{r}',t)\rangle - \langle \hat{n}_\sigma(\mathbf{r},t)\rangle\langle \hat{n}_\sigma(\mathbf{r}',t)\rangle. \tag{5.1}$$

In lattices, the field operators can be expanded, as in the previous section, as series by using localized Wannier functions

$$\hat{\Psi}_\sigma(\mathbf{r},t) = \sum_i w_{\sigma,i}(\mathbf{r},t)\hat{c}_{\sigma,i}$$
$$\hat{\Psi}^\dagger_\sigma(\mathbf{r},t) = \sum_i w^*_{\sigma,i}(\mathbf{r},t)\hat{c}^\dagger_{\sigma,i},$$

where w is a Wannier function and $\hat{c}$ is an annihilation operator.

In typical experiments, the trapped gas is released and let to expand. The gas is assumed to be dilute, and hence the rare collisions can be ignored during the expansion. Therefore, the expansion is adiabatic and ballistic, and after the expansion the density-density correlations reflect correlations in the momentum space at $t = 0$. After the expansion, the Wannier functions can be written as [55]

$$w_i(\mathbf{r},t) = A(t)e^{-iQ(\mathbf{r})\cdot\mathbf{R}_i},$$

where $A(t)$ is a time dependent scaling factor and

$$Q(\mathbf{r}) = \frac{m\mathbf{r}}{\hbar t}.$$

In other words, the Wannier functions become plane waves at long times, the condition of which is obtained using the saddle point approximation to be $t \gg md^2/\hbar$.

5.1.1 Ground state

In order to be able to calculate the density-density correlations we have to identify the appropriate many-body state for the system.

On a mean-field level the ground state ansatz at zero temperature which includes the possibility of the BCS-state, the BP/Sarma-state, and the one mode FFLO-state can be expressed as [51]

$$|\Psi_{GS}\rangle = \prod_{\mathbf{k}\in G_3} \hat{c}^\dagger_{\downarrow,-\mathbf{k}+\mathbf{q}} \prod_{\mathbf{k}\in G_2} \hat{c}^\dagger_{\uparrow,\mathbf{k}} \prod_{\mathbf{k}\in G_1} (u_{\mathbf{k},\mathbf{q}} + v_{\mathbf{k},\mathbf{q}}\hat{c}^\dagger_{\uparrow,\mathbf{k}}\hat{c}^\dagger_{\downarrow,-\mathbf{k}+\mathbf{q}})|0\rangle, \tag{5.2}$$

where $|0\rangle$ is the vacuum state. In region G_1, both quasiparticle dispersions $E_{+,\mathbf{k},\mathbf{q}}, E_{-,\mathbf{k},\mathbf{q}}$ are positive, in region G_2 quasiparticle dispersions $E_{-,\mathbf{k},\mathbf{q}} \geq 0$ and $E_{+,\mathbf{k},\mathbf{q}} < 0$, and in region G_3 $E_{+,\mathbf{k},\mathbf{q}} \geq 0$ and $E_{-,\mathbf{k},\mathbf{q}} < 0$. Region G_1 is populated

by pairs with a quasi-momentum $\mathbf{q}$. Region G_2 is populated by atoms of the component $\uparrow$ in the quasi-momentum states $\mathbf{k} \in G_2$ whereas region G_3 is populated by $\downarrow$-atoms in the quasi-momentum states $-\mathbf{k}+\mathbf{q}$. The Bogoliubov-dispersions are determined as in chapter 3.

With the Bogoliubov transformation, the ground state ansatz becomes

$$|\Psi_{GS}\rangle = \prod_{\mathbf{k}\in G_1} \hat{\gamma}^\dagger_{+,\mathbf{k},\mathbf{q}} \prod_{\mathbf{k}\in G_2} \hat{\gamma}^\dagger_{-,\mathbf{k},\mathbf{q}}|0\rangle, \tag{5.3}$$

in region G_1 $E_{+,\mathbf{k},\mathbf{q}} < 0$ and in region G_2 $E_{-,\mathbf{k},\mathbf{q}} < 0$. This ground state ansatz is a vacuum state for the quasiparticles, and implies expectation values.

$$\begin{aligned}
&\langle\Psi_{GS}|\hat{\gamma}^\dagger_{\alpha,\mathbf{k},\mathbf{q}}\gamma_{\beta,\mathbf{k}',\mathbf{q}}|\Psi_{GS}\rangle = \delta_{\alpha\beta}\delta_{\mathbf{k},\mathbf{k}'}f(E_{\alpha,\mathbf{k},\mathbf{q}}),\\
&\langle\Psi_{GS}|\hat{\gamma}^\dagger_{\alpha,\mathbf{k},\mathbf{q}}\gamma^\dagger_{\beta,\mathbf{k}',\mathbf{q}}|\Psi_{GS}\rangle = \langle\Psi_{GS}|\hat{\gamma}_{\alpha,\mathbf{k},\mathbf{q}}\gamma_{\beta,\mathbf{k}',\mathbf{q}}|\Psi_{GS}\rangle = 0.
\end{aligned}$$

5.1.2 Noise correlations in optical lattices

The noise correlations in lattices are given by the functions

$$\begin{aligned}
G_{\alpha\beta}(\mathbf{r},\mathbf{r}',t) =& A(t)^4 \sum_{i,j,m,n} e^{iQ(\mathbf{r})\cdot\mathbf{R}_{ij}+iQ(\mathbf{r})\cdot\mathbf{R}_{mn}}\langle\hat{c}^\dagger_{\alpha,i}\hat{c}_{\alpha,j}\hat{c}^\dagger_{\beta,m}\hat{c}_{\beta,n}\rangle\\
&- \langle\hat{n}_\alpha(\mathbf{r},t)\rangle\langle\hat{n}_\beta(\mathbf{r}',t)\rangle,
\end{aligned}$$

where $\mathbf{R}_{ij} = \mathbf{R}_i - \mathbf{R}_j$. In above we have written the field operators at long times as

$$\begin{aligned}
\hat{\Psi}_\alpha(\mathbf{r}) &= A(t)\sum_m e^{-iQ(\mathbf{r})\cdot\mathbf{R}_m}\hat{c}_{\alpha,m}\\
\hat{\Psi}^\dagger_\beta(\mathbf{r}') &= A(t)\sum_n e^{iQ(\mathbf{r}')\cdot\mathbf{R}_n}\hat{c}^\dagger_{\beta,n},
\end{aligned}$$

and we have put these field operators in the definition of the noise correlation functions. Since the ground state ansatz is given in the momentum space, it is more convenient to take the Fourier transform of the operators. After this the noise correlations are given by

$$\begin{aligned}
&G_{\alpha\beta}(\mathbf{r},\mathbf{r}',t) =\\
&\frac{A(t)^4}{M^2}\sum_{\substack{i,j,m,n,\\ \mathbf{k}_1,\mathbf{k}_2,\mathbf{k}_3,\mathbf{k}_4}} \left(e^{iQ(\mathbf{r})\cdot\mathbf{R}_{ij}+iQ(\mathbf{r}')\cdot\mathbf{R}_{mn}}e^{-i\mathbf{k}_1\cdot\mathbf{R}_i+i\mathbf{k}_2\cdot\mathbf{R}_j-i\mathbf{k}_3\cdot\mathbf{R}_m+i\mathbf{k}_4\cdot\mathbf{R}_n}\langle\hat{c}^\dagger_{\alpha,\mathbf{k}_1}\hat{c}_{\alpha,\mathbf{k}_2}\hat{c}^\dagger_{\beta,\mathbf{k}_3}\hat{c}_{\beta,\mathbf{k}_4}\rangle\right)\\
&- \langle\hat{n}_\alpha(\mathbf{r},t)\rangle\langle\hat{n}_\beta(\mathbf{r}',t)\rangle.
\end{aligned}$$

Finally one can calculate the expectation values, and find after lengthy algebra,

$$
\begin{aligned}
G_{\uparrow\downarrow}(\mathbf{r},\mathbf{r}',t) &= A(t)^4 \sum_{\mathbf{k}} \Bigg[\delta\left(\mathbf{r} - \frac{\hbar t \tilde{\mathbf{k}}}{m}\right) \delta\left(\mathbf{r}' + \frac{\hbar t(\tilde{\mathbf{k}'} - \mathbf{q})}{m}\right) \\
&[f(E_{\uparrow,\mathbf{k},\mathbf{q}}) f(E_{\downarrow,\mathbf{k},\mathbf{q}}) + (1 - f(E_{\uparrow,\mathbf{k},\mathbf{q}}))(1 - f(E_{\downarrow,\mathbf{k},\mathbf{q}}))] |u_{\mathbf{k},\mathbf{q}}|^2 |v_{\mathbf{k},\mathbf{q}}|^2 \Bigg], \\
G_{\downarrow\uparrow}(\mathbf{r},\mathbf{r}',t) &= A(t)^4 \sum_{\mathbf{k}} \Bigg[\delta\left(\mathbf{r} + \frac{\hbar t(\tilde{\mathbf{k}} - \mathbf{q})}{m}\right) \delta\left(\mathbf{r}' - \frac{\hbar t \tilde{\mathbf{k}'}}{m}\right) \\
&[f(E_{\uparrow,\mathbf{k},\mathbf{q}}) f(E_{\downarrow,\mathbf{k},\mathbf{q}}) + (1 - f(E_{\uparrow,\mathbf{k},\mathbf{q}}))(1 - f(E_{\downarrow,\mathbf{k},\mathbf{q}}))] |u_{\mathbf{k},\mathbf{q}}|^2 |v_{\mathbf{k},\mathbf{q}}|^2 \Bigg], \\
G_{\uparrow\uparrow}(\mathbf{r},\mathbf{r}',t) &= A(t)^4 \sum_{\mathbf{k}} \Bigg[\delta\left(\mathbf{r} - \frac{\hbar t \tilde{\mathbf{k}}}{m}\right) \delta\left(\mathbf{r}' - \frac{\hbar t \tilde{\mathbf{k}'}}{m}\right) \\
&[f(E_{\uparrow,\mathbf{k},\mathbf{q}}) f(E_{\downarrow,\mathbf{k},\mathbf{q}}) + (1 - f(E_{\uparrow,\mathbf{k},\mathbf{q}}))(1 - f(E_{\downarrow,\mathbf{k},\mathbf{q}}))] |u_{\mathbf{k},\mathbf{q}}|^2 |v_{\mathbf{k},\mathbf{q}}|^2 \\
&- |u_{\mathbf{k},\mathbf{q}}|^2 f(E_{\uparrow,\mathbf{k},\mathbf{q}}) - |v_{\mathbf{k},\mathbf{q}}|^2 (1 - f(E_{\downarrow,\mathbf{k},\mathbf{q}})) \Bigg] + \delta(\mathbf{r} - \mathbf{r}') \langle \hat{n}_{\uparrow}(\mathbf{r},t) \rangle, \\
G_{\downarrow\downarrow}(\mathbf{r},\mathbf{r}',t) &= A(t)^4 \sum_{\mathbf{k}} \Bigg[\delta\left(\mathbf{r} - \frac{\hbar t(\tilde{\mathbf{k}} - \mathbf{q})}{m}\right) \delta\left(\mathbf{r}' - \frac{\hbar t(\tilde{\mathbf{k}'} - \mathbf{q})}{m}\right) \\
&[f(E_{\uparrow,\mathbf{k},\mathbf{q}}) f(E_{\downarrow,\mathbf{k},\mathbf{q}}) + (1 - f(E_{\uparrow,\mathbf{k},\mathbf{q}}))(1 - f(E_{\downarrow,\mathbf{k},\mathbf{q}}))] |u_{\mathbf{k},\mathbf{q}}|^2 |v_{\mathbf{k},\mathbf{q}}|^2 \\
&- |u_{\mathbf{k},\mathbf{q}}|^2 f(E_{\downarrow,\mathbf{k},\mathbf{q}}) - |v_{\mathbf{k},\mathbf{q}}|^2 (1 - f(E_{\uparrow,\mathbf{k},\mathbf{q}})) \Bigg] + \delta(\mathbf{r} - \mathbf{r}') \langle \hat{n}_{\downarrow}(\mathbf{r},t) \rangle,
\end{aligned}
\tag{5.4}
$$

where

$$
\tilde{\mathbf{k}} = \mathbf{k} + \sum_{i=1}^{3} \frac{\hbar 2 n_i \pi t \hat{x}_i}{md},
$$

where n_i are integers. Above we have implicitly assumed that the lattice is large i.e. $M >> 1$. Note that functions of type

$$
\delta\left(\mathbf{r} - \frac{\hbar t \tilde{\mathbf{k}}}{m}\right)
$$

are not real delta-functions, but rather kind of peak functions. Because in the FFLO state, momenta $\mathbf{k}$ and $-\mathbf{k} + \mathbf{q}$ are correlated, the noise correlation signal is pronounced only if

$$
\mathbf{r} + \mathbf{r}' = \frac{\hbar t \tilde{\mathbf{q}}}{m} + \sum_{i=1}^{3} \frac{\hbar 2 n_i \pi t \hat{x}_i}{md}.
$$

The BCS continuum result [55] is similar, but peaks appear when $\mathbf{r} + \mathbf{r}' = 0$. In the continuum limit of low densities and long wavelengths, this result reduces to the known result.

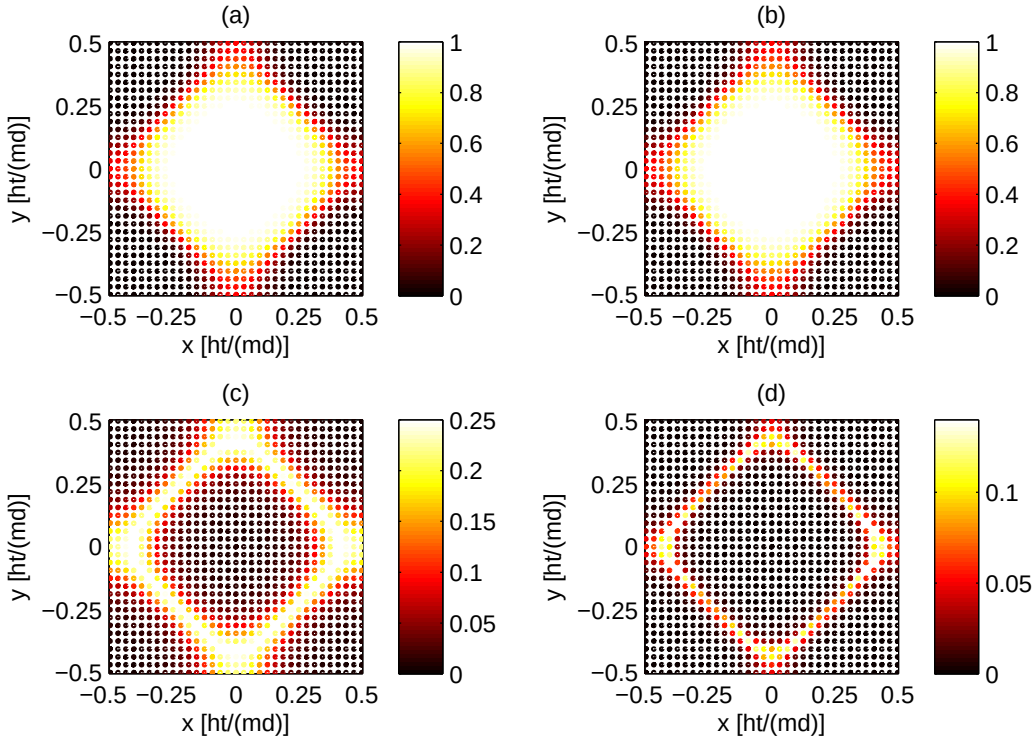

Figure 5.1: Figure (a) shows a cut of the BCS-state density in the $z = 0$ plane for $k_BT/(2J) = 0.196$ (just below T_c) while figure (b) shows a cut of the normal-state density in the $z = 0$ for $k_BT/(2J) = 0.20$ (just above T_c). Figures (c) and (d) show the integrated BCS-state noise correlations between components at temperatures $k_BT/(2J) = 0$ and $k_BT/(2J) = 0.196$, respectively. The other parameters used were $n_\uparrow = n_\downarrow = 0.20$, $U/(2J) = -1.86$. In figures (a) and (d) $\Delta/(2J) = 0.09$ and in figure (c), $\Delta/(2J) = 0.35$.

Although densities do not change much when the phase transition between the BCS phase and the normal phase takes place (as shown in figures 5.1 (a) and (b)), the noise correlations change crucially. In the normal phase the noise correlation between components are zero ($u_{\mathbf{k}}v_{\mathbf{k}} = 0$ in the normal phase), but in the BCS phase it is not zero, as shown in figure 5.1 (d). In the experiments, one takes typically a two-dimensional picture from the cloud of atoms [42, 41]. For this reason, it is of importance to investigate also the column integrated noise correlation signals, which are given by

$$G_{\uparrow,\downarrow}(x,y) = \int dz\, G_{\uparrow,\downarrow}\left(x, y, z, -x + \hbar t q_x/m, -y + \hbar t q_y/m, -z + \hbar t q_z/m\right).$$

Figures 5.1 (c) and (d) show the integrated noise correlations.

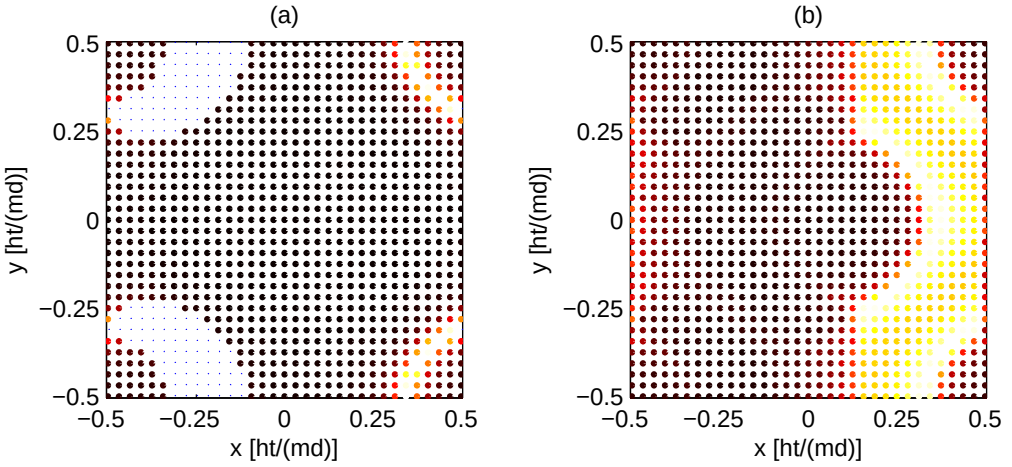

Figure 5.2: FFLO-state noise correlation ($G_{\uparrow\downarrow}$) at temperature $T = 0$. In (a), we show a cut in the $z = 0$ plane while (b) shows the column integrated signal. The parameters are $q_x = 0.25(\pi/d), q_y = q_z = 0$, polarization $P = (n_\uparrow - n_\downarrow)/(n_\uparrow + n_\downarrow) = 0.168$, $\Delta/(2J) = 0.16$, and $U/(2J) = -1.86$. In figure (a), correlations vanish in the dotted areas. We choose $\mathbf{r} + \mathbf{r}' - (\hbar t/m)\mathbf{q} = 0$ and color-coding is such that light colors imply high peaks and dark colors low.

The BCS state noise correlation of a single component shows similar antibunching behavior as the ideal Fermi gas noise correlation [41]. If $\mathbf{r} = \mathbf{r}' + \sum_{i=1}^{3} 2\hbar n_i \pi t \hat{x}_i/(md)$ and and $n_i \neq 0$ for at least one i, the noise correlation of a single component shows the holes. However, the BCS-state noise correlation of a single component shows also the bunching peak when $\mathbf{r} = \mathbf{r}'$. This result differs from the ideal gas result where such a peak is absent. This antibunching is due the Pauli exclusion principle, while the bunching peak is related to the BCS transition.

The FFLO noise correlations differ crucially from the BCS noise correlations. In the FFLO case the noise correlations are not symmetric contrary to the BCS correlations, as shown figure 5.2. This is due to the fact that in the FFLO case the Fermi surfaces are shifted by $\mathbf{q}$. Although at non-zero temperatures Fermi surfaces are rounded and sharp peaks are weakened due to thermal fluctuations, the shift in the positions of the peaks persists **IV**.

One can also use the noise correlations to detect multimode FFLO states, since multimode FFLO states leave clear signatures on the noise correlations. For example, for the two-mode FFLO-state, i.e., the state where the gap is given by $\Delta(\mathbf{R_i}) = \Delta_0 \cos(\mathbf{q} \cdot \mathbf{R}_i)$, the order parameter can be written in the momentum

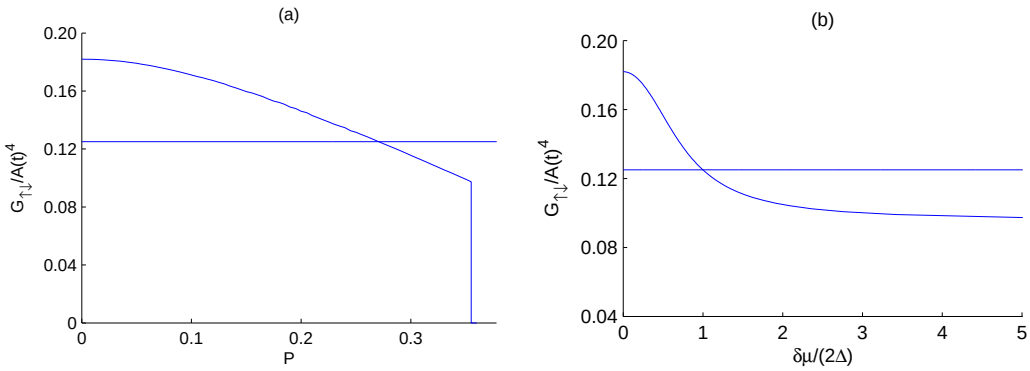

Figure 5.3: This figure demonstrates how the polarization contributes to the maximum peak height. (a) shows the maximum peak height as a function of the polarization while (b) shows the maximum peak height as a function of the chemical potential difference $(\mu_\uparrow - \mu_\downarrow)/(2\Delta) = \delta\mu/(2\Delta)$. We used the parameters $k_B T/(2J) = 0.45$ and an average filling fraction $(n_\uparrow + n_\downarrow)/2 = 0.30$. We have canceled the time dependence of the maximum peak height by dividing the maximum peak height by the scaling factor $A(t)^4$. The horizontal lines show value $1/8$.

space as

$$\Delta(\mathbf{R}_i) = \Delta_0 \cos(\mathbf{q}\cdot\mathbf{R}_i) = \Delta_0 \left(\frac{e^{i\mathbf{q}\cdot\mathbf{R}_i} + e^{-i\mathbf{q}\cdot\mathbf{R}_i}}{2} \right)$$
$$= -U\langle \hat{c}_{\uparrow,i}\hat{c}_{\downarrow,i}\rangle = \frac{-U}{M}\sum_{\mathbf{k},\mathbf{k}'} e^{-i(\mathbf{k}+\mathbf{k}')\cdot\mathbf{R}_i}\langle \hat{c}_{\uparrow,\mathbf{k}}\hat{c}_{\downarrow,\mathbf{k}'}\rangle$$
$$= e^{i\mathbf{q}\cdot\mathbf{R}_i}\frac{-U}{M}\sum_{\mathbf{k}}\langle \hat{c}_{\uparrow,\mathbf{k}}\hat{c}_{\downarrow,-\mathbf{k}-\mathbf{q}}\rangle + e^{-i\mathbf{q}\cdot\mathbf{R}_i}\frac{-U}{M}\sum_{\mathbf{k}}\langle \hat{c}_{\uparrow,\mathbf{k}}\hat{c}_{\downarrow,-\mathbf{k}+\mathbf{q}}\rangle.$$

Therefore the only non-vanishing expectation values in the momentum space are $\langle \hat{c}_{\uparrow,\mathbf{k}}\hat{c}_{\downarrow,-\mathbf{k}+\mathbf{q}}\rangle$ and $\langle \hat{c}_{\uparrow,\mathbf{k}}\hat{c}_{\downarrow,-\mathbf{k}-\mathbf{q}}\rangle$. This implies that an $\uparrow$-atom in the momentum state $\mathbf{k}$ is paired with $\downarrow$-atoms in the momentum states $-\mathbf{k}+\mathbf{q}$ and $-\mathbf{k}-\mathbf{q}$. Because in the single mode FFLO-state points $\mathbf{r}$ and $-\mathbf{r}+\hbar t\mathbf{q}/m$ are correlated after free expansion, in the two mode FFLO-state $\mathbf{r}$ is correlated with $-\mathbf{r}+\hbar t\mathbf{q}/m$ and $-\mathbf{r}-\hbar t\mathbf{q}/m$ after free expansion. For this reason with the two mode FFLO state one can see pronounced correlation peaks, when $\mathbf{r}+\mathbf{r}' \pm \hbar t\mathbf{q}/m = 0$.

The noise correlations offer a potential tool to detect the gapless BP/Sarma state, i.e., a state where $\mathbf{q} = 0$ and one of the quasiparticle dispersions $E_{\sigma,\mathbf{k}}$ is negative for some values of the momentum $\mathbf{k}$. This implies that in the gapless state $|\delta\mu| = |\mu_\uparrow - \mu_\downarrow| > 2\Delta$ (when the hopping strengths are equal).

It may not be easy to detect the gapless states via noise correlations, since the noise correlations of the gapless BP/Sarma state and non-gapless BP/Sarma

state appear quite similar. On the other hand, by monitoring the peak heights at $z = 0$ (and $\mathbf{r}' = -\mathbf{r}$), one can identify the gapless states. The reason for this is that in the gapless BP state the maximum peak height is always smaller than $A(t)^4/8$ whereas in the gapped state the maximum is always greater than this. This can be obtained from the fact that the term $|u_{\mathbf{k}}|^2|v_{\mathbf{k}}|^2$ peaks on the Fermi surface corresponding to the average chemical potential. On the other hand, near this surface the peak heights are

$$\begin{aligned}&|u_{\mathbf{k}}|^2|v_{\mathbf{k}}|^2[f(E_{\uparrow,\mathbf{k}})f(E_{\downarrow,\mathbf{k}}) + (1 - f(E_{\uparrow,\mathbf{k}}))(1 - f(E_{\downarrow,\mathbf{k}}))]\\ &\approx \frac{1}{4}[f(\Delta + \delta\mu/2)f(\Delta - \delta\mu/2) + (1 - f(\Delta - \delta\mu/2))(1 - f(\Delta + \delta\mu/2))],\end{aligned}$$

where $\delta\mu = \mu_\uparrow - \mu_\downarrow$ and then the term in the square brackets is bigger than $1/2$, when $\Delta \pm \delta\mu/2 > 0$ and otherwise always lower than $1/2$. This effect is shown in 5.3.

5.2 Superfluid density

Pairing does not necessarily imply superfluidity. There can be pairing without superfluidity [80], or the paired state can be unstable [81]. Superfluid density is a coefficient of inertia under the phase shift of the system [82]. If a linear phase shift is imposed on the system, the order parameter has a position depended phase, and if the gas is normal the order parameter is zero. Thus the phase shift does nothing to the normal gas. Superfluid density can be described the free-energy in the uniform case as

$$\Omega_{v_s} = \Omega_0 + \frac{1}{2}M_s v_s^2 = \Omega_0 + \frac{1}{2}V\tilde{\rho}_s v_s^2,$$

where Ω_{v_s} is the free-energy of moving gas, Ω_0 is the free-energy, when superfluid velocity $v_s = 0$, $\tilde{\rho}_s$ is the superfluid density, V is the system size. This superfluid velocity is related to the gradient of the phase of the pairing field [83]. When the pairing field is written as $\Delta(\mathbf{r}) = |\Delta(r)|e^{i\theta(\mathbf{r})}$, the superfluid velocity is defined as

$$\mathbf{v}_s(\mathbf{r}) = \frac{\hbar^2}{2m}\nabla\theta(\mathbf{r}),$$

For uniform BCS gas the superfluid density is given by [84]

$$\tilde{\rho}_s = \tilde{\rho} + \frac{2\hbar^2}{V}\sum_{\mathbf{k}} k_x^2 \frac{\partial f(E_{\mathbf{k}})}{\partial E_{\mathbf{k}}} = \tilde{\rho} + \frac{2\hbar^2}{3V}\sum_{\mathbf{k}} k^2 \frac{\partial f(E_{\mathbf{k}})}{\partial E_{\mathbf{k}}},$$

where $\tilde{\rho}$ is the total mass density, $E_{\mathbf{k}} = \sqrt{\epsilon_{\mathbf{k}}^2 + \Delta^2}$, and $\epsilon_{\mathbf{k}} = \hbar^2|\mathbf{k}|^2/(2m) - \mu$. This equation is known as Landau's formula.

5.2.1 Superfluid density in optical lattices

Here, we consider two-components Fermi gases, whose components are two different hyperfine states of ^{6}Li, in optical lattices. Let us start the mean-field Hamiltonian $\hat{H}_0$ (3.5) If one imposes a linear phase variation $\mathbf{\Theta}\cdot\mathbf{R}_i = (\Theta_x/(M_x d), \Theta_y/(M_y d), \Theta_z/(M$
$\mathbf{R}_i$ [82, 85], to the order parameter, the Hamiltonian is given by

$$\begin{aligned}\hat{H}_{\mathbf{\Theta}} = &-\sum_{\sigma=\uparrow,\downarrow}\left(J_{\sigma,x}\sum_{\langle i,j\rangle_x}+J_{\sigma,y}\sum_{\langle i,j\rangle_y}+J_{\sigma,z}\sum_{\langle i,j\rangle_z}\right)\hat{c}^\dagger_{\sigma,i}\hat{c}_{\sigma,j}\\ &-\sum_i(\mu_\uparrow c^\dagger_{\uparrow,i}\hat{c}_{\uparrow,i}+\mu_\downarrow c^\dagger_{\downarrow,i}\hat{c}_{\downarrow,i})\\ &+\sum_i|\Delta|e^{i(\mathbf{q}+2\mathbf{\Theta})\cdot\mathbf{R}_i}\hat{c}^\dagger_{\uparrow,i}\hat{c}^\dagger_{\downarrow,i}+|\Delta|e^{-i(\mathbf{q}+2\mathbf{\Theta})\cdot\mathbf{R}_i}\hat{c}_{\downarrow,i}\hat{c}_{\uparrow,i}.\end{aligned} \tag{5.5}$$

If one makes transformation $\hat{c}_{\sigma,i}\to\hat{c}_{\sigma,i}e^{i\mathbf{\Theta}\cdot\mathbf{R}_i}$, the Hamiltonian becomes

$$\begin{aligned}\hat{H}_{\mathbf{\Theta}} = &-\sum_i(\mu_\uparrow c^\dagger_{\uparrow,i}\hat{c}_{\uparrow,i}+\mu_\downarrow c^\dagger_{\downarrow,i}\hat{c}_{\downarrow,i})\\ &+\sum_i|\Delta|e^{i\mathbf{q}\cdot\mathbf{R}_i}\hat{c}^\dagger_{\uparrow,i}\hat{c}^\dagger_{\downarrow,i}+|\Delta|e^{-i\mathbf{q}\cdot\mathbf{R}_i}\hat{c}_{\downarrow,i}\hat{c}_{\uparrow,i}\\ &-\sum_\sigma\left[\sum_n\left(J_{\sigma,x}(e^{i\Theta_x/M_x}\hat{c}^\dagger_{\sigma,n}\hat{c}_{\sigma,n+d\hat{x}}+e^{-i\Theta_x/M_x}\hat{c}^\dagger_{\sigma,n}\hat{c}_{\sigma,n-d\hat{x}}\right.\right.\\ &+J_{\sigma,y}(e^{i\Theta_y/M_y}\hat{c}^\dagger_{\sigma,n}\hat{c}_{\sigma,n+d\hat{y}}+e^{-i\Theta_y/M_y}\hat{c}^\dagger_{\sigma,n}\hat{c}_{\sigma,n-d\hat{y}})\\ &\left.\left.+J_{\sigma,z}(e^{i\Theta_z/M_z}\hat{c}^\dagger_{\sigma,n}\hat{c}_{\sigma,n+d\hat{z}}+e^{-i\Theta_z/M_z}\hat{c}^\dagger_{\sigma,n}\hat{c}_{\sigma,n-d\hat{z}})\right)\right].\end{aligned} \tag{5.6}$$

We further assume that Θ_α/M_α are small, which is important to avoid effects other than the collective flow of the superfluid component. Under this assumption we can approximate the exponent functions using a few first terms of the Taylor expansion

$$e^{i\frac{\Theta_\alpha}{M_\alpha}}\approx 1+i\frac{\Theta_\alpha}{M_\alpha}-\frac{\Theta_\alpha^2}{2M_\alpha^2}.$$

Thus the Hamiltonian is given by

$$\begin{aligned}\hat{H}_{\mathbf{\Theta}} = \hat{H}_0 + H' \approx \hat{H}_0 + \sum_{\sigma} \Bigg[& \frac{\Theta_x^2}{2M_x^2} \sum_{\langle i,j\rangle_x} J_{\sigma,x} \hat{c}^\dagger_{\sigma,i} \hat{c}_{\sigma,j} + \\ & \frac{\Theta_y^2}{2M_y^2} \sum_{\langle i,j\rangle_y} J_{\sigma,y} \hat{c}^\dagger_{\sigma,i} \hat{c}_{\sigma,j} + \frac{\Theta_z^2}{2M_z^2} \sum_{\langle i,j\rangle_z} J_{\sigma,z} \hat{c}^\dagger_{\sigma,i} \hat{c}_{\sigma,j} \\ & - i\frac{\Theta_x}{M_x} \sum_i J_{\sigma,x} (\hat{c}^\dagger_{\sigma,i} \hat{c}_{\sigma,i+d\hat{x}} - \hat{c}^\dagger_{\sigma,i} \hat{c}_{\sigma,i-d\hat{x}}) \\ & - i\frac{\Theta_y}{M_y} \sum_i J_{\sigma,y} (\hat{c}^\dagger_{\sigma,i} \hat{c}_{\sigma,i+d\hat{y}} - \hat{c}^\dagger_{\sigma,i} \hat{c}_{\sigma,i-d\hat{y}}) \\ & - i\frac{\Theta_z}{M_z} \sum_i J_{\sigma,z} (\hat{c}^\dagger_{\sigma,i} \hat{c}_{\sigma,i+d\hat{z}} - \hat{c}^\dagger_{\sigma,i} \hat{c}_{\sigma,i-d\hat{z}}) \Bigg].\end{aligned} \tag{5.7}$$

Furthermore, we obtain in the momentum space

$$\begin{aligned}\hat{H}_{\mathbf{\Theta}} \approx \hat{H}_0 + \sum_{\sigma,\alpha} \Bigg[& \frac{\Theta_\alpha^2}{2M_\alpha^2} \sum_{\mathbf{k}} 2J_{\sigma,\alpha} \cos(k_\alpha d) \hat{c}^\dagger_{\sigma,\mathbf{k}} \hat{c}_{\sigma,\mathbf{k}} \\ & + \frac{\Theta_\alpha}{M_\alpha} \sum_{\mathbf{k}} 2J_{\sigma,\alpha} \sin(k_\alpha d) \hat{c}^\dagger_{\sigma,\mathbf{k}} \hat{c}_{\sigma,\mathbf{k}} \Bigg].\end{aligned} \tag{5.8}$$

We can write the grand potential of the system with a perturbing phase gradient as a series [86]

$$\Omega_{\mathbf{\Theta}} = \Omega_0 - \sum_{n=1}^{\infty} \frac{(-1)^n}{n\hbar^n} \int_0^{\beta\hbar} d\tau_1 \cdots \int_0^{\beta\hbar} d\tau_n \, \langle T_\tau \hat{H}'(\tau_1) \cdots \hat{H}'(\tau_n) \rangle_0, \tag{5.9}$$

where τ is imaginary time, Ω_0 is the grand canonical potential in the absence of the perturbation. The brackets $\langle \dots \rangle_0 = \mathrm{Tr}[\exp(-\beta(\hat{H}_0 - \mu_\uparrow \hat{N}_\uparrow - \mu_\downarrow \hat{N}_\downarrow)) \dots]$ denote the thermodynamic average evaluated in the equilibrium state of the unperturbed system. Since all the twisting angles Θ_α are small, we can ignore higher than Θ_α^2 order terms. With this approximation, the grand potential is expressed as

$$\Omega_{\mathbf{\Theta}} \approx \Omega_0 + \frac{1}{\beta\hbar} \int_0^{\beta\hbar} d\tau \, \langle T_\tau \hat{T}(\tau) \rangle_0 - \frac{1}{\beta\hbar^2} \int_0^{\beta\hbar} \int_0^{\beta\hbar} d\tau \, d\tau' \langle T_\tau \hat{J}(\tau) J(\tau') \rangle_0,$$

where

$$\hat{T} = \sum_{\sigma,\alpha} \left[\frac{\Theta_\alpha^2}{2M_\alpha^2} \sum_{\mathbf{k}} 2J_{\sigma,\alpha} \cos(k_\alpha d) \hat{c}^\dagger_{\sigma,\mathbf{k}} \hat{c}_{\sigma,\mathbf{k}} \right]$$

$$\hat{J} = \sum_{\sigma,\alpha} \left[\frac{\Theta_\alpha}{M_\alpha} \sum_{\mathbf{k}} 2J_{\sigma,\alpha} \sin(k_\alpha d) \hat{c}^\dagger_{\sigma,\mathbf{k}} \hat{c}_{\sigma,\mathbf{k}} \right].$$

The first perturbation term is given by

$$\frac{1}{\beta\hbar}\int_0^{\beta\hbar} d\tau\,\langle T_\tau \hat{T}(\tau)\rangle_0 = \sum_{\sigma,\alpha}\left[\frac{\Theta_\alpha^2}{2M_\alpha^2}\sum_{\mathbf{k}} 2J_{\sigma,\alpha}\cos(k_\alpha d)N_{\sigma,\mathbf{k}}\right], \tag{5.10}$$

where $N_{\sigma,\mathbf{k}}$ is number of particles of the σ-component in the momentum state $\mathbf{k}$. By applying Wick's theorem, the second perturbation assumes the form

$$\begin{aligned}
&-\frac{1}{2\beta\hbar^2}\int_0^{\beta\hbar}\int_0^{\beta\hbar} d\tau\,d\tau'\,\langle T_\tau \hat{J}(\tau)\hat{J}(\tau')\rangle_0 \\
&= -\frac{1}{2\beta\hbar^2}\int_0^{\beta\hbar}\int_0^{\beta\hbar} d\tau\,d\tau'\left[\sum_{\sigma,\sigma',\alpha,\alpha'}\frac{\Theta_\alpha\Theta_{\alpha'}}{M_\alpha M_{\alpha'}}\sum_{\mathbf{k},\mathbf{k}'} 4J_{\sigma,\alpha}J_{\sigma',\alpha'}\sin(k_\alpha d)\sin(k'_{\alpha'}d)\right. \\
&\left.\times\left((1-\delta_{\sigma\sigma'})\delta_{\mathbf{k}+\mathbf{q},-\mathbf{k}'+\mathbf{q}}F(\mathbf{k},\tau,\tau')F^\dagger(\mathbf{k}',\tau,\tau') - \delta_{\sigma\sigma'}\delta_{\mathbf{k}\mathbf{k}'}G_\sigma(\mathbf{k},\tau,\tau')G_{\sigma'}(\mathbf{k}',\tau,\tau')\right)\right],
\end{aligned}$$

where the Green's function are defined by

$$\begin{aligned}
G_\sigma(\mathbf{k},\tau,\tau') &= -\langle T_\tau \hat{c}_{\sigma,\mathbf{k}}(\tau)\hat{c}^\dagger_{\sigma,\mathbf{k}}(\tau)\rangle_0, \\
F(\mathbf{k},\tau,\tau') &= -\langle T_\tau \hat{c}_{\uparrow,\mathbf{k}+\mathbf{q}}(\tau)\hat{c}_{\downarrow,-\mathbf{k}+\mathbf{q}}(\tau)\rangle_0.
\end{aligned}$$

These Green's functions can be calculated from the definition of the Green's functions in the momentum space [87]

$$\begin{pmatrix} i\hbar\omega_n - \epsilon_{\uparrow,\mathbf{k}+\mathbf{q}} & \Delta \\ \Delta & -\hbar\frac{\partial}{\partial\tau} + \epsilon_{\downarrow,-\mathbf{k}+\mathbf{q}}\end{pmatrix} G(\mathbf{k},\omega_n) = \hbar\mathbb{I},$$

where $\mathbb{I}$ is 2×2 unit matrix and the fermionic Matsubara frequencies are given by

$$\omega_n = \frac{\pi(2n+1)}{\hbar\beta},$$

where n is an integer. Finally, the one particle dispersions are

$$\epsilon_{\sigma,\mathbf{k}} = \sum_\alpha 2J_{\sigma,\alpha}(1-\cos(k_{\alpha d}) - \mu_\sigma.$$

By multiplying the both sides of the Green's function equation by factor $G^{-1}(\mathbf{k},\omega_n)$ one finds

$$\hbar G^{-1}(\mathbf{k},\omega_n) = \begin{pmatrix} i\hbar\omega_n - \epsilon_{\uparrow,\mathbf{k}+\mathbf{q}} & \Delta \\ \Delta & -\hbar\frac{\partial}{\partial\tau} + \epsilon_{\downarrow,-\mathbf{k}+\mathbf{q}}\end{pmatrix}.$$

Since this matrix is a 2×2-matrix, it can be inverted analytically. It turns out that the Green's function matrix in the momentum space is given by

$$G(\mathbf{k},\omega_n) = \begin{pmatrix} -\frac{\hbar(i\hbar\omega_n+\epsilon_{\downarrow,-\mathbf{k}+\mathbf{q}})}{(E_{+,\mathbf{k},\mathbf{q}}-i\hbar\omega_n)(E_{-,\mathbf{k},\mathbf{q}}+i\hbar\omega_n)} & \frac{\hbar\Delta_0}{(E_{+,\mathbf{k},\mathbf{q}}-i\hbar\omega_n)(E_{-,\mathbf{k},\mathbf{q}}+i\hbar\omega_n)} \\ \frac{\hbar\Delta_0}{(E_{+,\mathbf{k},\mathbf{q}}-i\hbar\omega_n)(E_{-,\mathbf{k},\mathbf{q}}+i\hbar\omega_n)} & -\frac{\hbar(i\hbar\omega_n-\epsilon_{\uparrow,\mathbf{k}+\mathbf{q}})}{(E_{+,\mathbf{k},\mathbf{q}}-i\hbar\omega_n)(E_{-,\mathbf{k},\mathbf{q}}+i\hbar\omega_n)}\end{pmatrix},$$

where the quasiparticle dispersions $E_{+,\mathbf{k},\mathbf{q}}$ and $E_{-,\mathbf{k},\mathbf{q}}$ are the same as we used in chapter 3. The Green's function matrix can be simplified by using factors $u_{\mathbf{k},\mathbf{q}}$ and $v_{\mathbf{k},\mathbf{q}}$, and is then rewritten in the form

$$G(\mathbf{k},\omega_n)=\hbar\begin{pmatrix} \frac{|u_{\mathbf{k},\mathbf{q}}|^2}{i\hbar\omega_n-E_{+,\mathbf{k},\mathbf{q}}}+\frac{|v_{\mathbf{k},\mathbf{q}}|^2}{i\hbar\omega_n+E_{-,\mathbf{k},\mathbf{q}}} & \frac{u_{\mathbf{k},\mathbf{q}}v^*_{\mathbf{k},\mathbf{q}}}{i\hbar\omega_n+E_{-,\mathbf{k},\mathbf{q}}}-\frac{u_{\mathbf{k},\mathbf{q}}v^*_{\mathbf{k},\mathbf{q}}}{i\hbar\omega_n-E_{+,\mathbf{k},\mathbf{q}}} \\ \frac{u^*_{\mathbf{k},\mathbf{q}}v_{\mathbf{k},\mathbf{q}}}{i\hbar\omega_n+E_{-,\mathbf{k},\mathbf{q}}}-\frac{u^*_{\mathbf{k},\mathbf{q}}v_{\mathbf{k},\mathbf{q}}}{i\hbar\omega_n-E_{+,\mathbf{k},\mathbf{q}}} & \frac{|v_{\mathbf{k},\mathbf{q}}|^2}{i\hbar\omega_n-E_{+,\mathbf{k},\mathbf{q}}}+\frac{|v_{\mathbf{k},\mathbf{q}}|^2}{i\hbar\omega_n+E_{-,\mathbf{k},\mathbf{q}}} \end{pmatrix}. \quad (5.11)$$

The individual Green's functions can be identified explicitly to be

$$G_\uparrow(\mathbf{k},\omega_n)=\frac{|u_{\mathbf{k},\mathbf{q}}|^2}{i\hbar\omega_n-E_{+,\mathbf{k},\mathbf{q}}}+\frac{|v_{\mathbf{k},\mathbf{q}}|^2}{i\hbar\omega_n+E_{-,\mathbf{k},\mathbf{q}}},$$
$$G_\downarrow(\mathbf{k},\omega_n)=\frac{|u_{\mathbf{k},\mathbf{q}}|^2}{i\hbar\omega_n-E_{-,\mathbf{k},\mathbf{q}}}+\frac{|v_{\mathbf{k},\mathbf{q}}|^2}{i\hbar\omega_n+E_{+,\mathbf{k},\mathbf{q}}},$$
$$F(\mathbf{k},\omega_n)=\frac{u_{\mathbf{k},\mathbf{q}}v^*_{\mathbf{k},\mathbf{q}}}{i\hbar\omega_n+E_{-,\mathbf{k},\mathbf{q}}}-\frac{u_{\mathbf{k},\mathbf{q}}v^*_{\mathbf{k},\mathbf{q}}}{i\hbar\omega_n-E_{+,\mathbf{k},\mathbf{q}}}.$$

Furthermore, we obtain

$$G_\sigma(\mathbf{k},\tau,\tau')=\frac{1}{\sqrt{\beta\hbar}}\sum_{n=-\infty}^{\infty}e^{-i\omega_n(\tau-\tau')}G_\sigma(\mathbf{k},\omega_n)$$
$$F(\mathbf{k},\tau,\tau')=\frac{1}{\sqrt{\beta\hbar}}\sum_{n=-\infty}^{\infty}e^{-i\omega_n(\tau-\tau')}F(\mathbf{k},\omega_n).$$

Substitution of these Green's functions in the second order perturbation term, it assumes the form

$$-\frac{1}{2\beta\hbar^2}\int_0^{\beta\hbar}\int_0^{\beta\hbar}d\tau\,d\tau'\,\langle T_\tau\hat{J}(\tau)\hat{J}(\tau')\rangle_0=\sum_\alpha\frac{\Theta_\alpha^2}{M_\alpha^2}\sum_{\mathbf{k}}\Bigg[2J^2_{\uparrow,\alpha}\sin^2((k_\alpha+q_\alpha)d)$$
$$\times\Bigg(2|u_{\mathbf{k},\mathbf{q}}|^2|v_{\mathbf{k},\mathbf{q}}|^2\frac{f(E_{+,\mathbf{k},\mathbf{q}})+f(E_{-,\mathbf{k},\mathbf{q}})-1}{E_{+,\mathbf{k},\mathbf{q}}+E_{-,\mathbf{k},\mathbf{q}}}-$$
$$\beta|u_{\mathbf{k},\mathbf{q}}|^4f(E_{+,\mathbf{k},\mathbf{q}})(1-f(E_{+,\mathbf{k},\mathbf{q}}))-\beta|v_{\mathbf{k},\mathbf{q}}|^4f(E_{-,\mathbf{k},\mathbf{q}})(1-f(E_{-,\mathbf{k},\mathbf{q}}))\Bigg)+$$
$$2J^2_{\downarrow,\alpha}\sin^2((k_\alpha-q_\alpha)d)\Bigg(2|u_{\mathbf{k},\mathbf{q}}|^2|v_{\mathbf{k},\mathbf{q}}|^2\frac{f(E_{+,\mathbf{k},\mathbf{q}})+f(E_{-,\mathbf{k},\mathbf{q}})-1}{E_{+,\mathbf{k},\mathbf{q}}+E_{-,\mathbf{k},\mathbf{q}}}-$$
$$\beta|u_{\mathbf{k},\mathbf{q}}|^4f(E_{-,\mathbf{k},\mathbf{q}})(1-f(E_{-,\mathbf{k},\mathbf{q}}))$$
$$-\beta|v_{\mathbf{k},\mathbf{q}}|^4f(E_{+,\mathbf{k},\mathbf{q}})(1-f(E_{+,\mathbf{k},\mathbf{q}}))\Bigg)+$$
$$4J_{\uparrow,\alpha}J_{\downarrow,\alpha}\sin((k_\alpha+q_\alpha)d)\sin((k_\alpha-q_\alpha)d)$$
$$\times|u_{\mathbf{k},\mathbf{q}}|^2|v_{\mathbf{k},\mathbf{q}}|^2\Bigg(\frac{2(f(E_{+,\mathbf{k},\mathbf{q}})-f(E_{-,\mathbf{k},\mathbf{q}}))}{E_{+,\mathbf{k},\mathbf{q}}-E_{-,\mathbf{k},\mathbf{q}}}$$
$$-\frac{2f(E_{+,\mathbf{k},\mathbf{q}})-1}{2E_{+,\mathbf{k},\mathbf{q}}}-\frac{2f(E_{-,\mathbf{k},\mathbf{q}})-1}{2E_{-,\mathbf{k},\mathbf{q}}}\Bigg)\Bigg],$$

We can now write the twisted grand potential as

$$\Omega_{\mathbf{\Theta}} = \Omega_0 + \sum_{\alpha\alpha'} \delta\Omega_{\alpha\alpha'} \frac{\Theta_\alpha \Theta_{\alpha'}}{M_\alpha M_{\alpha'}},$$

and determine the components of the superfluid density tensor as

$$\tilde{\rho}_{\alpha\alpha'} = \frac{\delta\Omega_{\alpha\alpha'}}{\bar{J}_x} = \frac{2\delta\Omega_{\alpha\alpha'}}{J_{\uparrow,x} + J_{\downarrow,x}}.$$

These dimensionless elements are given by

$$\begin{aligned}
\tilde{\rho}_{\alpha\alpha} &= \sum_{\mathbf{k},\sigma} 2\tilde{J}_{\sigma,\alpha} \cos(k_\alpha d) N_{\sigma,\mathbf{k}} \\
&+ \sum_{\mathbf{k}} \Bigg[\tilde{J}^2_{\uparrow,\alpha} \sin^2((k_\alpha + q_\alpha/2)d) \\
&\times \Bigg(2|u_{\mathbf{k},\mathbf{q}}|^2 |v_{\mathbf{k},\mathbf{q}}|^2 \frac{f(E_{+,\mathbf{k},\mathbf{q}}) + f(E_{-,\mathbf{k},\mathbf{q}}) - 1}{E_{+,\mathbf{k},\mathbf{q}} + E_{-,\mathbf{k},\mathbf{q}}} \\
&- \beta |u_{\mathbf{k},\mathbf{q}}|^4 f(E_{+,\mathbf{k},\mathbf{q}})(1 - f(E_{+,\mathbf{k},\mathbf{q}})) \\
&- \beta |v_{\mathbf{k},\mathbf{q}}|^4 f(E_{-,\mathbf{k},\mathbf{q}})(1 - f(E_{-,\mathbf{k},\mathbf{q}})) \Bigg) + 2\tilde{J}^2_{\downarrow,\alpha} \sin^2((k_\alpha - q_\alpha/2)d) \\
&\times \Bigg(2|u_{\mathbf{k},\mathbf{q}}|^2 |v_{\mathbf{k},\mathbf{q}}|^2 \frac{f(E_{+,\mathbf{k},\mathbf{q}}) + f(E_{-,\mathbf{k},\mathbf{q}}) - 1}{E_{+,\mathbf{k},\mathbf{q}} + E_{-,\mathbf{k},\mathbf{q}}} \\
&- \beta |u_{\mathbf{k},\mathbf{q}}|^4 f(E_{-,\mathbf{k},\mathbf{q}})(1 - f(E_{-,\mathbf{k},\mathbf{q}})) \\
&- \beta |v_{\mathbf{k},\mathbf{q}}|^4 f(E_{+,\mathbf{k},\mathbf{q}})(1 - f(E_{+,\mathbf{k},\mathbf{q}})) \Bigg) \\
&+ 4\tilde{J}_{\uparrow,\alpha} \tilde{J}_{\downarrow,\alpha'} \sin((k_\alpha + q_\alpha/2)d) \sin((k_\alpha - q_\alpha/2)d) \\
&\times |u_{\mathbf{k},\mathbf{q}}|^2 |v_{\mathbf{k},\mathbf{q}}|^2 \Bigg(\frac{2(f(E_{+,\mathbf{k},\mathbf{q}}) - f(E_{-,\mathbf{k},\mathbf{q}}))}{E_{+,\mathbf{k},\mathbf{q}} - E_{-,\mathbf{k},\mathbf{q}}} \\
&- \frac{2f(E_{+,\mathbf{k},\mathbf{q}}) - 1}{2E_{+,\mathbf{k},\mathbf{q}}} - \frac{2f(E_{-,\mathbf{k},\mathbf{q}}) - 1}{2E_{-,\mathbf{k},\mathbf{q}}} \Bigg) \Bigg], \\
\tilde{\rho}_{\alpha\alpha'} &= 0,
\end{aligned} \tag{5.12}$$

and furthermore we can determine dimensionless superfluid fraction as

$$\rho_{\alpha\alpha'} = \frac{\tilde{\rho}_{\alpha\alpha'}}{N_\uparrow + N_\downarrow},$$

where N_σ is the total number of particles of the σ-component.

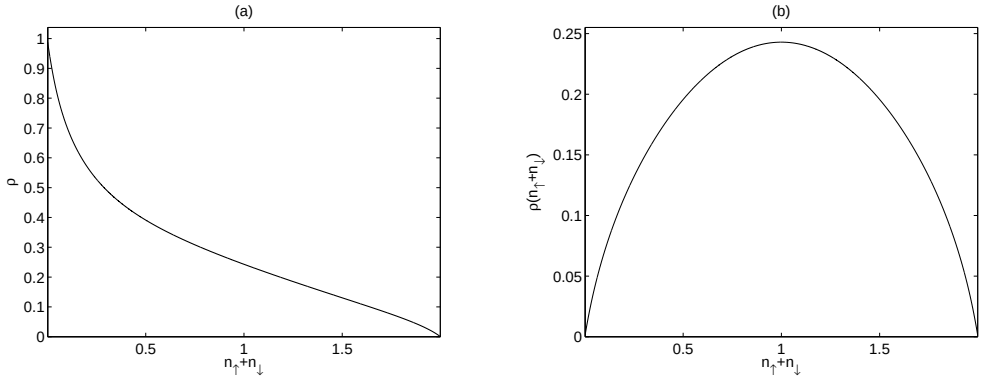

Figure 5.4: Figure (a) shows the BCS superfluid fraction $\rho = \rho_{xx} = \rho_{yy} = \rho_{zz}$ as a function of the total filling fraction $n_\uparrow + n_\downarrow = 2n_\uparrow = 2n_\downarrow$ at zero temperature. In figure (b) we show $\rho(n_\uparrow + n_\downarrow)$ as a function of the total filling fraction. All the hopping strengths are the same, i.e., $J = J_{\uparrow,\alpha} = J_{\downarrow,\alpha'}$,and $-U/J = 6.0$.

5.2.1.1 BCS and the Sarma phase superfluid density

As described in chapter 3, momentum vector $\mathbf{q}$ is zero in the standard BCS phase and in the Sarma phase. Thus one obtains the BCS/Sarma superfluid density from equation (5.12) by replacing q_α by zero.

In the BCS continuum limit, where $\mu_\uparrow = \mu_\downarrow$, $J_{\uparrow,\alpha} = J_{\downarrow,\beta} = J$, and $d \to 0$, but Jd^2 remains a constant, the superfluid fraction becomes

$$\rho_{\alpha\alpha} = \rho = 1 + \frac{2\hbar^2}{m_a n V} \sum_{\mathbf{k}} k_x^2 \frac{\partial f(E_{\mathbf{k}})}{\partial E_{\mathbf{k}}},$$

where $m_a = \hbar^2/(2Jd^2)$ is the effective mass, $n = n_\uparrow + n_\downarrow$ is the total number density and V is the size of the system. This equation is precisely the Landau's formula as it should be. This continuum limit can be realized in the limit of vanishing total filling fraction, as shown in figure 5.4 (a). Figure 5.4 (b) shows the particle-hole symmetry of the BCS superfluid density. This symmetry arises from the particle-hole symmetry of the mean-field Hubbard model.

The superfluid fraction can be different in different directions, when the hopping strengths are different in different directions, as shown in figure 5.5 (a). Since the hopping strengths are different in different directions, the effective masses are different in different directions and since the superfluid fraction components are different in different directions. In figure 5.5 (b), we show the BCS superfluid fraction as a function of the dimensionless coupling strength $-U/J$ at zero temperature. As we can observe from the figure, the superfluid fraction decreases with increasing $-U/J$ contrary to the free space result, where the superfluid fraction is a constant as a function of the coupling strength. This is due to the

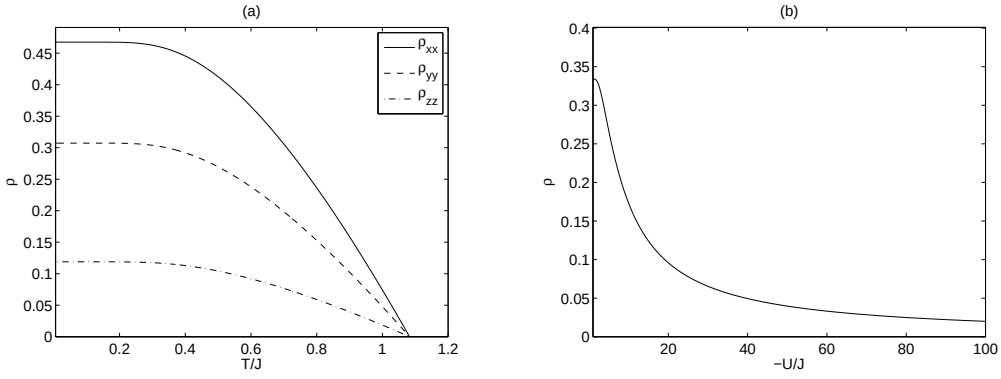

Figure 5.5: Figure (a) shows the BCS superfluid fraction as a function of temperature in the case, where the hopping strengths are different in different directions. Figure (b) shows the BCS superfluid fraction as a function of a dimensionless coupling strength $-U/J$ at zero temperature. In figure (a) $J_{\uparrow,y} = J_{\downarrow,y} = 0.8J_{\uparrow,x} = 0.8J_{\downarrow,x}$ and $J_{\uparrow,z} = J_{\downarrow,z} = 0.5J_{\uparrow,x} = 0.5J_{\downarrow,x}$. In figure (b) $J_{\sigma,\alpha} = J_{\sigma',\alpha'} = J$ and in the both figures $-U/J_{\uparrow,x} = 6.0$.

fact that as $-U/J$ increases the movement of the atoms decreases in the lattice. In other words the larger $-U/J$ is the smaller Cooper pairs are, and the more localized atoms are.

The Sarma phase superfluid fraction is very similar to the BCS phase superfluid fraction. In the both phases Sarma- and BCS phase the superfluid fraction proportional to $|\Delta|^2$, as shown in figure 5.6 (b).

5.2.1.2 One mode FFLO phase superfluid density

If the momentum vector $\mathbf{q}$ is finite, the phase is the one mode FFLO phase, and the superfluid density of this phase was given in equation (5.12). The one mode FFLO superfluid fraction can be in principle asymmetric, even in the case where all the hopping strengths are equal. This is due to vector $\mathbf{q}$. However, it turns out that, in cubic lattices, the free energy is minimized for the vector $\mathbf{q}$ lieyng alongside an principal axis, and since the one mode FFLO superfluid density is symmetric. This is due to the fact if the lattice is cubic and all the hoping strengths are equal, the system does not favour any of these axis.

The one mode FFLO superfluid density is not directly proportional to $|\Delta|^2$, unlike the BCS/Sarma superfluid density. As shown in figure 5.7. We can observe the phase transition between the Sarma phase and the FFLO phase as a gusp in the curve at $P \approx 0.15$ in figure 5.7 (a).

For strong interactions and low temperatures, the one mode FFLO superfluid density can be negative. This indicates that the phase is dynamically unsta-

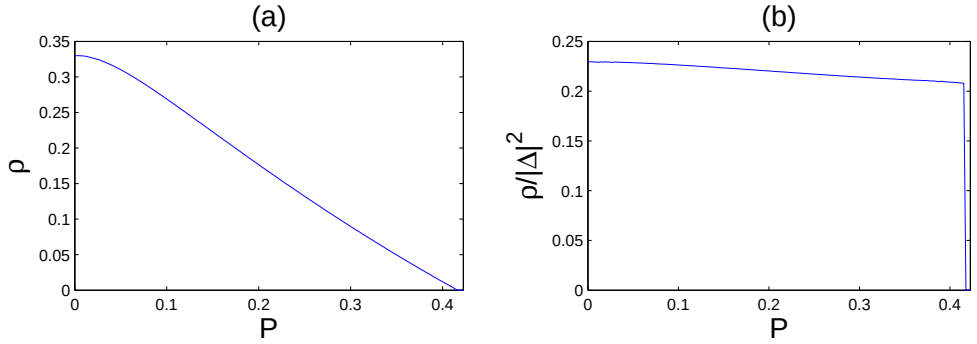

Figure 5.6: Figure (a) shows the Sarma phase superfluid fraction as a function of the polarization at constant temperature. In figure (b) we show the Sarma phase superfluid fraction divided by $|\Delta|^2$. The parameters, which were used, are $k_BT/J \approx 0.46$, $U/J = -5.1$, and the average filling fraction is $n_{av} = (n_\uparrow + n_\downarrow)/2 = 0.2$, All the hopping strengths were equal. The sudden drop in figure (b) at $P \approx 0.45$ in indicates that the pairing field becomes zero.

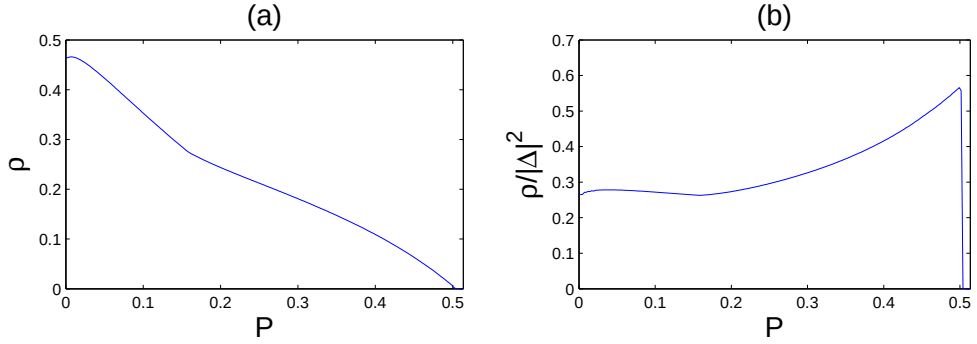

Figure 5.7: Figure (a) shows first the Sarma- and after that the FFLO phase superfluid fraction as a function of the polarization at constant temperature. In figure (b) we show the Sarma- and FFLO phase superfluid density divided by $|\Delta|^2$. The parameters are $k_BT/J \approx 0.23$, $U/J \approx -5.1$, and the average filling fraction is $n_{av} = (n_\uparrow + n_\downarrow)/2 = 0.2$. All the hopping strengths are equal. The sudden drop in figure (b) at $P \approx 0.5$ in indicates that the pairing field becomes zero.

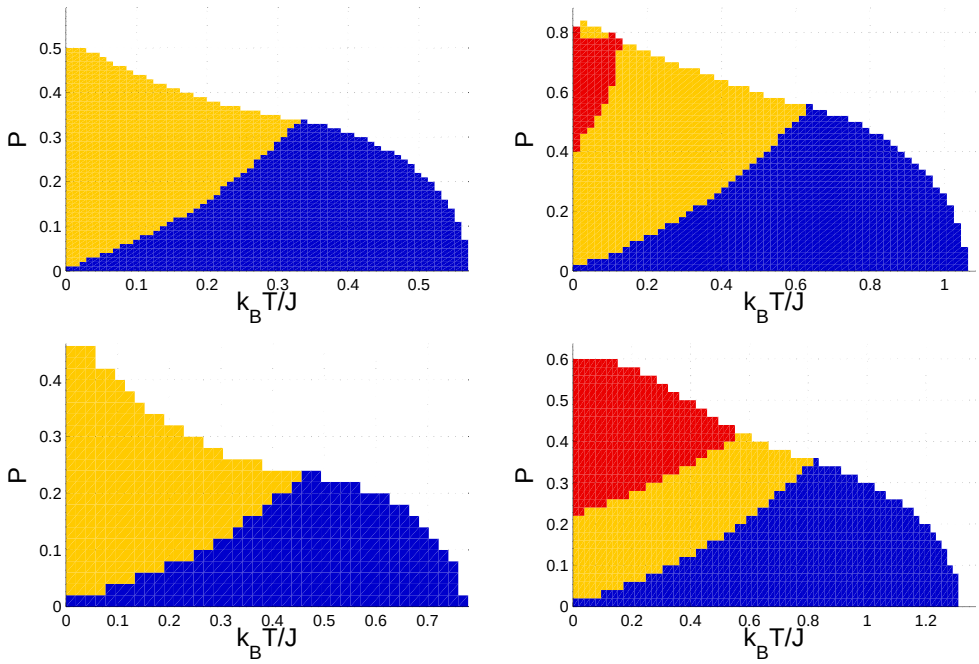

Figure 5.8: Phase diagrams of a two-components Fermi gas with two different average filling fractions and two different interaction strengths in a cubic lattice. The average filling fraction and the interaction strengths are from top left to bottom right: $n_{av} = 0.2$, $U/J \approx -4.4$; $n_{av} = 0.2$, $U/J \approx -6.3$; $n_{av} = 0.5$, $U/J \approx -4.4$; $n_{av} = 0.5$, $U/J \approx -6.3$. All the hopping strengths are equal. The color scheme is as follows: BCS/Sarma=blue, stable FFLO=yellow, unstable FFLO=red, normal gas=white. In the to right figure the yellow area between the red areas is due to the numerical uncertainties.

ble [81]. However,the one mode FFLO phase is stable if $-U/J < 4.0$. We can observe the unstable regions of the phase diagram from figure 5.8. This instability is also connected to the filling fraction, when the average filling fraction increases (up to 0.5 after that the regions decreases, which due to the particle hole symmetry) the unstable regions increases, as shown figure 5.8. Note that we do not take the phase separation into account. These dynamical instabilities indicate that the one mode FFLO is not the ground state. The ground state may be some kind of phase separation or the multimode FFLO states [88, 89]. The superfluid density can be measured by measuring the frequency of the collective modes [90].

Chapter 6

Conclusions

The superfluidity of Fermi gases arises from pairing of two different species of fermions. Different types of paired states were described in this thesis. First, we studied within the mean-field theory two-components Fermi gases in optical lattices and showed that the Fulde-Ferrel-Larkin-Ovchinnikov state is energetically favorable in a large region of the phase diagram in a cubic lattice. We generalized the Hubbard Hamiltonian to the higher bands, and found that there can, under our assumptions, be two different types of paired states between the bands.

Next we focused on a three-component Fermi gas, and showed that the BCS theory can be generalized to this case. We demonstrated that a three-component Fermi gas in a harmonic trap is a very rich system. We discussed also three-component Fermi gases in optical lattices and showed that it is possible to tune the lattices in such a way that the Hamiltonian approaches $SU(3)$-symmetric form.

In the last part of this thesis it is discussed how these different paired states can be experimentally observed and investigated. We showed that the noise correlations are a useful tool to detect different phases in optical lattices. Furthermore, we calculated the superfluid densities, and found that the FFLO superfluid density differs crucially from the BCS/Sarma superfluid density in lattices. We also showed that there can be dynamical instabilities in the FFLO phase.

Multitude of new directions for future studies have been opened. The multi-band Hubbard models can be used to study the crossover physics, which means physics near the Feshbach resonance, in optical lattices. Also analogs between the QCD and three-component Fermi gases offer lot of new possibilities. Furthermore, beyond mean-field corrections should be studied more extensively.

Bibliography

[1] S. N. Bose. Plancks gesetz und lichtquantenhypothese. *Z. Phys.*, 26:178, 1924.

[2] A. Einstein. Quantentheorie des einatomigen idealen Gases: Zweite Abhandlung. *Sitzungber. Preuss. Akad. Wiss.*, 1925(0):3, January 1925.

[3] M. H. Anderson, J. R. Ensher, M. R. Matthews, C. E. Wieman, and E. A. Cornell. Observation of Bose-Einstein condensation in a dilute atomic vapor. *Science*, 269:198–201, 1995.

[4] K. B. Davis, M.-O. Mewes, M. R. Andrews, N. J. van Druten, D. S. Durfee, D. M. Kurn, and W. Ketterle. Bose-Einstein condensation in a gas of sodium atoms. *Phys. Rev. Lett.*, 75:3969–3973, 1995.

[5] C. S. Adams and E. Riis. Laser cooling and trapping of neutral atoms. *Prog. Quant. Electr.*, 21:1–79, 1997.

[6] H. J. Metcalf and P. van der Straten. *Laser Cooling and Trapping.* Springer, New-York, 1999.

[7] C. J. Pethick and H. Smith. *Bose-Einstein Condensation in Dilute Gases.* CUP, Cambridge, 2001.

[8] C.J. Myatt, E.A. Burt, R.W. Ghrist, E.A. Cornell, and C.E. Wieman. Production of two overlapping Bose-Einstein condensates by sympathetic cooling. *Phys. Rev. Lett.*, 78:586, 1997.

[9] U. Fano. Effects of configuration interaction on intensities and phase shifts. *Phys. Rev.*, 124:1866, 1961.

[10] H. Feshbach. A unified theory of nuclear reactions. *Ann. Phys.*, 19:287, 1962.

[11] M. Bartenstein, A. Altmeyer, S. Riedl, R. Geursen, S. Jochim, C. Chin, J. Hecker Denschlag, R. Grimm, A. Simoni, E. Tiesinga, C. J. Williams, and P. S. Julienne. Precise determination of li-6 cold collision parameters by radio-frequency spectroscopy on weakly bound molecules. *Phys. Rev. Lett.*, 94:103201, 2005.

[12] J. Bednorz and K. Müller. Possible high tc superconductivity in the ba-la-cu-o system. *Z. Physik, B*, 64:189, 1986.

[13] J. Bardeen, L. N. Cooper, and J. R. Schrieffer. Theory of superconductivity. *Phys. Rev.*, 108:1175, 1957.

[14] L. N. Cooper. Bound electron pairs in a degenerate Fermi gas. *Phys. Rev.*, 104:1189 – 1190, 1956.

[15] C. A. Regal, C. Ticknor, J. L. Bohn, and D. S. Jin. Creation of ultracold molecules from a Fermi gas of atoms. *Nature*, 424:47, 2003.

[16] K.E. Strecker, G.B. Partridge, and R.G. Hulet. Conversion of an atomic Fermi gas to a long-lived molecular Bose gas. *Phys. Rev. Lett.*, 91:080406, 2003.

[17] J. Cubizolles, T. Bourdel, S. J. J. M. F. Kokkelmans, G. V. Shlyapnikov, and C. Salomon. Production of long-lived ultracold li molecules from a Fermi gas. *Phys. Rev. Lett.*, 91:240401, 2003.

[18] S. Jochim, M. Bartenstein, A. Altmeyer, G. Hendl, C. Chin, J. H. Denschlag, , and R. Grimm. Pure gas of optically trapped molecules created from Fermionic atoms. *Phys. Rev. Lett.*, 91:240402, 2003.

[19] S. Jochim, M. Bartenstein, A. Altmeyer, G. Hendl, S. Riedl, C. Chin, J. Hecker Denschlag, and R. Grimm. Bose-Einstein condensation of molecules. *Science*, 302:2101–2103, 2003.

[20] C. A. Regal, M. Greiner, and D. S. Jin. Emergence of a molecular Bose-Einstein condensate from a Fermi gas. *Nature*, 426:537, 2003.

[21] M. W. Zwierlein, C. A. Stan, C. H. Schunck, S. M. F. Raupach, S. Gupta, Z. Hadzibabic, and W. Ketterle. Observation of Bose-Einstein condensation of molecules. *Phys. Rev. Lett.*, 91:250401, 2003.

[22] T. Bourdel, L. Khaykovich, J. Cubizolles, J. Zhang, F. Chevy, M. Teichmann, L. Tarruell, S. J. J. M. F. Kokkelmans, and C. Salomon. Experimental study of the BEC-BCS crossover region in lithium 6. *Phys. Rev. Lett.*, 93:050401, 2004.

[23] C.A. Regal, M. Greiner, and D.S. Jin. Observation of resonance condensation of Fermionic atom pairs. *Phys. Rev. Lett.*, 92:040403, 2004.

[24] M. W. Zwierlein, C. A. Stan, C. H. Schunck, S.M.F. Raupach, A.J. Kerman, and W. Ketterle. Condensation of pairs of fermionic atoms near a feshbach resonance. *Phys. Rev. Lett.*, 92:120403, 2004.

[25] J. Kinast, S. L. Hemmer, M. E. Gehm, A. Turlapov, and J. E. Thomas. Evidence for superfluidity in a resonantly interacting Fermi gas. *Phys. Rev. Lett.*, 92:150402, 2004.

[26] M. Bartenstein, A. Altmeyer, S. Riedl, S. Jochim, C. Chin, J. H. Denschlag, and R. Grimm. Crossover from a molecular Bose-Einstein condensate to a degenerate Fermi gas. *Phys. Rev. Lett.*, 92:120401, 2004.

[27] J. Kinast, A. Turlapov, J. E. Thomas, Q. Chen, J. Stajic, and K. Levin. Heat capacity of a strongly interacting Fermi gas. *Science*, 307:1296–1299, 2005.

[28] M. W. Zwierlein, J.R. Abo-Shaeer, A. Schirotzek, C.H. Schunck, and W. Ketterle. Vortices and superfluidity in a strongly interacting Fermi gas. *Nature*, 435:1047–1051, 2005.

[29] P. S. Jessen and I. H. Deutsch. Optical lattices. *Adv. At. Mol. Opt. Phys.*, 37:95–138, 1996.

[30] K. I. Petsas, A. B. Coates, and G. Grynberg. Crystallography of optical lattices. *Phys. Rev. A*, 50:5173–5189, 1994.

[31] C. Orzel, A. K. Tuchman, M. L. Fenselau, M. Yasuda, and M. A. Kasevich. Squeezed states in a Bose-Einstein condensate. *Science*, 291:2386, 2001.

[32] M. Greiner, I. Bloch, O. Mandel, T. W. Hänsch, and T. Esslinger. Exploring phase coherence in a 2d lattice of Bose-Einstein condensates. *Phys. Rev. Lett.*, 87:160405, 2001.

[33] S. Burger, F. S. Cataliotti, C. Fort, F. Minardi, M. Inguscio, M. L. Chiofalo, and M. P. Tosi. Superfluid and dissipative dynamics of a Bose-Einstein condensate in a periodic optical potential. *Phys. Rev. Lett.*, 86:4447, August 2001.

[34] Z. Hadzibabic, S. Stock, B. Battelier, V. Bretin, and J. Dalibard. Interference of an array of independent Bose-Einstein condensates. *Phys. Rev. Lett.*, 93:180403, 2004.

[35] M. Köhl, H. Moritz, T. Stöferle, K. Günter, and T. Esslinger. Fermionic atoms in a three dimensional optical lattice: Observing Fermi surfaces, dynamics, and interactions. *Phys. Rev. Lett.*, 94:080403, 2005.

[36] J. K. Chin, D. E. Miller, Y. Liu, C. Stan, W. Setiawan, C. Sanner, K. Xu, and W. Ketterle. Evidence for superfluidity of ultracold fermions in an optical lattice. *Nature*, 443:961–964, 2006.

[37] N. W. Ashcroft and N. D. Mermin. *Solid State Physics*. Saunder College Publishing, New York, 1976.

[38] G. H. Wannier. The structure of electronic excitation levels in insulating crystals. *Phys. Rev.*, 52:191, 1937.

[39] T. Stöferle, H. Moritz, K. Günter, M. Köhl, and T. Esslinger. Molecules of Fermionic atoms in an optical lattice. *Phys. Rev. Lett.*, 96:030401, 2006.

[40] R. Jördens, N. Strohmaier, H. Moritz, and T. Esslinger. A mott insulator of fermionic atoms in an optical lattice. *Nature*, 455:204, 2008.

[41] T. Rom, Th. Best, D. van Oosten, U. Schneider, S. Foelling, B. Paredes, and I. Bloch. Free fermion antibunching in a degenerate atomic Fermi gas released from an optical lattice. *Nature*, 444:733–736, 2006.

[42] S. Foelling, F. Gerbier, A. Widera, O. Mandel, T. Gericke, and I. Bloch. Spatial quantum noise interferometry in expanding ultracold atom clouds. *Nature*, 434:481–484, 2005.

[43] E. Burovski, E. Kozik, N. Prokof'ev, B. Svistunov, and M. Troyer. Critical temperature curve in the BEC-BCS crossover. *Phys. Rev. Lett.*, 101:090402, 2008.

[44] P. Fulde and R. A. Ferrell. Superconductivity in a strong spin-exchange field. *Phys. Rev.*, 135:A550, 1964.

[45] A. I. Larkin and Y. N. Ovchinnikov. Nonuniform state of supercon-ductors. *Zh. Eksp. Teor. Fiz.*, 47:1136, 1964.

[46] G. Sarma. *J. Phys. Chem. Solids*, 24:1029, 1963.

[47] W. V. Liu and F. Wilczek. Interior gap superfluidity. *Phys. Rev. Lett.*, 90:047002, 2003.

[48] A. M. Clogston. Upper limit for the critical field in hard superconductors. *Phys. Rev. Lett.*, 9:266–267, 1962.

[49] T. K. Koponen, T. Paananen, J.-P. Martikainen, M. R. Bakhtiari, and P. Törmä. FFLO state in 1, 2, and 3 dimensional optical lattices combined with a non-uniform background potential. *New Journal of Physics*, 10:045104, 2008.

[50] K. B. Gubbels, M. W. J. Romans, and H. T. C. Stoof. Sarma phase in trapped unbalanced Fermi gases. *Phys. Rev. Lett.*, 97:210402, 2006.

[51] Daniel E. Sheehy and Leo Radzihovsky. BEC-BCS crossover, phase transitions and phase separation in polarized resonantly-paired superfluids. *Annals of Physics*, 322:1790, 2007.

[52] T. Müller, S. Flling, A. Widera, and I. Bloch. State preparation and dynamics of ultracold atoms in higher lattice orbitals. *Phys. Rev. Lett.*, 99:200405, 2007.

[53] R. B. Diener and T. H. Lo. Two-component Fermion systems in strong coupling. *Phys. Rev. Lett.*, 96:010402, 2006.

[54] J.-P. Martikainen, E. Lundh, and T. Paananen. Interband physics in an ultra-cold Fermi gas in an optical lattice. *Phys. Rev. A*, 78:023607, 2008.

[55] E. Altman, E. Demler, and M. D. Lukin. Probing many-body states of ultracold atoms via noise correlations. *Phys. Rev. A*, 70:013603, 2004.

[56] C. Chin, M. Bartenstein, A. Altmeyer, S. Riedl, S. Jochim, J. H. Denschlag, and R. Grimm. Observation of the pairing gap in a strongly interacting Fermi gas. *Science*, 305:1128–1130, 2004.

[57] J. Kinnunen, M. Rodriguez, and P. Törmä. Pairing gap and in-gap excitations in trapped Fermionic superfluids. *Science*, 305:1131–1133, 2004.

[58] Y. Shin, C. H. Schunck, A. Schirotzek, and W. Ketterle. Tomographic rf spectroscopy of a trapped Fermi gas at unitarity. *Phys. Rev. Lett.*, 99:090403, 2007.

[59] M. G. Alford and G. Cowan. Single-flavour and two-flavour pairing in three-flavour quark matter. *J. Phys. G*, 32:511–528, 2006.

[60] C. Honerkamp and W. Hofstetter. BCS pairing in Fermi systems with n different hyperfine states. *Phys. Rev. Lett.*, 92:170403, 2004.

[61] A. Rapp, W. Hofstetter, and G. Zarand. Trionic phase of ultracold Fermions in an optical lattice: A variational study. *Phys. Rev. B*, 77:144520, 2008.

[62] T. B. Ottenstein, T. Lompe, M. Kohnen, A. N. Wenz, and S. Jochim. Collisional stability of a three-component degenerate Fermi gas. *Phys. Rev. Lett.*, 101:203202, 2008.

[63] N. N. Bogoliubov. *Sov. Phys. JETP*, 34:41, 1958.

[64] J. G. Valatin. *Il Nuovo Cimento*, 8:843, 1958.

[65] P. G. de Gennes. *Superconductivity of metals and alloys*. Addison-Wesley, New York, 1989.

[66] Y. Shin, M. W. Zwierlein, C. H. Schunck, A. Schirotzek, and W. Ketterle. Observation of phase separation in a strongly-interacting imbalanced Fermi gas. *Phys. Rev. Lett.*, 97:030401, 2006.

[67] M. W. Zwierlein, A. Schirotzek, C. H. Schunck, and W. Ketterle. Fermionic superfluidity with imbalanced spin populations. *Science*, 311:492, 2006.

[68] M. Haque and H.T.C. Stoof. Pairing of a trapped resonantly-interacting fermion mixture with unequal spin populations. *Phys. Rev. A*, 74:011602(R), 2006.

[69] J.-P. Martikainen. Ultracold polarized Fermi gas at intermediate temperatures. *Phys. Rev. A*, 74:013602, 2006.

[70] G. B. Partridge, W. Li, R. I. Kamar, Y. Liao, and R. G. Hulet. Pairing and phase separation in a polarized Fermi gas. *Science*, 311:506, 2006.

[71] G. B. Partridge, W. Li, Y. Liao, R. G. Hulet, M. Haque, and H. T. C. Stoof. Deformation of a trapped Fermi gas with unequal spin populations. *Phys. Rev. Lett.*, 97:190407, 2006.

[72] T. N. De Silva and E. J. Mueller. Surface tension in population imbalanced unitary Fermi gases. *Phys. Rev. Lett.*, 97:070402, 2006.

[73] J. Kinnunen, L. M. Jensen, and P. Törmä. Strongly interacting Fermi gases with density imbalance. *Phys. Rev. Lett.*, 96:110403, 2006.

[74] T. N. De Silva and E. J. Mueller. Profiles of near-resonant population-imbalanced trapped Fermi gases. *Phys. Rev. A*, 73:051602(R), 2006.

[75] O. Mandel, M. Greiner, A Widera, T. Rom, T. W. Hänsch, and I. Bloch. Controlled collisions for multi-particle entanglement of optically trapped atoms. *Nature*, 425:937, 2003.

[76] O. Mandel, M. Greiner, A Widera, T. Rom, T. W. Hänsch, and I. Bloch. Coherent transport of neutral atoms in spin-dependent optical lattice potentials. *Phys. Rev. Lett.*, 91:010407, 2003.

[77] V. N. Efimov. Weakly bound states of three resonantly-interacting particles. *Sov. J. Nuc. Phys.*, 12:589, 1971.

[78] V. N. Efimov. Low-energy properties of three resonantly interacting particles. *Sov. J. Nuc. Phys.*, 29:546, 1979.

[79] T. Kraemer, M. Mark, P. Waldburger, J. G. Danzl, C. Chin, B. Engeser, A. D. Lange, K. Pilch, A. Jaakkola, H.-C. Nägerl, and R. Grimm. Evidence for Efimov quantum states in an ultracold gas of caesium atoms. *Nature*, 440:315–318, 2006.

[80] C. H. Schunck, Y. Shin, A. Schirotzek, M. W. Zwierlein, and W. Ketterle. Pairing without superfluidity: The ground state of an imbalanced Fermi mixture. *Science*, 316:867–870, 2007.

[81] B. Wu and Q. Niu. Landau and dynamical instabilities of the superflow of Bose-Einstein condensates in optical lattices. *Phys. Rev. A*, 64:061603, 2001.

[82] R. Roth and K. Burnett. Superfluidity and interference pattern of ultracold bosons in optical lattices. *Phys. Rev. A*, 67:031602, 2003.

[83] P. W. Anderson. Considerations on the flow of superfluid helium. *Rev. Mod. Phys.*, 38:298, 1966.

[84] E. M. Lifshitz and L. P. Pitaevskii. *Statistical Physics, Part 2.* Butterworth-Heinemann, Oxford, 2002.

[85] J.-P. Martikainen and H. T. C. Stoof. Spontaneous squeezing of a vortex in an optical lattice. *Phys. Rev. A*, 70:013604, 2004.

[86] G. D. Mahan. *Many-Particle Physics, 3rd ed.* Kluwer Academic/Plenum Publishers, New York, 2000.

[87] A. L. Fetter and J. D. Walecka. *Quantum theory of many-particle systems.* Dover, New York, 2003.

[88] Meera M. Parish, Stefan K. Baur, Erich J. Mueller, and David A. Huse. Quasi-one-dimensional polarized Fermi superfluids. *Phys. Rev. Lett.*, 99:250403, 2007.

[89] M. Iskin and C. J. Williams. Population imbalanced fermions in harmonically trapped optical lattices. *Phys. Rev. A*, 78:011603(R), 2008.

[90] S. Riedl, E. R. Sanchez Guajardo, C. Kohstall, A. Altmeyer, M. J. Wright, J. Hecker Denschlag, R. Grimm, G. M. Bruun, and H. Smith. Collective oscillations of a Fermi gas in the unitarity limit: Temperature effects and the role of pair correlations. *Phys. Rev. A*, 78:053609, 2008.